

ANDREAS KILIMATOS

FEASIBILITY OF  
CONCRETE SHELLS  
USING FLEXIBLE  
MOULD  
PREFABRICATED  
CONCRETE  
ELEMENTS

**Cover photo:**

Military aircraft hanger by Pier Luigi Nervi-Orvieto, Italy, 1935  
(Source: concretevinyl)

# Feasibility of concrete shells using flexible mould prefabricated concrete elements

MASTER THESIS

by

Andreas Kilimatos

in partial fulfilling of of the requirement for the degree of

**Master of Science**  
in Civil Engineering

in Delft University of Technology

To be defended publicly on Monday June 4<sup>th</sup>, 2018

Student number: 4359909  
Supervisor: Dr.ir. H.R.Schipper  
Thesis committee: Prof.ir. R. Nijse  
Ir. P. Egenraam

An electronic version of this thesis is available at  
<http://repository.tudelft.nl/>



# Abstract

Shell structures appear quite often in our daily life. From aircraft fuselages to storage silos and boat hulls, these structures are employed for their structural efficiency and the aesthetics they provide. They are characterised by a small thickness in comparison to their other dimensions and by curvature in their unstressed state.

Despite their structural efficiency transferring loads in their plane, thin concrete shells are not employed quite often. The traditional construction method is a labour intensive process which includes the fabrication of a formwork system, usually made out of plywood, on which concrete is cast. The necessary reinforcement in the form of bars although it is quickly placed, it has the drawback of requiring frequent joints and overlapping. Its bending and assembling is also considered difficult for curved shapes like shells. As it can be seen, great costs emerge from this process and this was a trigger factor for the formation of the research question.

A different approach for the construction of shells employs prefabricated elements which are connected on site and create the complete thickness of the concrete shell. Although high construction speed and high quality are achieved with this method, significant reduction of costs is still not feasible, as the formwork is very expensive and re-use of it, is only occasionally possible.

However, an adjustable mould can produce elements of different dimensions, shape and curvature, decreasing substantially the formwork costs which comprise large part of the total shell construction costs. The flexible mould method and the principle of deformation after casting that were introduced by Prof. R.H. Schipper find application in this project. The research question is the following:

“Is it possible to construct a shell structure using flexible mould prefabricated elements without putting at risk the stability of the shell?”

A comparison between the structural feasibility of a monolithic shell and the one of a segmented prefabricated shell is the method that will be utilised to answer the research question.

The result of the traditional construction method is a shell of 100mm thickness using C 50/60. For the case of the prefabricated shell, a construction method that makes use both of prefabricated elements and cast in-situ concrete is applied. However, the properties of the connection between the elements have not been thoroughly investigated and only a limited number of applications and researches has been realised. Instead of proceeding in the definition of the connection properties, a conservative assumption according to which the prefabricated elements function solely as formwork elements takes place. This construction method offers significant benefits compared to the traditional method, since the elements are produced faster and easier, and complex shell configurations are allowed. In addition, the formwork elements are integrated in the final structure, avoiding the arduous process of removing them.

The behavior of the elements is examined throughout the different construction stages and a connection model is introduced that employs FRP strips, in order to account for the large tensile forces. During these analyses it was concluded that 40mm thick formwork elements with three supports per side of element, are sufficiently strong to sustain their weight and the applied load from the reinforcement and wet concrete. With this conclusion, the construction of the shell of the 'Bezoekerscentrum Waalbos' is indeed possible using the flexible mould prefabricated elements, answering positively to the set research question.



# Acknowledgments

I would like to take the opportunity to express my gratitude to everyone who contributed to the completion of this thesis. Initially, I would like to thank my graduation committee for their assistance and support throughout the progress of the thesis. Thank you Rob Nijssse, Roel Schipper, Peter Eigenraam for your interest and advice. Special thanks to my friends, fellow engineers, Maria Alexiou, Anna Ioannidou-Kati and Pratik Rao, who shared generously their thoughts, ideas and knowledge with me. Their contribution was priceless. Furthermore, I would like to thank the Fanourakis Foundation for their financial support during the first year of my studies. Finally and most importantly, I deeply thank my parents, my brother and my grandmother for believing and supporting me and for offering their love during harsh times.

Andreas S. Kilimatos  
Delft, May 2018

# Table of Contents

<b>1. 1 SHELL STRUCTURES.....</b>	<b>2</b>
1.1 SURFACE GEOMETRY.....	2
1.2 SHELLS IN FREE-FORM ARCHITECTURE.....	3
1.3 STATE OF AFFAIRS.....	4
1.4 PROBLEM DESCRIPTION AND SCOPE.....	6
<b>2. 2 THEORY OF SHELLS.....</b>	<b>8</b>
2.1 MEMBRANE THEORY OF SHELLS.....	8
2.2 BENDING THEORY.....	11
<b>3. 3 FORMWORK TYPES FOR CONCRETE SHELLS.....</b>	<b>14</b>
3.1 INTRODUCTION.....	14
3.2 DESCRIPTION OF THE PROBLEM WITH TIMBER FORMWORK.....	15
3.3 PNEUMATIC INFLATED FORMWORK.....	16
3.4 EARTH MOULDS.....	17
3.5 POLYURETHANE FOAM FORMWORK.....	18
3.6 RAISED STEEL SKELETON METHOD.....	19
3.7 3D-PRINTING.....	19
3.8 PREFABRICATED CONCRETE ELEMENTS.....	20
3.9 MOULDS FOR PREFABRICATED CONCRETE ELEMENTS-METHODS OF CONSTRUCTION.....	21
3.9.1 <i>Timber moulds</i> .....	21
3.9.2 <i>Steel moulds</i> .....	22
3.9.2.1 Hoto Fudo.....	22
3.9.3 <i>Textile formwork</i> .....	23
3.9.3.1 Palazetto dello Sport.....	24
3.9.3.2 Spencer Dock Bridge.....	25
<b>4. 4 ANALYSIS OF APPROXIMATING STRUCTURAL FORMS.....</b>	<b>26</b>
4.1 INTRODUCTION.....	26
4.2 VERIFICATION PROCESS.....	27
4.3 LOADS .....	28
4.3.1 <i>Permanent loads</i> .....	28
4.3.2 <i>Variable loads</i> .....	29
4.3.2.1 Snow load.....	29
4.3.2.2 Wind load.....	30
4.4 FLAT SLAB.....	30
4.4.1 <i>Description of flat slab behaviour</i> .....	31
4.4.2 <i>Load Combinations</i> .....	32
4.4.3 <i>Analysis of results-Comparison</i> .....	32
4.4.3.1 Theoretical results.....	32
4.4.3.2 FEA results .....	34
4.4.3.3 Theoretical results.....	36
4.4.3.4 FEA results .....	37
4.5 ARCH.....	38
4.5.1 <i>Load combinations</i> .....	40
4.5.2 <i>Analysis of results</i> .....	41

4.6	CYLINDRICAL SHELL.....	45
4.6.1	<i>Load combinations</i> .....	49
4.6.2	<i>Theoretical results</i> .....	49
4.6.3	<i>FEA results</i> .....	51
4.6.4	<i>Comparison</i> .....	51
4.7	SPHERICAL SIDE PART.....	52
4.7.1	<i>Side part-Dome</i> .....	52
<b>5. 5</b>	<b>ANALYSIS OF THE CASE STRUCTURE 'BEZOEKERSCENTRUM WAALBOS'.....</b>	<b>56</b>
5.1	DESCRIPTION OF THE STRUCTURE.....	56
5.2	VERIFICATION OF THE FINAL MODEL.....	58
5.3	SUPPORTS.....	60
5.4	DISCUSSION ON THE RESULTS OF THE ANALYSIS.....	62
5.5	ANALYSIS WITH SERVICE LOADS.....	63
5.5.1	<i>Permanent Loads</i> .....	63
5.5.2	<i>Variable Loads</i> .....	63
5.5.2.1	<i>Live load</i> .....	64
5.5.2.2	<i>Snow Load</i> .....	64
5.5.3	<i>Wind Load</i> .....	65
5.5.4	<i>Load combinations</i> .....	68
5.6	RESULTS OF LINEAR STATIC ANALYSIS.....	69
5.7	MESH SIZE STUDY.....	70
5.7.1	<i>Process</i> .....	70
5.8	INVESTIGATION OF THE THICKNESS OF THE SHELL.....	75
5.9	INVESTIGATION OF CONCRETE GRADE.....	76
<b>6. 6</b>	<b>ANALYSIS OF THE PREFABRICATED CONCRETE SHELL.....</b>	<b>78</b>
6.1	SEGMENTATION OF THE SHELL.....	78
6.1.1	<i>Boundary -Conforming Grids</i> .....	78
6.1.2	<i>Structured grids</i> .....	79
6.1.3	<i>Block-Structured Grids</i> .....	79
6.1.4	<i>Translational grids</i> .....	80
6.1.5	<i>Grid generation for dome structures</i> .....	81
6.2	SEGMENTATION OF 'BEZOEKERSCENTRUM WAALBOS'.....	81
<b>7. 7</b>	<b>ANALYSIS OF THE SEGMENTED STRUCTURE.....</b>	<b>85</b>
7.1	CONSTRUCTION METHOD-CONNECTIONS BETWEEN ELEMENTS.....	85
7.2	TYPES OF CONNECTIONS.....	85
7.2.1	<i>Wet connection</i> .....	85
7.2.2	<i>Bolted connection/welded connection</i> .....	86
7.2.3	<i>Post-tensioning connection</i> .....	86
7.2.4	<i>Glued connection</i> .....	86
7.2.5	<i>Prefabricated connection</i> .....	86
7.3	PROPOSED CONSTRUCTION METHOD FOR 'BEZOEKERSCENTRUM WAALBOS'.....	87
7.3.1	<i>Description of construction method</i> .....	87
7.3.2	<i>Evaluation of the method</i> .....	88
7.4	SEGMENTED SHELL CHARACTERISTICS AND ANALYSIS.....	89
7.4.1	<i>Introduction</i> .....	89
7.4.2	<i>Dimensions of the elements-Transportation to the building site</i> .....	89
7.4.3	<i>FRP reinforcement of concrete structures</i> .....	97
7.5	CONCLUSIONS.....	105

<b>8. 8 CONCLUSIONS AND RECOMMENDATIONS.....</b>	<b>106</b>
8.1 CONCLUSIONS.....	106
8.2 RECOMMENDATIONS.....	109
<b>BIBLIOGRAPHY.....</b>	<b>113</b>
<b>APPENDIX A.....</b>	<b>117</b>

# List of Figures

Illustration 1.1: Types of Gaussian curvature [2].....	2
Illustration 1.2: Examples of free-form designs [54], [53].....	3
Illustration 1.3: Concept of deformation after casting [52].....	6
Illustration 2.1: Shell element membrane forces.....	9
Illustration 2.2: Membrane free body.....	10
Illustration 3.1: Shapes, formwork and skeleton shuttering[9].....	15
Illustration 3.2: Examples of elaborated timber formwork for concrete shells[9], [25] .....	15
Illustration 3.3: The plane concrete plate is produced and the membrane is inflated [10].....	16
Illustration 3.4: Forming soil mould for concrete shell [8].....	17
Illustration 3.5: Excavation of mould through archways [8].....	18
Illustration 3.6: Double polyurethane foam formwork for concrete shells [23].....	18
Illustration 3.7: Central mast and steel rebars [8].....	19
Illustration 3.8: Jubilee Church, Rome [19].....	22
Illustration 3.9: Hoto Fudo with Mt. Fuji in the background [20].....	23
Illustration 3.10: Cross-section of Hoto Fudo shell [22].....	23
Illustration 3.11: Ribbed roof -Palazzetto dello Sport [26].....	25
Illustration 3.12: Spencer Dock Bridge-Double-curved parapets [27].....	25
Illustration 4.1 Plan view of the structure [28].....	26
Illustration 4.2: Part of structure considered as a slab.....	31
Illustration 4.3: Slab 1.....	33
Illustration 4.4: Bending moments in a flat slab supported by 2 columns [34].....	33
Illustration 4.5: Infinitely rigid part of column support [34].....	34
Illustration 4.6: Strips for moment distribution-Original flat slab.....	35
Illustration 4.7: Slab 2.....	36
Illustration 4.8: Continuous beam on three supports approximating the behaviour of Slab 2.....	37
Illustration 4.9: Three-hinged arch.....	40
Illustration 4.10: Parabolic arch under uniform load action [35].....	40
Illustration 4.11: Free body diagram of a three hinged arch under self-weight.....	42
Illustration 4.12: Normalised moments for a two-hinged arch.....	45
Illustration 4.13: Normalised moments for a three-hinged arch.....	45
Illustration 4.14: Parts of the design case structure.....	45
Illustration 4.15: Behaviour of long barrel shell - Beam action [36].....	46
Illustration 4.16: Part of the structure considered as a cylindrical roof.....	46
Illustration 4.17: Supports in transverse direction for cylindrical roof.....	47
Illustration 4.18: Cylindrical shell roof-Plan view and cross-section.....	47
Illustration 4.19: Free body diagram of shell beam.....	50
Illustration 4.20: Ellipsoid side parts.....	53
Illustration 4.21: Membrane forces on infinitesimal load element.....	54
Illustration 5.1: Model of the structure.....	56
Illustration 5.2: Structure with its surroundings.....	57
Illustration 5.3: Supporting arch at the facade opening.....	57
Illustration 5.4: Stresses on a cross section.....	59
Illustration 5.5: Stresses of the chosen cross-section.....	59
Illustration 5.6: Total stresses-DIANA.....	60
Illustration 5.7: Initial deformations of the structure.....	61

Illustration 5.8: Deformations due to self-weight in the z-axis – arch support.....	62
Illustration 5.9: Hoop stresses-self weight.....	62
Illustration 5.10: Meridional stresses-self weight.....	63
Illustration 5.11: Snow load shape coefficients for cylindrical roof.....	64
Illustration 5.12: Recommended values of Ce for different topographies.....	65
Illustration 5.13: Exposure factor according to Eurocode.....	66
Illustration 5.14: Illustration 5.11: External pressure coefficients cpe,10 for domes with circular base.....	67
Illustration 5.15: Distribution for vaulted roofs.....	67
Illustration 5.16: Wind distribution in the circumferential direction.....	68
Illustration 5.17: Structural failure modes for shells.....	70
Illustration 5.18: Influence length of edge disturbances in a spherical dome.....	70
Illustration 5.19: Error function of displacement in relation to mesh size.....	71
Illustration 5.20: Vertical deformation diagram-LC1.....	72
Illustration 5.21: Deflection diagram of two-span beam with uniformly distributed load .....	72
Illustration 5.22: Global stresses in the circumferential direction-LC2.....	73
Illustration 5.23: Global stresses in the meridional direction-LC2.....	73
Illustration 5.24: Moments in the x-axis (left) and y-axis (right).....	74
Illustration 5.25: First buckling mode-LC2.....	75
Illustration 5.26: Second buckling mode-LC2.....	75
Illustration 6.1: Boundary conforming quadrangular and triangular grid [3].....	79
Illustration 6.2: Types of interface between contiguous blocks: (a) discontinuous, (b and c) non-smooth, (d) smooth [3].....	80
Illustration 6.3: Segmentation of translational surface [3].....	80
Illustration 6.4: Basic grid patterns [2].....	80
Illustration 6.5: Grid configuration for some shapes [3].....	81
Illustration 6.6: Triangular elements at the sides of the domes.....	83
Illustration 6.7: Final segmentation at the sides of the dome.....	83
Illustration 6.8: Segmented shell-top view.....	84
Illustration 6.9: Segmented shell-front view.....	84
Illustration 7.1: Glued connection [42].....	86
Illustration 7.2: Different versions of prefabricated connection [44].....	87
Illustration 7.3: Prefabricated connection model design.....	88
Illustration 7.4: Representation of static and dynamic loads [45].....	90
Illustration 7.5: Crane lifting element.....	91
Illustration 7.6: Element to be examined under its own weight.....	91
Illustration 7.7: Displacements in the vertical axis.....	92
Illustration 7.8: Local stresses y-axis.....	92
Illustration 7.9: Illustration 7.8: Local stresses x-axis.....	92
Illustration 7.10: Prefabricated elements supported by props.....	94
Illustration 7.11: Basic control (critical) perimeter for corner support.....	96
Illustration 7.12: Rigid FRP strips [48].....	98
Illustration 7.13: Hand layup FRP laminates [48].....	98
Illustration 7.14: Model of the connection.....	99
Illustration 7.15: Indicative fibre properties given in JRC2016.....	100
Illustration 7.16: Indicative resin properties given in JRC2016.....	100
Illustration 7.17: Materials in DIANA model.....	102
Illustration 7.18: Connection-Deformations z-axis.....	102
Illustration 7.19: Connection-Stresses x-axis.....	102
Illustration 7.20: Connection-Stresses y-axis.....	103

# List of Tables

Table 4.1: Dead Loads.....	29
Table 4.2: Recommended values of $C_e$ for different topographies.....	30
Table 4.3: Geometric dimensions of slab.....	31
Table 4.4: Geometrical dimensions of Flat Slab.....	32
Table 4.5: Position of square columns in Slab1.....	33
Table 4.6: Bending moments of Slab1 per meter of strip Theoretical results.....	33
Table 4.7: Bending moments of Slab1 FEA results.....	34
Table 4.8: Deviation of FEA results from theoretical results.....	35
Table 4.9: Position of circular columns in Slab 2.....	36
Table 4.10: Bending moments of Slab 2 Theoretical results.....	37
Table 4.11: Bending moments of Slab 2 FEA results.....	38
Table 4.12: Percentages of deviation in Slab 2.....	38
Table 4.13: Resultant horizontal reaction forces of the arch .....	41
Table 4.14: Resultant horizontal reaction forces of the arch .....	41
Table 4.15: Angles $\alpha$ and $\beta$ of check points.....	42
Table 4.16: Internal forces of the arch for different load cases-FEA results.....	43
Table 4.17: Internal forces of the arch for different load cases-theoretical results.....	43
Table 4.18: Maximum bending moments in the arch.....	44
Table 4.19: Geometric dimensions of cylindrical shell roof.....	49
Table 4.20: Moment at midspan Cylindrical roof.....	49
Table 4.21: Maximum tensile force Cylindrical roof theoretical results.....	50
Table 4.22: Maximum unit shear at support of cylindrical roof theoretical results.....	50
Table 4.23: Moment at midspan Cylindrical roof FEA results.....	51
Table 4.24: Maximum tensile force Cylindrical roof FEA results.....	51
Table 4.25: Maximum unit shear force at support Cylindrical roof FEA results.....	51
Table 4.26: Bending moment Cylindrical roof FEA results.....	51
Table 4.27: Deviation between theoretical and FEA results Cylindrical roof.....	52
Table 4.28: Geometrical dimensions Side part-Dome.....	53
Table 5.1: Deviation of numerical and analytical calculation quantities.....	60
Table 5.2: Results of the analysis of the model due to its self-weight.....	61
Table 5.3: Snow load values.....	65
Table 5.4: External pressure on the shell.....	67
Table 5.5: ULS load combinations.....	68
Table 5.6: Applied load cases.....	69
Table 5.7: Results of applied load cases-Linear static analysis.....	71
Table 5.8: Results of analysis for different shell thickness.....	76
Table 7.1: Properties of C90/105.....	92
Table 7.2: Analysis results multiplied by amplification factor.....	94
Table 7.3: Element on props-Construction loads.....	96
Table 7.4: Element on props-Three prop supports per side.....	96
Table 7.5: Properties of FRP laminate.....	102

Table 7.6: Properties of the composite material (C90/105 and FRP).....	102
Table 7.7: Properties for "composite material" for the 2mm and 6mm FRP strip....	104
Table 7.8: Results of analysis of connected elements of 20mm thickness.....	105
Table 7.9: Mechanical properties of epoxy resin matrix HS CFRP .....	105
Table 7.10: Results of analysis of connected elements for element thickness of 40mm .....	106



# CHAPTER 1

## 1 Shell structures

### 1.1 Surface geometry

Shell structures are form-resistant structures that carry the applied loads primarily in membrane action, which means pure axial and shear action along their middle plane due to their curvature and continuity. Ideally, they resist loads in pure compression, although generally tension and shear do occur, accompanied by bending at the boundaries. Concrete shells are structures that exist quite regularly in our daily life.

From stadium roofs, to cooling towers and water tanks, shells are often employed as they provide two main advantages: aesthetic provisions of high quality and structural efficiency. The latter comes from the fact that shells are structures that support themselves and external loads using their geometry and particularly their continuity and curvature [1]. Shells are structurally continuous in the sense that they can transfer forces in all directions on the surface of the shell, as required. Moreover they have a different mode of action from skeletal structures, like trusses and frames, which are able to transfer forces only along their distinct structural members.

Curvature and particularly the Gaussian curvature which is defined as the product of the two main curvatures of a surface, can serve as a means of surface classification, useful for the description of shells. When the Gaussian curvature is positive, both curvatures point in the same direction, and the resulting surface is called synclastic. In the opposite case, where the Gaussian curvature is negative, the curvatures point in opposite directions and the surface is called anticlastic. When one of the curvatures is zero, a monoclastic surface with zero Gaussian curvature is received. In this case, the structure due to its geometry behaves as a vault, losing its ability of efficient load transfer. Zero Gaussian curvature comes out also as a result, when both curvatures are zero, in the case of a flat surface.

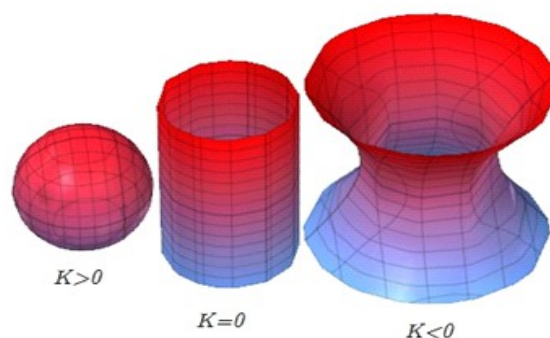


Illustration 1.1: Types of Gaussian curvature [2]

Surfaces are also classified in a continuous manner according to the way they are developed. Ruled surfaces are produced by sliding each end of a straight line on their own generating curve, while retaining the straight line parallel to a prescribed direction or plane. The generated straight line is not necessarily at right angles to the plane containing the generating director curves. Translational surfaces are generated by sliding a plane curve along another plane curve while retaining the orientation of the sliding constant. Finally surfaces of revolution are produced by the revolution of a plane curve, the meridional curve, about an axis, the axis of revolution.

A final distinction of surfaces is done between developable and non-developable surfaces. A surface is considered developable, when it can be flattened onto a plane without distortion (i.e. “stretching” or “compressing”). Conversely, they are surfaces that can be generated by transforming a plane by “folding”, “bending”, “cutting”[4], among other ways, characterized mathematically by zero curvature. Finally, in three dimensions, all developable surfaces are ruled surfaces but not vice versa. However, most smooth surfaces are non-developable surfaces. Non-developable surfaces are referred to as having “double curvature”, “compound curvature”, or “non-zero Gaussian curvature” Examples of these, are the sphere, the hyperbolic paraboloid and the hyperboloid.

## 1.2 Shells in Free-Form Architecture

The recent tendency to integrate calculations (analysis), design and production, driven by the possibility to exchange data between CAD software and FEM software [3] has led to the opening of new creative horizons in the architectural field. This gave the architects the ability to construct innovative and complex shapes and buildings of unprecedented sophisticated designs. All the above are features which distinguish free-form architecture. Free-form architecture is characterized by “a free-flowing expression that seeks to simultaneously reflect and reconcile the inevitability of a diversity of forces influencing any architectural design”[5]. With its flexibility and plasticity, free-form surfaces have to be rationalized with planar, single and double curved panels. This is where the idea of the flexible mould method for the production of curved concrete panels using a unique mould finds its application.



Illustration 1.2: Examples of free-form designs [54], [53]

A lot of knowledge has been developed to describe the mechanical behavior of geometrically regular curved surfaces like most shells are formed by, due to the fact that these surfaces can be described by simple analytical mathematical models [6]. For irregular curved surfaces however, like the ones that are employed by free-form architecture, very little analytical mathematical models exist, and the development of formulas is difficult in order to describe their mechanical behavior. As it was mentioned before, the Finite Element Analysis software, provide a partial solution to the problem, as they solely provide quantitative information about the results (like the magnitude of stresses and displacements), without any qualitative data and graphical and analytical methods have been developed for the analysis of the shell structural behaviour

### **1.3 State of Affairs**

The emergence of concrete shells dates back to antiquity, with the construction of the still standing Pantheon in Rome, which was completed about 125 CE [49]. Modern concrete shells, which began to appear in the 1920s, are made out of thin steel reinforced concrete, sometimes relying wholly on the shell structure itself [50]. In-plane casting is historically the most commonly used construction method in shell constructions. Large quantities of timber formwork supported by a dense wooden or steel scaffolding to keep curvature precise are put together by high quality carpenters, in a labor intensive procedure [51]. Traditional construction method of shells makes use of reinforcement bars, which are quickly placed but has the drawback of needing frequent joints and overlapping. Its bending and assembling is also considered difficult for curved shapes like shells.

Despite the structural advantage of monolithic shells transferring the loads very efficiently, and the economical design due to low thickness-to-span ratio, the cost that emerges during this production method, limits their prevalence in the building environment. The economy is of great importance, a term that intends to describe the design and construction of the best building at the least cost. Shells require a minimum of structural materials [15]. The quantity of concrete and reinforcement are factors that determine the cost. Formworks come next in importance determining what is possible to build and in certain cases representing up to 60% of the overall costs of concrete structures.

Different approaches are followed for the construction of modern shell structures. In each case, certain factors like the economy of the construction, the necessary durability of the shell and the ease of maintenance of the final structure led to different realization methods and characteristics of the final structure. Account of these aspects should be thus taken during the design and the execution of the project. There is no standard procedure and method that is currently in use. It is also noticed that in large significant projects, where the purpose is the

creation of a 'monument', economy could not dominate since the production of unique elements that freeform architecture requires are realized with the use of unique moulds.

Over the years attempts have been made to reduce the construction costs and ease the construction of shells, mainly on academic level. One of these attempts concerns the prefabrication of concrete elements. Prefabricating structures is a popular building method, where manufacturing takes place in a controlled environment, providing at the same time fast and simple erection on site. Prefabrication for shells means their segmentation in curved concrete panels, and their subsequent placement and connection at the building site. Benefits of this type of construction are the higher concrete quality that can be utilized, the higher building speed and the better logistic organization compared to in-situ cast concrete structures [42]. Substantial reduction of the costs is, however, not yet achieved for concrete shells, as the formwork is still very expensive and re-use of the form is only occasionally possible. Currently prefabricated panels applied for shell structures are produced with standard fixed formworks. The problem that arises is that for each different element a new form has to be made, and re-use of this form is almost impossible due to the specific geometry of each element.

Unless the use of flexible formwork is applied, no financial mitigation is possible. The original concept for the flexible mould is attributed to the ideas of Renzo Piano. That involved the placement of a scale model in a machine, where the height of certain points would be measured. The results would be transferred electronically to a system of vertical pistons, which will scale up the received measurements, and estimate the exact height. Subsequently, a mat would be placed on top of the pistons to create a mould. Most developments of the adjustable formwork are based on this idea. The formwork could adapt its shape, to the required geometry of each single panel comprising the shell. This concept is based on the principle of deformation of an originally flat sheet of any material into a double curved surface. More specifically deformation after casting was a concept formed by H.R.Schipper(2015) in his PhD study, which includes:

- filling of the flexible mould with self-compacting concrete
- waiting for a period of 30-60 minutes
- deforming the concrete element
- letting the deformed element harden for 24 hours and
- demoulding it.

The flexible mould method proposed by the same author offers a cost-efficient method for the manufacturing of elements with a reusable mould. Further research is recommended, addressing different aspects, with the quality and properties of connections being a very

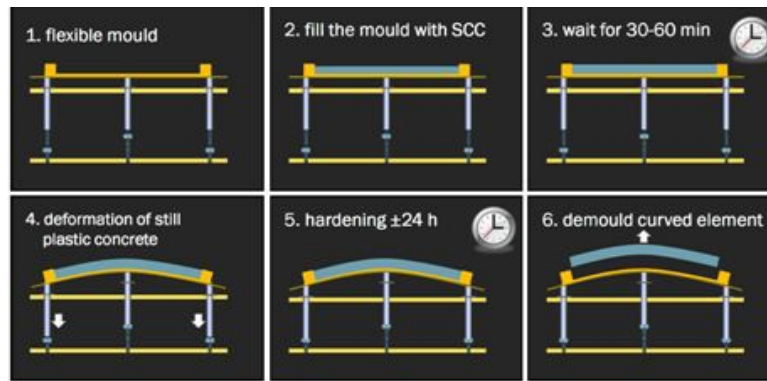


Illustration 1.3: Concept of deformation after casting [52]

crucial one, as loss of stiffness of the connections might lead to reduction of the buckling stability. For this reason shell stability shall be researched further and the properties of the required connections should be determined.

#### 1.4 Problem description and Scope

No shell construction technique, as it is organized and executed currently, provides a flawless, financially efficient, and effortless result. A comparison is considered wise to be carried out between the afore-mentioned shell construction methods, concerning their influence on the stability of a shell structure. There is a spectrum of aspects that have strong influence on the construction process and the economy of concrete shells. Traditional construction methods differ quite significantly from the method that adopts prefabricated elements and consequently the construction and design aspects involved differ significantly as well (e.g. different concrete and reinforcement type). Little implementation though, of flexible formwork prefabricated elements has taken place, and their structural behavior has not been fully researched. Thus further investigation should be conducted, examining whether a transition from a fully cast in-situ concrete shell to a prefabricated shell is feasible without jeopardizing the stability of the shell. Regarding the construction of the shells with prefabricated double curved elements, distinction can be made between complete prefabricated elements and thin curved elements topped with in-situ concrete. Research variables such as type of concrete, reinforcement, formwork and connections among others should be examined independently as factors that may influence dependent variables according to a principle of scientific research known as ‘*ceteris paribus*’. Their possible mutual dependencies should be examined as well.

This thesis intends to define whether the construction of the proposed shell structure of ‘Rijsoordse Molen’ is feasible using flexible mould prefabricated elements. In addition it will determine how these elements will be used and how the connection between them will affect the structural integrity of the shell. The current thesis will add to the research of the ‘flexible mould method’ by studying a practical application of the double-curved elements produced with the adjustable formwork. The structure should be optimized with regard to adre-

mentioned design and construction aspects, and a solution should be concluded that satisfies the set criteria, which are the following:

- the structure should satisfy the strength and stiffness requirements for shells.
- the construction and design of the structure should be cost-efficient
- the final design should not diverge greatly from the original design of the architect.

The structural behavior of the shell structure will be analyzed using a finite element analysis (FEM) program, Diana FEA. One reason for using this software, is that it has already been used in similar master thesis projects, providing consequently a continuation of the research and facilitating the comparison of results. It is, furthermore, equipped with powerful solvers that enable advanced analyses and is utilized by global engineering consultants and research institutions

# CHAPTER 2

## 2 Theory of shells

A lot of theories have been developed for the description of the mechanical behavior of shells. Among them, a well-known one is the membrane theory, in which it is assumed that the thickness of the shell is much smaller than the other two dimensions. For this reason its flexural rigidity is much smaller than its extensional rigidity [3]. Shells are thus structures that carry the applied loads with membrane action, this is in pure tension and compression along the middle of the shell thickness. However, bending action is also present, where the membrane theory does not hold, for example in regions where the extension of shells is prevented, like the supports. These disturbed zones, where the compatibility moments correct the thrust line of the structure will be described with the bending theory, which will be also addressed. It is considered wise to mention the principles of membrane theory, which deals with the extension of shells and the bending theory which describes the disturbed stress field of the shells. Initially the membrane theory will be explained, then a simplified method for deriving the membrane equation will follow for comparison. Finally, the bending theory will be mentioned.

### 2.1 Membrane theory of shells

#### KINEMATIC RELATION

The kinematic relation describes the relation between displacements and deformations. The deformation in the shell is only dependent on the translations of the middle surface, and since there is no bending, the rotations are not studied. For a shell of an arbitrary curvature, the kinematic equations are:

$$\varepsilon_{yy} = \frac{\partial u_x}{\partial x} + \frac{u_z}{r_x}$$

And in the y direction similarly

$$\varepsilon_{yy} = \frac{\partial u_y}{\partial y} + \frac{u_z}{r_y}$$

The curvatures already mentioned are:

$$k_x = 1/r_x \text{ and } k_y = 1/r_y$$

Additional shear rotation is necessary for a correct description of the surface deformation. The shell shear deformation is equal to the plate shear deformation:

$$\gamma_{xy} = \frac{\partial u_x}{\partial y} + \frac{\partial u_y}{\partial x}$$

From all the above the kinematic relation yields:

$$\begin{bmatrix} \epsilon_{xx} \\ \epsilon_{yy} \\ \gamma_{xy} \end{bmatrix} = \begin{bmatrix} \partial/\partial x & 0 & -kx \\ 0 & \partial/\partial y & -ky \\ \partial/\partial y & \partial/\partial x & 0 \end{bmatrix} \begin{bmatrix} u_x \\ u_y \\ u_z \end{bmatrix} \quad e = Bu$$

## CONSTITUTIVE RELATION

Without any bending, the stresses and strains are uniformly distributed over its thickness. Furthermore, it is assumed that the shell behaves according to Hooke's law. Thus the stress strain relation for the linear elastic shell is described by:

$$\begin{bmatrix} \sigma_{xx} \\ \sigma_{yy} \\ \sigma_{xy} \end{bmatrix} = \frac{E}{1-\nu^2} \begin{bmatrix} 1 & \nu & 0 \\ \nu & 1 & 0 \\ 0 & 0 & \frac{1-\nu}{2} \end{bmatrix} \begin{bmatrix} \epsilon_{xx} \\ \epsilon_{yy} \\ \gamma_{xy} \end{bmatrix}$$

The stress resultants can be determined from the strains by multiplication with the thickness  $t$ :

$$\begin{bmatrix} n_{xx} \\ n_{yy} \\ n_{xy} \end{bmatrix} = \frac{Et}{1-\nu^2} \begin{bmatrix} 1 & \nu & 0 \\ \nu & 1 & 0 \\ 0 & 0 & \frac{1-\nu}{2} \end{bmatrix} \begin{bmatrix} \epsilon_{xx} \\ \epsilon_{yy} \\ \gamma_{xy} \end{bmatrix} \quad s = De$$

## EQUILIBRIUM RELATIONS

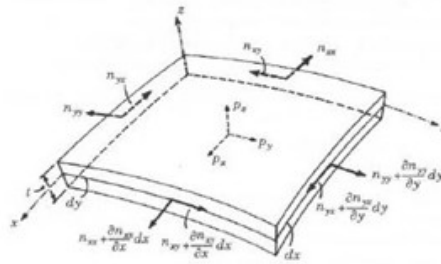


Illustration 2.1: Shell element membrane forces

Illustration 2.1 depicts the stress resultants and the load components on a shell element with dimensions  $dx$  and  $dy$ . The coordinates are placed in the direction of the principal curvatures.

Equilibrium in  $x$  and  $y$  direction gives:

$$-n_{xx} dy + n_{xx} dx + \frac{\partial n_{xx}}{\partial x} dx dy - n_{xy} dx + n_{xy} dy + \frac{\partial n_{yx}}{\partial y} dx dy + p_x dx dy = \frac{\partial n_{xx}}{\partial x} dx + \frac{\partial n_{yx}}{\partial y} dx + p_x dx = 0$$

and

$$-n_{yy} dx + n_{yy} dx + \frac{\partial n_{yy}}{\partial y} dx dy - n_{xy} dy + n_{xy} dy + \frac{\partial n_{yx}}{\partial y} dx dy + p_y dx dy = \frac{\partial n_{yy}}{\partial y} y + \frac{\partial n_{xy}}{\partial x} + p_y = 0$$

Equilibrium in the z-directions exists due to the curvature of the element:

$$k_x n_{xx} + k_y n_{yy} + p_z = 0$$

The equilibrium equation is obtained for a coordinate system placed in the principal direction

$$\begin{bmatrix} -\partial/\partial X & 0 & -\partial/\partial y \\ 0 & -\partial/\partial y & -\partial/\partial X \\ -k_x & -k_y & 0 \end{bmatrix} \begin{bmatrix} n_{xx} \\ n_{yy} \\ n_{xy} \end{bmatrix} = \begin{bmatrix} p_x \\ p_y \\ p_z \end{bmatrix} \quad \mathbf{B}^T \mathbf{s} = \mathbf{p}$$

For an arbitrary placed coordinate system, the previous relation becomes:

$$\begin{bmatrix} -\partial/\partial X & 0 & -\partial/\partial y \\ 0 & -\partial/\partial y & -\partial/\partial X \\ -k_x & -k_y & -2k_{xy} \end{bmatrix} \begin{bmatrix} n_{xx} \\ n_{yy} \\ n_{xy} \end{bmatrix} = \begin{bmatrix} p_x \\ p_y \\ p_z \end{bmatrix}$$

After the analysis of the membrane theory for thin shells, the membrane equation will be derived in a simplified way for a shell. For this reason, a flexible surface structure loaded with normal pressure is assumed. A surface element is shown. The element is cut along the principal curvatures, so that only axial forces resist the applied load. The curvatures along which forces act, are  $1/R_x$  and  $1/R_y$ . The edges of the free body are assumed to work as circular arcs, with curvatures constant along the edges. These arc lengths are:

$$a = \beta R_x \quad b = \alpha R_y$$

where  $\alpha$  and  $\beta$  are expressed in radians. The total pressure  $P$  is equal to:

$$P - pab = p(\beta R_x)(\alpha R_y)$$

The components of the membrane forces parallel to the resultant pressure  $P$  are:

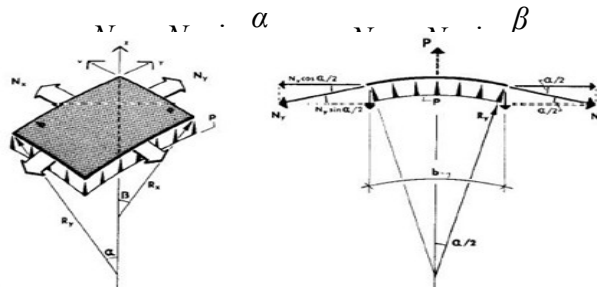


Illustration 2.2: Membrane free body

The resultant force  $P$  must be resisted by the sum of the vertical force components acting along the perimeter of the free body:

## 2.2 Bending theory

In regions where the membrane theory does not hold, due to edge disturbances, or for example in regions of zero Gaussian curvature, bending field components (compatibility moments) are required to compensate for the limitations of the membrane theory. This theory completes the description of the mechanical behavior of shells and will be briefly explained in the following paragraph. A premise is thus made for the shell in bending, that its behavior is described with a combination of the shell membrane theory and the bending theory of plates.

### KINEMATIC RELATION

The kinematic relation of describing a thin shell in bending is explained again, making use of a ring segment, This time though the kinematic relation for the ring segment in bending is found to be equal to:

$$\kappa_x = -d^2u_z/dx^2 \quad e = Bu$$

Combining the ring segment equations with y- direction and twisting curvature  $\rho_{xy}$ , the kinematic relation for a thin shell in bending is obtained:

$$\begin{bmatrix} \kappa_x \\ \kappa_y \\ \rho_{xy} \end{bmatrix} = \begin{bmatrix} -\frac{\partial^2}{\partial x^2} \\ -\frac{\partial^2}{\partial y^2} \\ -2\frac{\partial^2}{\partial x \partial y} \end{bmatrix} [u_z]$$

### CONSTITUTIVE RELATION

The constitutive relations between the curvatures and bending moments are described by the bending stiffness and a form for the lateral constraint [7]. The constitutive relation is:

$$\begin{bmatrix} m_{xx} \\ m_{yy} \\ m_{xy} \end{bmatrix} = \begin{bmatrix} D_b & \nu D_b & 0 \\ \nu D_b & D_b & 0 \\ 0 & 0 & D_b \left(\frac{1-\nu}{2}\right) \end{bmatrix} \begin{bmatrix} \kappa_{xx} \\ \kappa_{yy} \\ \rho_{xy} \end{bmatrix}$$

$D_b$  is the bending stiffness equal to  $\frac{Et^3}{12(1-\nu^2)}$

## EQUILIBRIUM RELATION

The equilibrium relations concerns the moments the out-of plane stresses and the external loads. The equilibrium is satisfied if:

$$\frac{\partial v_x}{\partial x} + \frac{\partial v_y}{\partial y} + p_z = 0$$

Equilibrium of moments in the x and y direction :

$$\frac{\partial m_{xx}}{\partial x} + \frac{\partial m_{yx}}{\partial y} - v_x = 0$$

$$\frac{\partial m_{yy}}{\partial y} + \frac{\partial m_{xy}}{\partial x} - v_y = 0$$

Thus, the equilibrium relation of a shell with membrane and bending action can be described as:

$$\begin{bmatrix} -\frac{\partial^2}{\partial x^2} \\ -\frac{\partial^2}{\partial y^2} \\ -2\frac{\partial^2}{\partial x \partial y} \end{bmatrix} \begin{bmatrix} m_{xx} \\ m_{yy} \\ m_{xy} \end{bmatrix} = [p_z] \quad B^T s = p$$

The combination of extension and bending gives the following relations:

## KINEMATIC RELATION

$$\begin{bmatrix} \epsilon_{xx} \\ \epsilon_{yy} \\ \gamma_{xy} \\ \kappa_{xx} \\ \kappa_{yy} \\ \rho_{xy} \end{bmatrix} = \begin{bmatrix} -\frac{\partial}{\partial x} & 0 & -\kappa_x \\ 0 & \frac{\partial}{\partial y} & -\kappa_y \\ \frac{\partial}{\partial y} & \frac{\partial}{\partial x} & -2\kappa_{xy} \\ 0 & 0 & -\frac{\partial^2}{\partial x^2} \\ 0 & 0 & -\frac{\partial^2}{\partial y^2} \\ 0 & 0 & -2\frac{\partial^2}{\partial x \partial y} \end{bmatrix} \begin{bmatrix} u_x \\ u_y \\ u_z \end{bmatrix}$$

## CONSTITUTIVE RELATION

$$\begin{bmatrix} n_{xx} \\ n_{yy} \\ n_{xy} \\ m_{xx} \\ m_{yy} \\ m_{my} \end{bmatrix} = \begin{bmatrix} D_m & \nu D_m & 0 & 0 & 0 & 0 \\ \nu D_m & D_m & 0 & 0 & 0 & 0 \\ 0 & 0 & D_b \left(\frac{1-\nu}{2}\right) & 0 & 0 & 0 \\ 0 & 0 & 0 & D_b & \nu D_b & 0 \\ 0 & 0 & 0 & \nu D_b & D_b & 0 \\ 0 & 0 & 0 & 0 & 0 & D_b \left(\frac{1-\nu}{2}\right) \end{bmatrix} \begin{bmatrix} \varepsilon_{xx} \\ \varepsilon_{yy} \\ \gamma_{xy} \\ \kappa_{xx} \\ \kappa_{yy} \\ \rho_{xy} \end{bmatrix}$$

with  $D_m = \frac{Et}{12(1-\nu)}$  and  $D_b = \frac{Et^3}{12(1-\nu^2)}$

Finally, the equilibrium relation

$$\begin{bmatrix} -\frac{\partial}{\partial x} & 0 & \frac{\partial}{\partial y} & 0 & 0_b & 0 \\ 0 & -\frac{\partial}{\partial y} & -\frac{\partial}{\partial x} & 0 & 0 & 0 \\ -k_x & -k_y & -2k_{xy} & -\frac{\partial^2}{\partial x^2} & -\frac{\partial^2}{\partial y^2} & -2\frac{\partial^2}{\partial x \partial y} \end{bmatrix} \begin{bmatrix} x \\ n_{yy} \\ n_{xy} \\ m_{xx} \\ m_{yy} \\ m_{my} \end{bmatrix} = \begin{bmatrix} p_x \\ p_y \\ p_z \end{bmatrix}$$

# CHAPTER 3

## 3 Formwork types for concrete shells

### 3.1 Introduction

In order to realize the reasons for the high costs raised during concrete shell construction, a description will follow of the current practices and methods. Traditionally the main ways of constructing concrete shells are:

- Concreting over timber formwork
- Pneumatic formwork
- Ground mounding (Earth mould)
- Polyurethane foam formwork
- Raised steel skeleton method
- 3D-printing (will be included in prefabrication)
- Prefabricated elements, which will be analysed separately

Out of these methods, in-situ casting on timber formwork is applied in most cases and has been proved to provide high quality structural result, and that is because traditionally timber formwork have often been associated with concrete structures [8]. This method was extensively utilized by two famous shell architects of the 20th century, Felix Candela (1910-1997) and Heinz Isler (1926-2009). By using ruled surfaces, Candela achieved to simplify formwork, as this meant that his double curved surfaces (hyperbolic paraboloids, conoids, hyperboloids, cylinders and cones) could be constructed from straight board formwork, fulfilling moreover the idea of reusability, which otherwise would increase the costs. Isler's concrete shells were constructed by casting concrete onto a grid of prepared timber beams, acting as falsework. The beams were arranged radially or parallel, and should be adjusted to the right height and position by means of a complicated scaffolding system, which has to withstand deflections and loads [9].

The falsework structure should consequently be lowered in order to allow the removal of the formwork, which were fixed on it, at centres of approximately 25cm in the form of timber skeleton boarding. The actual shell membrane would be positioned on the top of the boarding, concrete would be then laid on the timber membrane, forming the shell itself (Illustration 3.1). When the weather conditions called for thermal insulation, Isler used insulation panels as permanent shuttering, in the desired form, which acted as lost formwork.

The insulation would be anchored with suitable fixings to the cast concrete. Important factor in the construction of Isler shells were moreover the concrete as a material.



Illustration 3.1: Shapes, formwork and skeleton shuttering[9]

And the concreting process itself. Concrete for Isler offered its plasticity and its flexibility in form-shaping, crucial characteristics for the construction of shells. Isler shells were cast in slopes of up to  $45^\circ$  [9]. The concreting process would be adjusted to the specific conditions of each construction. A usual method involved pouring concrete from a crane, or pumped concrete spraying procedures.

### 3.2 Description of the problem with timber formwork

The structural quality of the final shell result provided by the timber formwork causes no frustration, as the structure is stable and efficient enough to carry the applied loads. The “problem” concerns the apparent impracticality of the accepted construction of concrete shells [9]. For the construction of shell, a timber shell, has to proceed, as it was described above. In contrast with the concrete, the timber needs coaxing in order to adapt to varying cross sections. Adding the cost of timber, the time spent in design and construction, the labor costs, and realizing the impossibility of reuse, the costs appear to be unjustifiable and unbearable.



Illustration 3.2: Examples of elaborated timber formwork for concrete shells[9], [25]

In order to reduce the formwork costs, other materials have been proposed that could be utilized for the same purpose and with the same function. Cardboard and steel reduce the

formwork costs, and particularly the later offers reusability. Nonetheless, the need to construct an overpriced framework that does not form a part of the final structure is present.

### 3.3 Pneumatic inflated formwork

The 1940s saw the developments of pneumatic formwork, as a way of reducing the construction costs and building speed of concrete shells. In the works of Frei Otto there are extensive descriptions of the use of pneumatic formwork. Different alternatives exist concerning their application.

One of them proposes the use of elastic neoprene membranes that when inflated become the mould on which the casting of concrete will happen. Initially, the membrane is spread flat across the ground covering the area within the foundation [9]. The reinforcement is subsequently placed on the membrane, the first layer of concrete is casted, mixed with hardening retardant substances. Following this, a second membrane is set on top of the concrete layer. The edges of the membranes are fixed on the footings and the bottom membrane is inflated. The top membrane keeps the concrete in place. Once the hardening procedure is completed, the membrane is removed. Waterproofing layer is finally applied. An alternative of this procedure consists of inflating a membrane covered with freshly mixed concrete (Illustration 3.3).



Illustration 3.3: The plane concrete plate is produced and the membrane is inflated [10]

Another option suggests the fabrication of a double curved shell structure built from a flat circular shell made of concrete and a soft Styrofoam component between the concrete segments, which allows the deformation of the flat plate [11]. This method is particularly intended for the construction of domes based on the principle that a doubly curved surface is a non-developable surface. Thus, the flat plate from which the final shell will emerge, has to consist of these elements of the distorted flat plate. These are placed on a planar working surface and are subsequently assembled by tendons, both in the radial direction holding the elements together, as well as in the circumferential direction carrying the hoop forces after the removal of the pneumatic formwork. In order for the flat plate to get transformed into a double curved shell, pneumatic formworks are used, which are inflated and realize the final

shape. The gaps between the elements are grouted and post-tensioned. PVC membrane is used for the fabrication of the formwork and PVC glue glues parts of this membrane in order to obtain the required formwork shape. Nowadays, the use of pneumatic formwork is restricted to the fabrication of synclastic surfaces and particularly domes. Another issue that appears with the use of this formwork is the deflections that emerge during the curing process and the associated weakening of the concrete.

### 3.4 Earth moulds

The use of soil for creating moulds for shell structures, particularly for domes, has been applied in a few cases. The use of soil for this reason is firstly justified by its abundance as a natural material. In addition, soil contains natural binders which permit the soil to maintain a formed shape. Furthermore, its workability allows for more accurate shaping and moulding, than what is the case with timber. Initially the foundations are constructed around the periphery of the dome, with its type varying on the design characteristics of the dome to be built. Following this, a huge mound of soil is constructed, which forms the mould on which concrete will be cast.



Illustration 3.4: Forming soil mould for concrete shell [8]

Compaction of the soil is of ultimate importance, as the earth mound should be able to withstand the weight of the wet concrete. Before the casting of the concrete, sandblasting may be required to provide a smooth interior surface. In a different case, a thin layer of concrete is first cast, on top of which wax is applied, so as to provide the same result. The reinforcement is subsequently placed, and the concrete is sprayed in patterns of ascending rings around the mould. An important issue is the removal of the soil from the interior of the casted dome. The excavation should start strictly from the centre in order to ensure dome action and to prevent the collapse of the structure

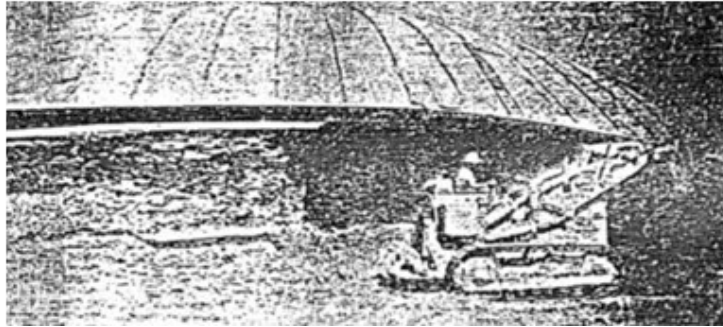


Illustration 3.5: Excavation of mould through archways [8]

The aforementioned technique can be realized either by constructing the dome around the mould at its final elevation, or the dome is initially cast on the ground, and then lifted up to its final elevation in the case of dome roofs [8]. The earth mould should be able to support the weight of the cast concrete, and for this reason proper soil compaction is essential.

### 3.5 Polyurethane foam formwork

An alternative to the case of timber formwork is the method that employs polyurethane foam formwork, instead of a plywood membrane, on which the concrete is cast. Polyurethane is a fluid in its original state, but hardens quite rapidly [8]. It can be adjusted in any configuration but at the same time is capable of supporting

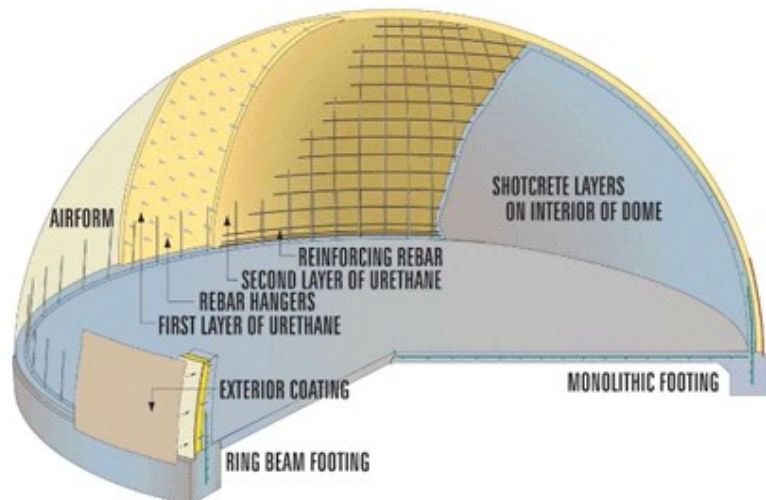


Illustration 3.6: Double polyurethane foam formwork for concrete shells [23]

The technique that makes use of these formworks proceeds in the following way:

- Inflate the shell membrane
- Spray the polyurethane foam on the inner surface
- Place reinforcement bars
- Cut out section of framed structure not in design
- Spray shotcrete
- Install openings[8]

The polyurethane formwork serves this way first as a formwork for the structure, and then it gets integrated in the construction, functioning as thermal and sound insulation reducing substantially the construction costs.

### 3.6 Raised steel skeleton method

The method of the raised steel skeleton, proposed by Sylwester Oleszki and Zbigniew Parzniewski [8], replaces the traditional timber formwork with reinforcing steel bars. This method was mainly utilized for domes and it will be briefly explained through a dome construction. A mast is raised at the centre of the dome, stabilized by guy wires and temporarily concreted after the foundation has been laid down. Reinforcing steel bars and wires are placed on the ground within the foundation [8]. The bars are linked together with sufficient flexibility and the steel structure is subsequently lifted by a movable crane.

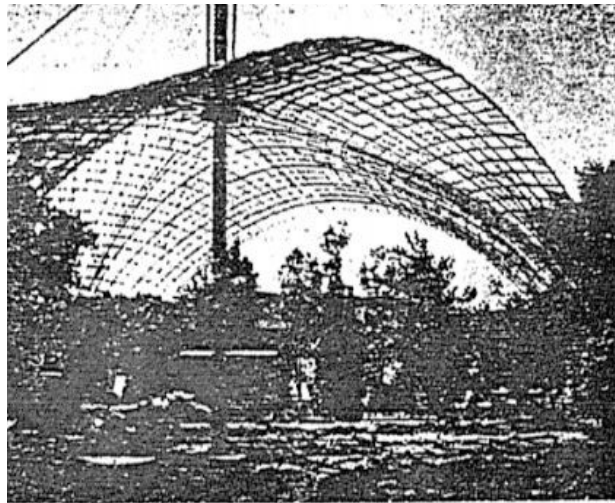


Illustration 3.7: Central mast and steel rebars [8]

The supports that have been added like the central mast are removed, the supporting bases are concreted and the skeleton is sprayed with shotcrete.

### 3.7 3D-Printing

An on-going promising high-tech technique which offers the advantages of faster construction, no need for formwork, decreased labor costs and increased allowable complexity and accuracy in the construction industry is 3D-printing. This method furthermore allows for structural customization, as it does not require that every structural element of a building be identical, for matters of costs or speed. Despite the obvious benefits of this method and the pioneering activities of some companies on this field, the building industry is still behind in the development of 3D concrete printing, mainly due to lack of research on the structural behavior of the materials to be used and the shape of the structures to be printed. 3D-Printing includes the on-site or off-site fabrication of buildings

or building components using industrial robots, gantry systems and tethered autonomous vehicles [12]. The method facilitates the production of new shapes, configurations and layouts that are more sustainable, since concrete is specifically placed where it is required, escaping from the need of solid and massive constructions.

The three most dominant printing techniques will be briefly mentioned. *Contour crafting*, one of the oldest still existing techniques, is a method that employs layered manufacturing making use of different materials (cement, ceramic slurry, polymer) to build large scale object with smooth surface finish [13]. *Concrete printing*, has a similar extrusion based construction method with contour crafting, but a smaller resolution of deposition allowing for greater printing freedom with more complex shapes [13]. Finally, the *D-Shape*, a printing process developed by Enrico Dini, makes use powder deposition and more specifically loose bed of sand layers selectively hardened by locally applying a binder material [13].

As far as shells are concerned, their construction using this technique might be considered to have limits. The reason is that concrete printing can only occur on previously printed concrete layers until an overhang of  $45^\circ$ , since after this angle supports are needed. Another issue that also emerges in printing architectural concrete is the unevenness of the final surface due to the very coarse concrete printing [14]. In smaller scale applications this issue did not exist, and higher printing accuracy was achieved.

### **3.8 Prefabricated concrete elements**

Apart from the high aesthetic quality provided by the shells, these structures offer the possibility of “covering an area with the least amount of material” [15]. Although this idea comprises the main core of shell structures, it was and still is regularly sidelined. After the flowering in concrete shell construction in the mids of the past century by great shell architects like Isler, Torroja, Candela and Nervi, a stale period followed. The construction of concrete shells became costly immoderate with reference to the principles governing this structural form and the “construction boom” ended. The traditional construction method made use of rigid timber formwork on top of which thin wooden boards were bent, which would host the reinforcement and the concrete casted on-site. This time consuming construction technique was feasible and cost-effective under the condition that the labor costs will be relatively lower than the material costs. At that moment, this relation was inverted, causing the aforementioned stagnation [16]. This evolution in the construction industry led to the shell construction method of prefabricated elements, combined with the intrinsic advantages of this method, which are:

- concrete of better quality is produced, as the manufacturing conditions are under control in a factory environment
- complex shapes can be realized with high accuracy levels
- the prefabricated structure can be disassembled and the elements be suitably used elsewhere
- higher construction speed is achieved than cast in-situ concrete
- the labour needed for the construction of the prefabricated elements can easily be trained
- weather is excluded as an influencing factor on the building process
- particularly for the case of shell structures, the quantity of the required falsework and scaffolding is substantially reduced
- better logistic organization than cast in-situ concrete

Over the past decade though, extensive progress has been realized in digitizing design and fabrication processes, enabling the analysis of complex geometries under consideration of multiple boundary conditions [16]. Developments in computation, storage, handling and cross-linking of digital information, allow for the integration to one process of activities starting from planning until the fabrication of the structure, due to the possibility of exchanging data between CAD-program (Computer Aided Design) and FEM-program (Finite Element Analysis). Further improvements have also occurred in the sector of material science, particularly on cementitious materials leading to composite materials with high tensile and bending tensile strength.

The technological progress mentioned before led architects and followingly engineers to the design and construction of complex shapes and configurations like the ones employed by free-form architecture, which behave like shells. This means that their structural behavior consists mainly of extensional forces and some bending moments due to edge disturbances. On the other hand, scientists try to rationalise the large-scale intricate surfaces with planar, single, double- curved panels. The construction of these panels entails the fabrication of unique moulds, singly used in most cases. The purpose of the adjustable formwork lies exactly on the point of reducing the mould fabrication, since this is what governs the panel cost.

### **3.9 Moulds for prefabricated concrete elements-Methods of construction**

#### *3.9.1 Timber moulds*

Apart from their use in cast in-situ shell construction, timber formworks are used for the fabrication of concrete panels. As an example, a case study where implementation of timber formwork for the construction of prefabricated concrete panels took place, will be mentioned.

This case study concerns the construction of the Rolex Learning Centre in Lausanne, where formwork tables of 2.50 x 5.50 m were constructed in factory by labor [17]. CNC-milling was also used for the fabrication of timber formwork. Each table consisted of two beams on which OSB plates were fixed. On top these plates, the final formwork on which the concrete would be cast were placed, consisting of 10cm wide wooden planks and a laminated chipboard nailed on these plates[17]. This final surface testified the final curves of the shell. Reusability of these moulds could be feasible by disassembling the formworks. When proper surface protection is provided, the moulds are reusable, but their lack of flexibility does not permit the use for different shapes [14].

### 3.9.2 *Steel moulds*

Steel moulds have been quite regularly utilised for the production of ceiling and wall panels or for entire structural parts like beams and supports, providing high accuracy in complex designs. Their resistance to wear allows for a high degree of repetition, compensating for their high costs [18]. However for curved elements, steel moulds are much less frequently employed. A prominent example, where fabrication of concrete elements by steel moulds took place is the Jubilee church in Rome. Known as La Chiesa del Dio Padre Misericordioso in Italian, this church was a part of pope John Paul II's millennium initiative to rejuvenate parish life in Italy [19]. It was inaugurated in 2003, and it is American architect's Richard Meier's



Illustration 3.8: Jubilee Church, Rome [19]

first church. The most distinctive feature of the church is the three curved shells walls that reach a height of 27,5 m above the building, made from prefabricated concrete elements with a marble-like finish, reinforced with steel and held together by post-tensioned cables

#### 3.9.2.1 Hoto Fudo

Hoto Fudo is restaurant located at the foot of Mt Fuji, in Japan, distinctive for its four continuous hemispheres symbolising the “soft clouds surrounding the mountain's summit” [21].



Illustration 3.9: Hoto Fudo with Mt. Fuji in the background [20]

In order to satisfy the local requirements regarding climate heavy snow and seismic activity special reinforced concrete sandwich shell was proposed, consisting of the main RC structure, sandwiched between a 60 mm hard urethane layer for heat insulation and other 15 mm glass fibre reinforced concrete for crack prevention.

In order to reduce the complexity of the formwork for the shell, a “truss wall system prefabricated formwork” method [22] was adopted, and 200 units of 3D formed rebar truss were transported on-site reducing the construction period and the complexity of the on-site formwork.

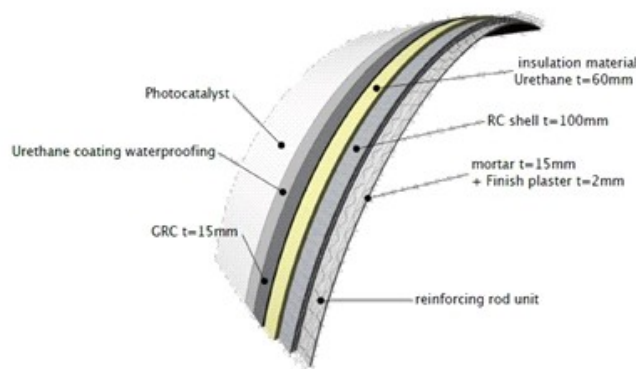


Illustration 3.10: Cross-section of Hoto Fudo shell [22]

### 3.9.3 Textile formwork

Textile membranes are widely used as tent structures and shelters. Last years however, these materials find implementation as a form of flexible formwork for the construction of shell structures, an idea that was first proposed by Prof. West at the CAST laboratory of the University of Manitoba [24]. However, other scholars have to be mentioned, like Kenzo Unno in Japan where he developed different methods for the optimization of the practical use of cast-in-place fabric-formed concrete walls. This method, starts as any other shell construction process with the modeling of the shell, in order for the textile to be cut in proper shapes and for the required formwork pretension to be defined.



Text 1: Fabric formwork and the resulting panel [24],

The pieces of the cutting pattern are, depending on the type of the fabric and the coating type, stitched or welded. Subsequently a minimum pretension-to guarantee the shape is applied. Fabric pretensioning is of crucial importance for the proper functioning of the formwork [24]. A first reason is that only certain amount of tension can be carried by the fabric. On the other hand, certain amount of pretensioning is necessary in order to account for the deformation of the fabric formwork after the casting of the concrete. Shotcrete is then sprayed on the formwork in several layers up to a certain thickness. Care should be taken of the displacement of the formwork after concreting. Some advantages of this method are the following:

- the installation of fabric formwork requires less manual labour and reduced material, storage and transportation costs
- the freedom in shape that it provides and the possibility of modifying the shape fast and easily
- design optimization is feasible as, design aspects can accommodate certain structural requirements through the shape flexibility.

Nonetheless, this technique seems to be in its infancy, as only research projects have been realized in an academic level, and further trust on the method should be gained.

#### 3.9.3.1 Palazetto dello Sport

With a seating capacity of 33,500, this indoor basketball arena was engineered by Pier Luigi Nervi for the 1960 Rome Olympic Games. The innovative ribbed dome consists of prefabricated Y-shaped ferrocement elements filled with cast-in-situ concrete, with a construction period of approximately 40 days.

The forces leading outward from the roof are picked up by Y-shaped buttresses that encircle the perimeter of the building. The prefabrication of the elements of the roof, was Nervi's tool to deal with the simultaneous construction of four important projects. More analytically,



Illustration 3.11: Ribbed roof -Palazzetto dello Sport [26]

Nervi's work on the prefabrication of concrete elements is found in the part of development of adjustable formwork.

### 3.9.3.2 *Spencer Dock Bridge*

With a length of 40 m, this bridge connects the Dublin city centre to the north docklands redevelopment area [28]. Double-curved prefabricated elements functioning as bridge parapets were constructed on-site using a Filcor Expanded Polystyrene (EPS) moulds covered with an epoxy resin and fiberglass to provide the necessary smooth texture [28]. A timber and plywood frame was supporting the moulds, that had been machined specifically for the project.

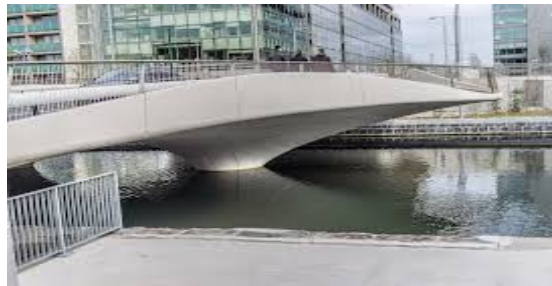


Illustration 3.12: Spencer Dock Bridge-Double-curved parapets [27]

# CHAPTER 4

## 4 Analysis of Approximating Structural Forms

### 4.1 Introduction

The 'Bezoekerscentrum Waalbos' will be the shell structure on which the application of the elements will be examined. The support conditions and the geometry of the structure do not qualify it strictly as a shell. As it can be seen from the picture, the shell-like roof covering is supported on columns. This cancels the shell function, as shells are self-supporting structures, which carry the applied loads through walls, edge beams or foundations.

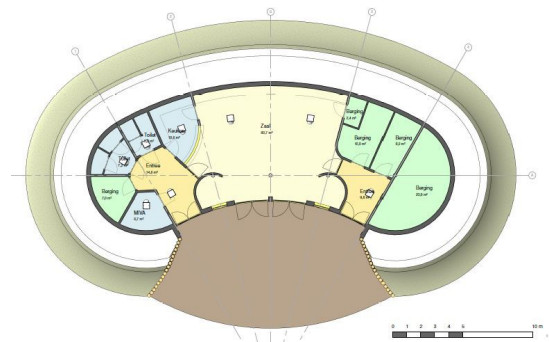


Illustration 4.1 Plan view of the structure [28]

The analysis of the complex geometry of the design case shell requires first an analysis of the force flow in structural forms that can approximate its structural behavior. Furthermore, in order to verify the Finite Element Analysis outcomes, a comparison will be carried out between the results of hand calculations of the analysis of the approximating structural forms and the ones obtained from the FEA software. This will also aid to determine which structural form simulates the design case structure the best and which modifications are necessary in order for the structure to behave as a shell. The main goals of this analysis are:

- Understanding the load transfer mechanism on the current design
- Getting familiar with the FEA software, as prior knowledge of the software did not exist
- Analyse the central part of the structure as this probably governs the thickness of the whole structure due to its geometry and supporting conditions
- Verifying the FEA software
-

The design case structure (“Bezoekerscentrum Waalbos”) proposed by Pr. Schipper with the permission of the architect, cannot be characterized as a pure shell according to its original design. This can be made obvious by the existence of supporting columns throughout the whole structure. The provided dimensions and curvatures moreover, led to the same conclusion. The scope thus, is to describe to what extent, the structure can be characterized as a shell, and what changes or improvements would be necessary for this characterization. From the above, it is clear that a first simulation of the structure as a shell is absolutely vital. The small curvature of the central part of the structure motivated the simulation of the roof as a point-supported flat slab, cantilevering on both sides. Furthermore, due to its form and the previously stated features (supporting conditions, geometry) regarding the central part of the building, the structure will be analysed also as an arch. Again, in order to proceed to this characterization, support conditions should be redefined or in a different case added to the original design. Finally, since the central part of the structure resembles to a cylinder, an approximation of the roof as a cylindrical shell roof will also take place.

Each of this three simulations will be executed, considering the required changes to the design, and the degree to which these changes influence the original design. After the verification of the software and the approximation process, the structure as a whole should be analysed. The remaining parts of the structure (side parts) will be first analysed, as only light modifications of their designs are necessary in order to consider them shell structures. The analysis of the whole structure itself will follow.

## **4.2 Verification process**

Verification refers to the method in which it is checked whether the FEA was conducted properly, whereas validation is the process in which we check whether the FEA results reflect the reality. The following simplification for the two terms is given as:

- Verification is how we see if we have solved the problem correctly
- Validation is how we see if we solved the correct problem

In the verification process the concern is to identify and remove errors from the model by comparing numerical calculations with analytical solutions. And that is exactly what will be conducted in this chapter [30].

In numerical problems and especially in FEA where the real world problems are solved, satisfying or even exactly formulating and developing the numerical scheme is often impossible and various types of assumptions are made and approximations are carried out [31]. Small errors in modeling and data input may have great impact on the performance and service life of the structure. Errors are inevitable in finite element models, and the more

complex the model, that higher the chance the they will occur. The important thing is to put a process in place to detect them before any damage occurs. The analysis must begin with clearly defined goals, accuracy requirements and key assumptions. Some typical items that this process has to contain are:

- Do key model dimensions agree with actual dimensions?
- Are the material properties correct and are they associated properly to model elements?
- Are the elements properly connected with interface elements?
- Is the mesh sufficiently refined to provide the required accuracy? Are the element formulations consistent with the application?
- Are the elements properties correct and are they associated properly to model elements?
- Does the self-weight produce the expected reaction forces as first indicator?
- Do the reaction forces balance the applied loads in each direction?
- Are the deformations and stresses realistic, and are they compared with hand calculations?

Most of these questions have been intrinsically set and answered in this chapter in order to execute the verification process. More analytically, the results are presented in the following paragraphs.

### **4.3 Loads**

Before proceeding to the analysis of the structure, the acting loads should be determined. Different load combinations will be examined, as it is not known in advance which load case will challenge the structure. The applied loads are categorised into groups of permanent, variable, accidental and time-dependent. Time dependent loads such as creep, shrinkage and temperature gradients are not considered for simplification reasons, although their effect on the structure might be severe. The same is valid for the accidental loads, since the purpose of the analysis of this chapter is restricted to preliminary design.

#### *4.3.1 Permanent loads*

The permanent loads for the construction consist of the dead weight of the structure, and additional weight produced by possible finishing, such as insulation or cladding. However, it is assumed that the shell does not contain any finishing, thus the extra covering load is not taken into account. The dead weight is calculated by multiplying the shell thickness with the

specific weight of concrete, for which a value of 2500 kg/m<sup>3</sup> is assumed. For the design case building though and according to the designs provided by the foundation, a soil covering is placed on top of the roof. Since no information is provided for the soil layer thickness, a uniform thickness of 0,2 m is assumed. In the same way, the soil weight is calculated, making use of soil specific weight of 15 kN/m<sup>3</sup>, as this value represents the unit weight of various soil types, like sandy loam soils, loam soils, and clay loam soils [32].

Type of Load	Load magnitude (kN/m <sup>2</sup> )
Self-weight	2,5
Soil load	3

Table 4.1: Dead Loads

### 4.3.2 Variable loads

According to EN 1991-1-1 a live load  $q_k$  may be selected within the range of 0,0 to 1,0 kN/m<sup>2</sup> and a point load  $Q_k$  value ranging from 0,9 to 1,5 kN. The recommended values are  $q_k = 0,4$  kN/m<sup>2</sup> and  $Q_k = 1$  kN. For reasons that will be explained later, a uniform distributed live load of 1,0 kN/m<sup>2</sup> is assumed for the construction.

#### 4.3.2.1 Snow load

To begin with, snow load is assumed to act vertically and refers to the horizontal projection of the roof.

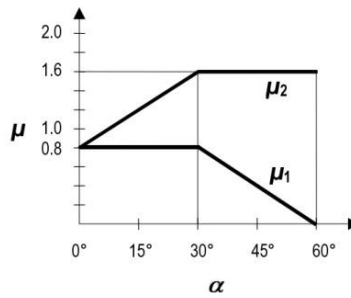
The calculation of the snow load on ground should proceed the calculation of the snow load on the roof. This reference value depends on the geographical location and the altitude of the building. EN1991-1-3 Annex C provides the characteristic values for the snow load on ground for European countries. For the location of Waalbos, a value of 0,4 kN/m<sup>2</sup> is taken from figure C.7 ( EN1991-1-3 Annex C).

The snow load on the roof surface is given by :

$$s = \mu_i * C_e * C_t * s_k$$

where  $\mu_i$  is the roof shape coefficient,  $C_e$  the exposure coefficient,  $C_t$  the thermal coefficient, and  $s_k$  the characteristic value of snow load at the ground.

The snow load shape coefficient depends on the shape of the roof. For monopitch roofs as it is the case for the central part of the design case building, the shape coefficient is given from Drawing 1, from which  $\mu = 0,8$ .



Drawing 1: Snow load shape coefficients monopitch roofs

$C_t$  is equal to 1 for normal situations, and  $C_e$  is obtained from Table 4.2 equal to 0,8 for windswept topographies.

Topography	$C_e$
Windswept <sup>a</sup>	0,8
Normal <sup>b</sup>	1,0
Sheltered <sup>c</sup>	1,2

<sup>a</sup> *Windswept topography*: flat unobstructed areas exposed on all sides without, or little shelter afforded by terrain, higher construction works or trees.  
<sup>b</sup> *Normal topography*: areas where there is no significant removal of snow by wind on construction work, because of terrain, other construction works or trees.  
<sup>c</sup> *Sheltered topography*: areas in which the construction work being considered is considerably lower than the surrounding terrain or surrounded by high trees and/or surrounded by higher construction works.

Table 4.2: Recommended values of  $C_e$  for different topographies

Thus, the resulting snow load for the case of a flat roof is equal to 0,256 kN/m<sup>2</sup>. The same value is also assumed for the cylindrical roof, for preliminary design purposes. Due to the small magnitude of snow load, this will not be taken separately into account, as the live load has already been increased to a value of 1,0 kN/m<sup>2</sup>.

#### 4.3.2.2 Wind load

As far as the wind load is concerned, no account of it is taken for the preliminary design of the approximating forms. However, during the analysis of the structure it will be examined and included as a variable load. Specifically for the case of the arch and for preliminary design purposes, wind loads may be neglected if the height-to-span ratio is  $h/L \leq 1/3$  [35].

### 4.4 Flat Slab

The idea of approximating the structure and particularly its central part with a slab, came up by examining the geometry of the structure, when during the analysis, it became obvious that the curvature of this part was small enough to consider it flat ( $\kappa=0,091$ ).

Another reason emerged when the final designs were published on the website of the foundation. The original shell structural form had been replaced by a shell-looking slab, supported by columns of unknown dimensions. The slab dimensions can be seen in Table 4.3. The support conditions should be examined, as these influence the load distribution and the

required thickness of the slab. Totally, this part is supported by five columns, two square columns at the rear part of the structure, and three circular ones at the front side. The originally assumed dimensions of the columns were chosen empirically, so as to support the applied loads.

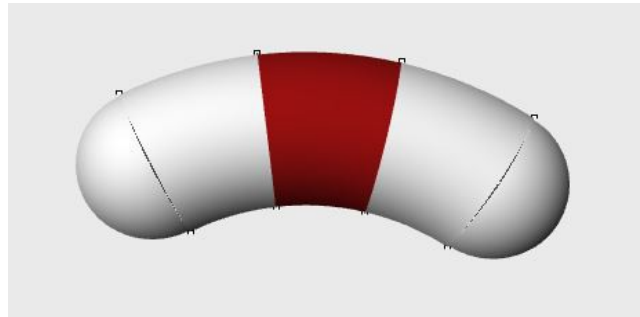


Illustration 4.2: Part of structure considered as a slab

Geometry Central Part	Dimensions
Maximum span x-direction	13,9 m
Minimum span x-direction	8,9 m
Span y-direction	10,0 m
Thickness	11,4 m
Radius of curvature	0,28 m
$l_{av}/t$	28

Table 4.3: Geometric dimensions of slab

#### 4.4.1 Description of flat slab behaviour

Whereas conventional slabs are supported by beams that extend along their edges, flat slabs simply rest on columns, on which they transfer the applied loads. In order to support heavy loads, the thickness of the slab is increased in regions close to the column supports, creating the so-called drops. In a different case, columns are provided with enlarged heads, called column heads or capitals. The absence of beams offers a flat soffit, providing higher aesthetic quality and additional fire resistance. Further advantages of a flat ceiling include the reduction in formwork costs, the simplicity of the construction and the more effective light diffuse.

For two-way single flat slab, a span to depth ration of 28 [33] is chosen as a thumb rule, through which the thickness of the slab is estimated. Table 4.4 shows the dimensions of the assumed flat slab.

Geometry Flat Slab	Dimensions
Span x-direction	11,4 m
Span-y direction	10 m
Thickness	0,28 m

Table 4.4: Geometrical dimensions of Flat Slab

#### 4.4.2 Load Combinations

During the preliminary design of the structure and the verification of the design, certain load cases were chosen. For the slab, three load cases are examined. For a rapid and straightforward comparison of results, the self-weight is only applied to the structure without load factors. For the ultimate limit state design (ULS), the second load combination includes the self-weight multiplied by a load factor of 1,35 the soil load multiplied by the same factor, and the live load by 1,5. Finally a serviceability limit state design case is applied on the slab with all the action load multiplied by a factor of 1,0.

#### 4.4.3 Analysis of results-Comparison

In order to verify the outcome of the FEA software, a comparison will be executed between the bending moments of the slab. First, the theoretical calculations will be presented, followed by the finite element analysis results. Finally, a comparison will take place, and conclusions will be drawn.

##### 4.4.3.1 Theoretical results

Due to the position of the columns provided by the designs of the building, only horizontal alignment of them is feasible. For this reason and in order to facilitate the hand calculations, the flat slab will be examined and analysed as two separate slabs. The first slab (Slab 1) will contain the two square columns and the second slab (Slab 2) the three circular ones. Each slab will have a length of 11,4 in the x-direction, and a length of 5 m the y-direction.

#### **Slab 1**

Slab 1 (Illustration 4.3) is supported by two square columns at a distance of 7 m from each other. The position of the columns can be seen in the Table 4.5. The bottom left corner of this slab is considered the beginning of the axes. The bending moments were established as a first comparison criterion for the slabs.

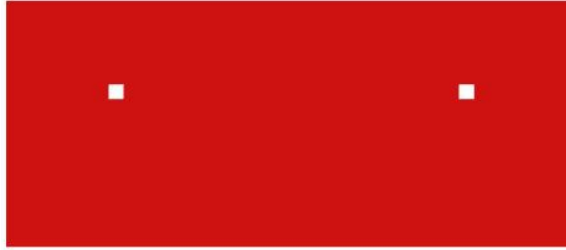


Illustration 4.3: Slab 1

Column	Position x-direction	Position y-direction
SQ1	2,05	2,85
SQ2	9,05	2,85

Table 4.5: Position of square columns in Slab1

For a flat slab supported by two columns, formulas are provided for the calculation of bending moments, shown in Illustration 4.4.

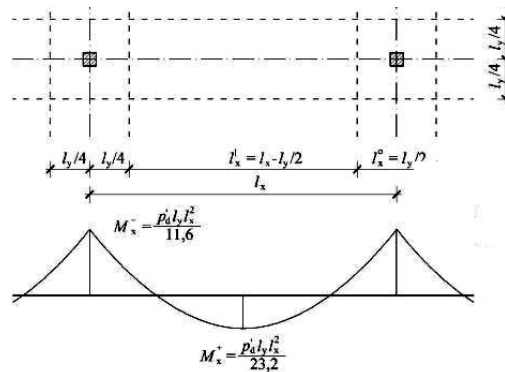


Illustration 4.4: Bending moments in a flat slab supported by 2 columns [34]

The application of these formulas results in the bending moments at the width of the columns

strip, which in this case is  $2 \frac{l_x}{4} = 2 \frac{7}{4} = 3,5 \text{ m}$ . For this reason, the resulting moments should be divided by the strip width of 3,5 m, in order to obtain the design moment for 1 m wide strip of the slab (Table 4.6).

$M_{xx}$ (kNm)	LC1	LC2	LC3
Left support	-30,17	-90,51	-69,4
Middle span	15,08	45,26	34,69
Right support	-30,17	-90,51	-69,4

Table 4.6: Bending moments of Slab1 per meter of strip Theoretical results

The application of these formulas is a part of the Equivalent Frame Method, for the design of flat slabs. It is the most commonly used method, where the slab is divided longitudinally and transversely into columns and slab strips. No further elaboration of the method is necessary, as the purpose of its use is only to verify the software results. Negative bending moments occur at the points of supports (hogging moments) and positive moments at the middle of the span. Positive bending moments are present at the side spans as well, but due to their smaller value, they are not mentioned.

#### 4.4.3.2 FEA results

For the case of the finite element analysis, a certain procedure will be followed in order to get realistic results for the moments at supports. Only a certain part of the column head is regarded infinitely rigid, thus the peak value of the moment determined at the column axis is rounded down along the infinitely rigid part of the support (Illustration 4.5).

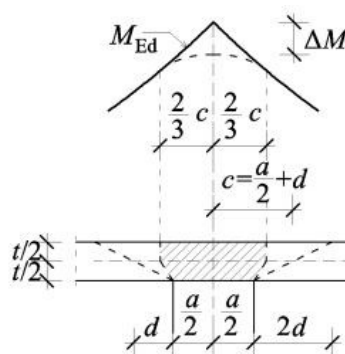


Illustration 4.5: Infinitely rigid part of column support [34]

In order to estimate the moments occurring in the perimeter of  $c=0,27\text{m}$  around the column, the average of the moments of this perimeter from DIANA is calculated. The results can be seen in Table 4.7.

$M_{xx}$ (kNm)	LC1	LC2	LC3
Left support	-30,54	-91,36	-65,16
Middle span	15,17	32,74	24
Right support	-32,37	-89,55	-65,7

Table 4.7: Bending moments of Slab1 FEA results

Following this, a comparison of the theoretical and FEA results will take place. It has to be mentioned that since the original flat slab has been analysed as two different slabs, moments in the y-direction are not examined. This would be possible if a more complete and elaborate

analysis of the flat slab of the structure would be realised. Table 4.8 contains the percentage of deviation.

$\Delta M_{xx}(\%)$	LC1	LC2	LC3
Left support	1,2	0,2	6,1
Middle span	-0,6	27,6	-30,8
Right support	6,6	0,8	4,9

Table 4.8: Deviation of FEA results from theoretical results.

From the comparison it is clearly seen that the theoretical and FEA results match quite well, apart from the case of sagging moments at spans. The great difference in these values can be justified by the combined plate action of the original slab that reduces the occurring bending moments. Furthermore, due to the geometry of Slab 1, there was only a column strip considered but no middle strip. In reality the cooperation between Slab 1 and Slab 2, gives the opportunity for considering a middle strip, and thus a different moment distribution is applied. The moment distribution of the sagging moment between the column strip and the middle strip (55%/45%), would produce a much smaller bending moment on the column strip, which would comply with the results of the finite element analysis. This also justifies the small difference in the average bending moment (-7,60/-6,15) at the column strip of Slab 1 and a hypothetical middle strip of the original slab (Illustration 4.5).

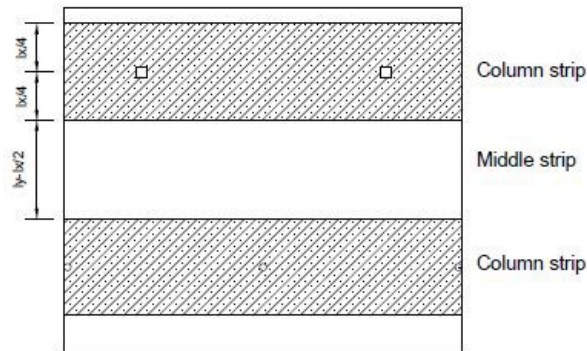


Illustration 4.6: Strips for moment distribution-Original flat slab

## Slab 2

Slab 2 (Illustration 4.7) is supported by three circular columns at a distance of 5,6 m from each other. The position of the columns can be seen in Table 4.9. The bottom left corner of this slab is considered the beginning of the axes. The bending moments were established as a comparison criterion for the slabs, and hand calculations will proceed the finite element analysis.

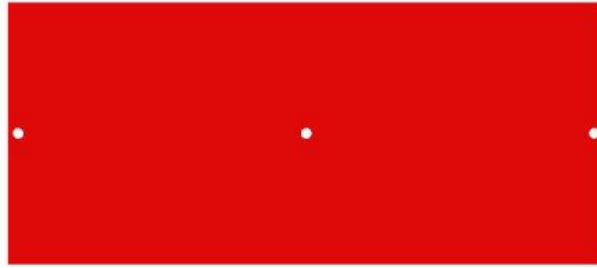


Illustration 4.7: Slab 2

Column	Position x-direction	Position y-direction
CIRC1	0,1	2,5
CIRC2	5,7	2,5
CIRC3	11,3	2,5

Table 4.9: Position of circular columns in Slab 2

In order to calculate the moments of Slab 2, which is supported by 3 columns, coefficients from Concise Eurocode 2 are used for the calculation. Table 15.3 of Concise Eurocode 2 provides these coefficients for beams and slabs of three or more spans. However, certain values for these coefficients are provided at the table comments for two span beams or slabs.

According to this table the design moments at supports are equal to:

$$\text{coeff} * n * \text{span}^2$$

For the design moments at spans:

$$(\text{coeff } g_k * \text{span} * \gamma_G g_k + \text{coeff } q_k * \text{span} * \gamma_Q q_k) * \text{span}^2$$

with a requirement of minimum span  $\geq 0,85$  maximum span.

Furthermore, the same loads and same load combinations are applied to Slab 2 as in Slab .

#### 4.4.3.3 Theoretical results

The condition of *minimum span*  $\geq 0,85$  *maximum span* is satisfied, since the two spans are of equal length.

The effective span of the slab between the two columns is:

$$l_{\text{eff}} = l_x - 2d_{\text{col}} + d, \text{ where}$$

$l_x$  is the span between the columns

$d_{\text{col}}$  is the diameter of the columns and

$d$  the efficient depth of the slab.

From the above,  $l_{\text{eff}} = 5,6$  m.

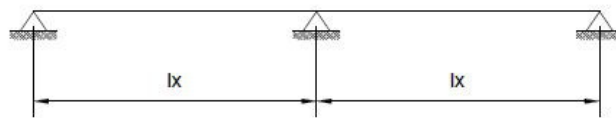


Illustration 4.8: Continuous beam on three supports approximating the behaviour of Slab 2

The formulas and coefficients of Table 15,3 will now be used for the calculation of moments. Table 4.10 shows the results for the three load combinations for the sagging moment at the middle of the span and the hogging moment at the point of the internal support. Since the moments derived from the formulas concern the column strip width, they have to be divided by it, in order to get the moments per meter of width. The strip in the x-direction that is being studied, is a column strip, which according to Eurocode takes up 70% of the acting per meter hogging moment, and 50% of the acting per meter sagging moment.

$M_{xx}$ (kNm/m))	LC1	LC2	LC3
Moment at span	17,64	38,23	28,06
Moment at internal support	-29,09	-62,33	-45,7

Table 4.10: Bending moments of Slab 2 Theoretical results

#### 4.4.3.4 FEA results

The results obtained from the finite element analysis will be processed, in order to obtain a more realistic representation of the actual behavior of the slab. For this reason, an averaged value for the support moment will be estimated at a cross section of width equal to the column dimension and length equal to the column strip width. For the sagging moment at the centre of the spans, the maximum positive moment obtained from the FEA is chosen for the comparison. If an average of the sagging moments for the width of the column strip had been chosen instead, a much smaller value would have been produced. This was not considered representative enough, and for this reason the idea was abandoned. Another feature from the FEA that has to be mentioned is the hogging moments at the end supports. Due to the position of the central axis of the two end columns at a distance of 0,1m towards the interior of the slab, negative moments occur which do not agree with the theoretical calculation, and for this reason they are not taken into account.

$M_{xx}$ (kNm/m))	LC1	LC2	LC3
Moment at span	15,17	32,74	24
Moment at internal support	-35,53	-76,67	-56,22

Table 4.11: Bending moments of Slab 2 FEA results

Following the finite element analysis, a comparison of the theoretical and FEA results will take place. Table 4.8 contains the percentage of deviation of the FEA results from the theoretical ones.

$\Delta M_{xx}$ (%)	LC1	LC2	LC3
Moment at span	14	14,4	14,5
Moment at internal support	-22	-23,1	-23

Table 4.12: Percentages of deviation in Slab 2

From the comparison of the results, a standard deviation of 14% is observed for the sagging moment at spans, and of 23% for the hogging moments at supports. For the case of the span moment this deviation could be considered expected and justified, as the same occurred for Slab 1, where bigger percentages of deviation were noticed. For the support moments, even though an averaging procedure was followed, there is still quite a significant percentage of deviation between theoretical and FEA results. The main reason that justifies the percentages of deviation, is that most finite element programs work with an elastic moment distribution, and materials that obey Hooke's law. This may be suitable for e.g. steel plates, but not for concrete which is an elasto-plastic material, since after it cracks its behavior is not linear. Consequently, the support moments are overestimated, and the deflection of the slab is underestimated. These support moments are unlikely to be realised under service loads due to cracking, and thus the service span moments will be correspondingly increased. In other words, underestimation of the sagging moments is a result of the FEA as well, for the case of the flat slabs.

## 4.5 Arch

When a shell is longitudinally supported by deep beams, walls or foundations, the forces are carried in the transverse direction to the supports. The shell in this case, works as a series of parallel arches, the so-called “funicular arches” responding to the applied loads solely in compression. However, the assumed loads do not remain constant, and that leads to flexure in the arch, since the rigid arch cannot readjust its shape in contrast to the cables. This means that the series of parallel arches, respond to forces by bending and axial force action. Their primary structural response is not membrane type action, and they can be approximated as arches.

Certain adjustments in the design are mandatory, in order to achieve the application of the arch action on the structure. The displacement at the base of the arch, has to be resisted by a horizontal thrust force, which means that the arch should be connected to the foundation. As far as the central part of the constructions is concerned, connection to the foundation is only provided from one side of the building. Extension of the roof at the facade should be realised and a proper arch configuration should be defined. From a material point of view, the arch should have a funicular shape. However, true funicular arches cannot be constructed for all applied loading conditions. For certain cases though, where the fixed dead weight comprises the largest portion of the total applied load, the arch geometry can be selected so that the pressure line is kept within the middle third of the member cross section, resulting in no tension across the arc length. Creating a critical loading envelope, by superimposing the effects of various loading cases on the arch, would provide an optimal geometrical shape [35]. The complexity though of this optimisation process dictates the use of the dead load pressure line as arch form, so that moments are generated only by live load action. The catenary form is obtained through this process, but since its mathematical expression is quite complicated, a second-degree parabola is used instead. As far as the height of the arch is concerned, the original design height will be kept. Taking also into account that for height-to-span ratio ( $h/L$ ) smaller than  $1/5$ , an arch can be treated as parabola, a span of 15 m is obtained [35].

The assumed arch might be considered as three-hinged, two-hinged or fixed. In a fixed arch, translation and rotation are prevented at the supports. The lack of hinges does not allow the structure to move freely, thus inducing bending moments. Due to its indeterminacy, this alternative is not considered. As far as two-hinged arches are concerned, they were first introduced at the late nineteenth century, with the development in structural analysis. They are one degree indeterminate structures, where the horizontal reaction is treated as the redundant, and it is subsequently evaluated by the virtual work method. This form of arch is vulnerable to foundation movement, and for this reason is not preferred. Finally, three-hinged arches are used extensively in prefabricated concrete constructions, due to their simple structural analysis, their adaptability to movements without being stressed, and easier transportation, execution and assembly. However two-hinged arches can be approximated as three-hinged arches for preliminary design purpose.

For the arch, the same structural forms will be determined using theoretical hand calculations and a FEA software. The strength and stability results of each method will be analysed and compared. Initially, the results of theoretical calculations will be analysed, then the ones obtained from the software and a comparison will complete the chapter. As it was mentioned previously, different load cases will be examined, as it is not known beforehand which loading situation will govern the design. A simple way of verifying the FEA model is to



Illustration 4.9: Three-hinged arch

compare the vertical and horizontal reaction forces. For the three-hinged arch, the reactions are obtained in the same manner as for a three-hinged portal frame, and are equal to:

$$A_v = B_v = \frac{wL}{2} \quad \text{and} \quad A_h = B_h = \frac{M}{h} = \frac{wL^2}{8h}$$

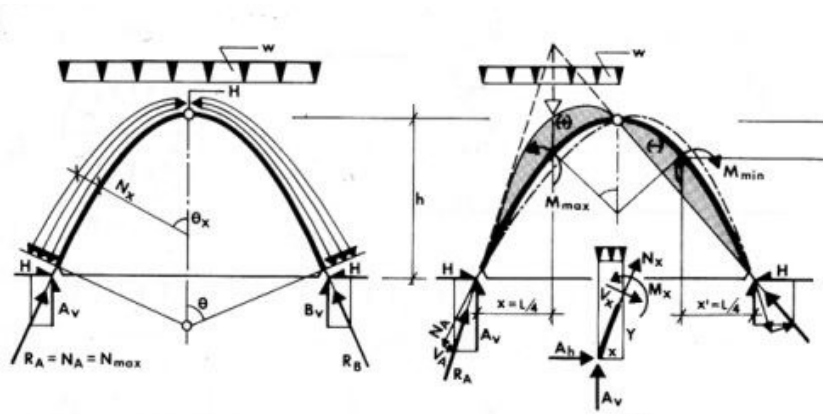


Illustration 4.10: Parabolic arch under uniform load action [35]

The slope of the arch is :

$$\tan\theta_o = \frac{A_v}{A_h} = \frac{4h}{L}$$

#### 4.5.1 Load combinations

The first case concerns the loading of the structure with its self-weight. No load factors were applied, in order to be able to compare the theoretical and FEA results in a fast and simple manner.

In the second load combination, the self-weight of the structure, the soil load due to the roof covering, and the assumed live load of 1,0 kN/m<sup>2</sup>, are applied. A load factor of 1,35 is chosen for the dead load (self-weight and soil load) and 1,5 for the live load. This load combination represents an ultimate limit state (ULS) design case, in order to calculate the maximum stresses. No bending and shear is present along the arch due to its symmetric loading-the forces are resisted in pure axial manner-and for this reason, asymmetric loading with the

same load factors is applied as a third load case. In this load case, apart from the self-weight that normally acts on the structure, the soil load and live load are only applied at the left half of the arch. This way, bending moments can be examined and compared

#### 4.5.2 Analysis of results

The following tables contain the reactions forces for all load combinations, for both the theoretical calculations and the FEA analysis results. Also, their relative difference is calculated.

		LC1	LC2	LC3
Theory	$R_h$	46,87	80,32	121,64
FEA	$R_h$	43,85	89,3	114,64
	$\Delta R_h[\%]$	6,4	-11,2	5,63

Table 4.13: Resultant horizontal reaction forces of the arch

For the vertical reaction forces, the LC3 produces different values on the two supports due to the asymmetric loading on the arch.

		LC1	LC2	LC3 (Left/Right)
Theory	$R_v$	37,5	100,59	81,8/61
FEA	$R_v$	38,41	97,3	91,96/60,48
	$\Delta R_v[\%]$	-2,4	3,3	-12,4/-0,85

Table 4.14: Resultant horizontal reaction forces of the arch

It is demonstrated that large thrust forces have to be resisted, with the necessary capacity being provided by the soil and the foundation, rods or buttresses. The large horizontal reaction forces are justified by the geometry of the arch, being quite flat. Light steep arches produce small horizontal thrusts compared to heavy shallow arches.

Next, the internal forces will be calculated and compared. Formulas are utilised for the calculation of axial and shear forces. These formulas [36] are provided for different load situations and specifically:

- point load
- self-weight
- uniformly distributed load

The case of point loading is not examined further, as it acts on top of consecutive layers. Due to this, its effect becomes distributed when it reaches the concrete skeleton. It does not act consequently as a point load but as a distributed load. For this reason, an increase in the mag-

nitude of the live load is applied from 0,4 kN/m<sup>2</sup> to 1,0 kN/m<sup>2</sup>. For the other two cases, the formulas for axial and shear forces are equal to:

$$N(\alpha, \beta) = \frac{1}{2} R w (-2 \cos(\beta))^2 + \frac{(\cos(\alpha))^2 \sin(\beta)}{-1 + \sin(\alpha)} \quad \text{and}$$

$$V(\alpha, \beta) = \frac{1}{2} R w \cos(\beta) (1 + \sin(\alpha) - 2 \sin(\beta)) \quad [36]$$

As it is noticed, the equations describing the internal axial and shear forces, are a function of two factors. These factors represent angles, explained in Illustration 4.11. The angle  $\alpha$  represents the angle formed from the centre of curvature of the arch between the supports and the horizontal axis, and  $\beta$  any angle at which the internal forces will be calculated. Using the equations above, the internal forces will be manually calculated and compared to the ones obtained from the FEA software. The check will be executed in two points: the top of the arch and the base of the arch.

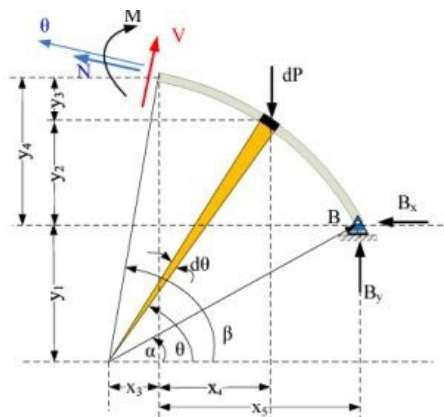


Illustration 4.11: Free body diagram of a three hinged arch under self-weight

Table 4.15 contains the angles  $\alpha$  and  $\beta$  for the two considered points.

	Angle $\alpha$	Angle $\beta$
Top of the arch	43,5°	90°
Base of the arch	43,5°	43,5°

Table 4.15: Angles  $\alpha$  and  $\beta$  of check points

First the results of the theoretical calculations will be presented, the the ones of the Finite Element Analysis, and subsequently a comparison will take place.

	LC1		LC2		LC38	
	Top	Bottom	Top	Bottom	Top	Bottom
$N_x$	-43,77	-61,26	-114,49	-160,46	-85,39	-131,42
$Q_y$	0	3,42	0	9,6	-10,7	5,35

Table 4.16: Internal forces of the arch for different load cases-FEA results

From the above, it is demonstrated that the arch responds to uniform distributed load (self-weight or other load type) with compression, justifying the characterisation of the arch as a “compressive structural system”. The axial compressive force reaches its highest value at the supports of the arch and decreases towards the crown. The shear force on the other hand gets a comparatively low value, and it varies only slightly from the support towards the top, until it reaches zero at the arch crown.

	LC1		LC2		LC4	
	Top	Bottom	Top	Bottom	Top	Bottom
$N_x$	-45,86	-60,16	-112,75	-147,96	-87	-114,26
$Q_y$	0	6,1	0	15,12	-10,31	1,36

Table 4.17: Internal forces of the arch for different load cases-theoretical results

This was expected due to the symmetric loading of the arch. The results of the hand calculations were taken using the aforementioned formulas. These formulas though could not be applied for the case of asymmetric load, as load combinations LC3. The loading of this combination was analysed in the following forms:

- since the self-weight is applied throughout the structure, the first part of the analysed loading consists of it. The equations above can properly be implemented.
- asymmetric loading consists of the live load and soil load, acting on the one of the two symmetrical parts of the arch (left part in DIANA analysis). The value of this load acting on the left part has been calculated to 5,5 kN/m. Thus, it can be analysed in a uniformly distributed symmetric load of  $5,5/2=2,75$  kN/m, and an asymmetric loading of the same value. For the first case again, use of the equations is allowed. Due to lack of formulas for the calculation of internal forces for the latter case, these are calculated assuming the arch as a beam, and estimating the forces correspondingly. The internal shear force at the support is calculated at  $ql/4 = Q_y = 2,75 \cdot 15/4 = 10,31$  kN.

Moreover, the internal moments have to be compared. For this reason, a derived equation is utilised, which is the product of [36]. The following formula has been derived for a three-hinged arch, and although the input of DIANA concerns a two-hinged arch, it is decided to be included, so a comparison of the order of magnitude of the occurring bending moment could be feasible. The same equation is valid for the self-weight and the external applied loads. The equation for the calculation of the internal moments is equal to:

$$M(\alpha, \beta) = \frac{1}{2}(R^2)w(-1 + \sin(\beta))(-\sin(\alpha) + \sin(\beta))$$

The assumption of a three-hinged arch results in zero bending moments at the position of the hinges. Thus, the bending moment is zero at the base of the arch and at its crown, a fact which is also confirmed by the results of the finite element analysis. These results show that the bending moment takes values extremely close to zero. For this reason these points cannot be considered as check points for the comparison between theoretical and FEA results. Instead, the maximum moment will be located by the result diagram of finite element analysis, and it will be compared with maximum moment obtained from theoretical calculations.

To accomplish this, the first derivative of the internal moment function will be calculated, considering angle  $\beta$  as the only variable of the function (angle  $\alpha$  is constant for the arch), and this will be set equal to  $43,5^\circ$ .

$$\frac{\partial M}{\partial \beta} = \frac{1}{2}(R^2)w \frac{\sin(x)(250\sin(x) - 211)}{125}$$

$$\frac{\partial M}{\partial \beta} = 0 \quad , \text{ from where } x=90^\circ \text{ or } x=57,56^\circ.$$

The first solution cannot be accepted since, at the point of  $90^\circ$  the moment becomes zero. Substituting the angle  $\beta$  with the value of  $57,56^\circ$ , the maximum bending moment on the arch is obtained.

		LC1	LC2
Theory	$M_z$ [kNm]	7,18	21,45
FEA	$M_z$ [kNm]	3,3	8,63

Table 4.18: Maximum bending moments in the arch

Large deviation in the results is a result of the different modeling of the arch in each case. The theoretical calculations assume a three-hinged arch whereas the finite element analysis deals with a two-hinged arch. The case of asymmetric loading is not taken into account, as no formulas are provided for the calculations of bending moments. The maximum bending moment from the finite element analysis is located at the crown of the arch, corresponding to the middle point. This is an expected fact if it is taken into account that the structural behavior of the arch can be approximated with this of a curved beam.

Concluding, comparing the behavior of the three-hinged and the two-hinged arch, the different moment distribution is pointed out. In the following pictures the normalised moment diagram for each case is schematised, in order to obtain a better understanding of the different behavior.

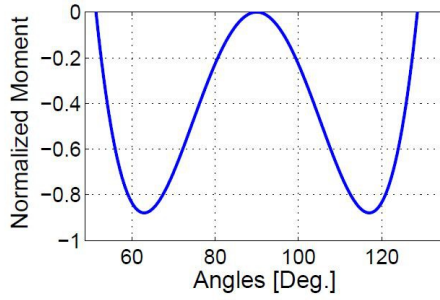


Illustration 4.13: Normalised moments for a three-hinged arch

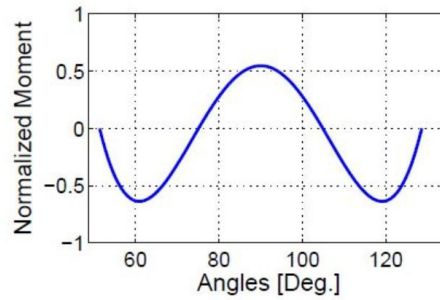


Illustration 4.12: Normalised moments for a two-hinged arch

## 4.6 Cylindrical shell

The design of the shell is clearly divided into two separate structural forms. A central part and two side parts (Illustration 4.14). The central part consists of a cylindrical roof and a side wall, connecting this roof to the foundation.

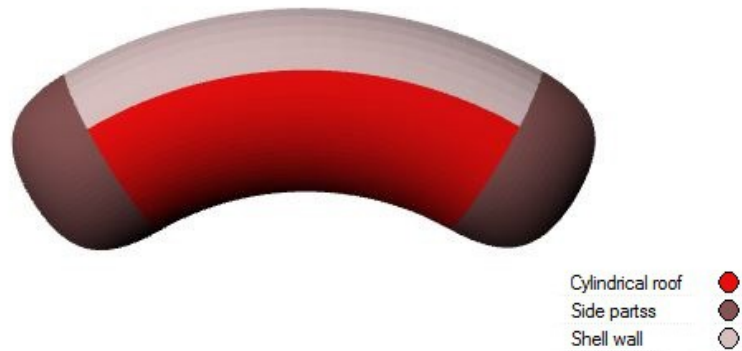


Illustration 4.14: Parts of the design case structure

Since the current supporting conditions do not qualify the structure as a cylindrical shell roof, design modifications are required in order to do so. Cylindrical shells are not only characterised by their shape but also by the type of supports in longitudinal and transverse direction, by the kind of diaphragms and edge beam conditions, and the continuity of the shell across several bays and spans [36]. As far as the supporting conditions are concerned, a distinction can be made as a result of the support direction. If the cylindrical shell is supported solely longitudinally by deep beams, frames or foundation, the forces are carried in the transverse direction to the supports, and its structural behavior can be approximated with the response of parallel arches. These arches respond to the applied loads by bending and axial force action. They cannot be considered shells as they respond primarily with bending and not with membrane action. These structures are called vaults and they can be designed as arches.

In the case where the shell is supported only in its transverse direction, it behaves like a beam spanning in the longitudinal direction. This means that the arch action in transverse direction

cannot be carried to the longitudinal supports like it is the case for vaults, but must be carried by internal shear forces which are a part of longitudinal beam action [36]. Consequently, their primary response action to the applied loads is beam action and not arch action like in the previous case. These structures are called long barrel shells or shell beams, and they can be visualised as shallow beams with curvilinear cross section .

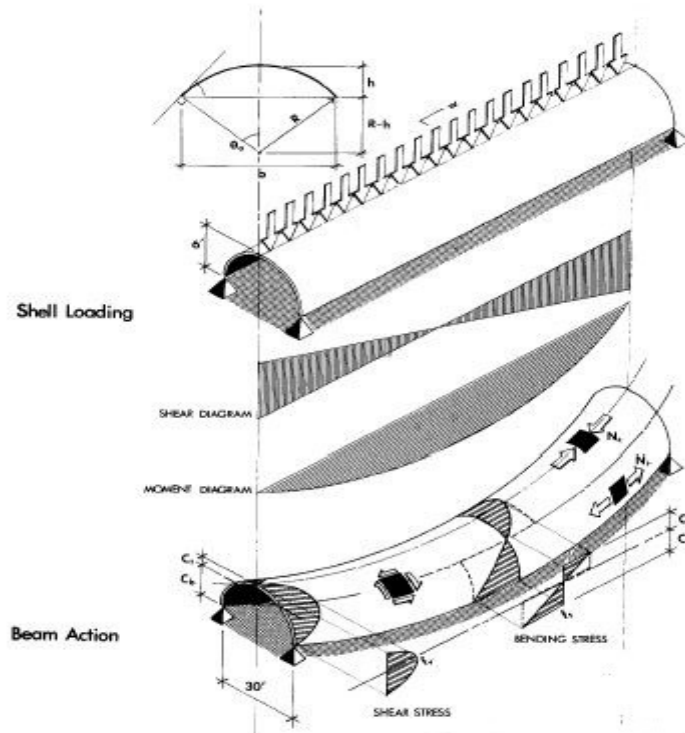


Illustration 4.15: Behaviour of long barrel shell - Beam action [36]

The transverse arch action which completes the analysis of shell beams will not be elaborated for practical reasons, mainly due to the complex geometry of the cylindrical roof of the design case building.

The cylindrical roof of the structure, as it was already mentioned, is connected on the side wall, without being supported by it. In the original design this part is supported as a slab by columns. Supports in the transverse direction are used for the cylindrical roof instead of the longitudinal direction. This choice causes less disturbances in the original design with a less complex construction process.

The introduction of walls (or columns) at the two sides of the cylindrical roof (Illustration 4.17) produces a long barrel shell, which will be analysed as an approximating structural form for the original design. In order though to consider the roof as a barrel shell, design modifications are mandatory.

The wall support is not necessary to extend until the rear wall of the structure, which is a shell itself, but only to the point that the considered roof starts. This is assumed to happen at



Illustration 4.17: Supports in transverse direction for cylindrical roof

a distance of 3,3 m from the wall-to-foundation connection. Instead of a wall, the roof can be supported by columns at its four corners. The roof has a chord width of 6,7 m and spans in an average length of 20,8 m.

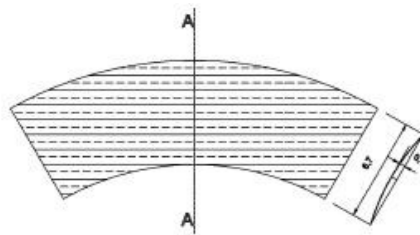


Illustration 4.18: Cylindrical shell roof-Plan view and cross-section

The shell will behave as a beam in the longitudinal direction and the loads will be transferred by internal shear forces that are part of the longitudinal beam action. It is assumed that the beam will not distort under the applied loads, so that linear stress distribution can be used. In order to prevent excessive deflections at the crown, the edges or buckling of the shell, longitudinal edge beams, transverse ribs ties, or diaphragms are introduced. Regular used height-to-span ratio for this kind of shells vary from 1:10 to 1:15. The selection of the height depends on aesthetic, functional and economical considerations. For the cylindrical roof of the structure the previously mentioned conditions cannot be strictly applied, as they do not fit to the geometry of the building. As a result, the roof dimensions are selected in order first to deviate the least from the original design, and provide a similar aesthetic result, and then to fulfill the requirements for considering the roof as a long barrel shell.

The current roof height of 0,4 m produces a radius of curvature, given from the following equation:

$$R = (b^2 + 4h^2) / 8h$$

where

R is the radius of curvature

b is the chord width and

h is the height of the roof measured from its supports equal to 14,23 m ( $\kappa = 1/14,23 = 0,0702$ ). However, in order for a cylindrical shell roof to be analysed as a shell beam the following condition has to be satisfied:

$$L/R > 2$$

where L is the span of the roof. The current span and radius produce a ratio of  $1,46 < 2$ . Thus, increase of the curvature and decrease of the radius is demanded in order for the roof to function as a shell beam. An increase of the maximum height of the roof from 0,4 to 0,6 m, produces a new radius of 9,6 m. This way the previously stated condition is fulfilled since  $L/R = 20,8/9,65 = 2,16 > 2$ . The maximum slope of the arch is equal to

$$\sin\theta_0 = \frac{b/2}{R}$$

and the arc length equal to

$$l = \pi R (\theta_0 / 90)$$

Table 4.19 contains the dimensions of the cylindrical shell roof. For an initial calculation of the thickness of the shell, different approaches are followed. Studies have shown that there is a relation between the thickness of the shell and the failure mode. Moreover, based on membrane theory, the nominal thickness can be calculated considering the normal force (n) in a pressurised cylinder due to self weight only. The thickness is estimated using the formula of critical membrane force  $n_{cr}$  and is equal to:

$$t^2 \geq p\alpha R \frac{\sqrt{3(1-\nu^2)}}{2EC}$$

from where we get  $t \geq 0,023$  m. The thickness is really small since the shell is assumed that it carries its self-weight. This value is calculated for a perfect cylindrical shell, which is clearly not the case in reality. Nevertheless, it demonstrates the structural efficiency of shells, as a shell of 6,7 m span can adequately carry its own load with a thickness of less than 3 cm. Actually, the thickness of the cylindrical shell rarely depends on strength considerations and it is generally and mainly used to provide enough coverage for the reinforcement. Only for very large shells, buckling may govern the shell thickness, although buckling of cylindrical shells is not as critical as for domes, because a relatively smaller portion of the shell is in compression. From the previous, it is made evident that a value can be proposed for the shell thickness. A thickness of 10 cm is adopted.

Cylindrical shell roof	Dimensions
Average span	20,8 m
Chord width	6,7 m
Thickness	0,1 m
Curvature	0,1036 1/m
Radius of curvature	9,65
Arc length	6,95 m
Slope at supports	26,9°

Table 4.19: Geometric dimensions of cylindrical shell roof

#### 4.6.1 Load combinations

The same approach will be followed here, as it has already been done for the previous structural forms. Initially only the self-weight of the structure will be applied without load factors. The second load case concerns the application of all the acting loads with the appropriate load factors for an ultimate limit state design case. Finally, the same loads in a serviceability limit state will be used. The wind load may be neglected for first-design purposes, and that is the reason why it is not taken into account in any of the combinations.

#### 4.6.2 Theoretical results

In order to analyse the cylindrical roof and calculate the internal forces, the stress approach can be followed. However, since this method requires the estimation of geometrical properties of the cylindrical roof which is a complex, lengthy and time-consuming procedure for a fast estimate, it will be abandoned. The shape of the roof as non-semicircular increases the complexity of the calculations. For this reason, the internal couple method will be applied.

The maximum moment at midspan is equal to

$$M_{max} = wL^2/8$$

where

w is the applied load and

L is the longitudinal span of the roof

Applying this equation for each of the load cases, the following results are obtained.

$M_{max}$	LC1	LC2	LC3
Moment at midspan (kNm)	135,2	464,1	378,56

Table 4.20: Moment at midspan Cylindrical roof

A location of the longitudinal steel reinforcement has to be assumed, in order to calculate internal tensile and compression forces using the internal couple method. For this reason, the position of the reinforcement is considered at 0,2 m from the base, so the effective depth is equal to  $d=0,6 - 0,2=0,4\text{m}$ . The lever arm for the compression-tension couple is estimated at  $z=0,9d=0,9*0,4=0,36\text{m}$  conservatively. The moment at midspan is resisted by internal force couple:

$$T(z)=C(z)=M$$

The maximum tensile force is thus equal to

$$T = M / z$$

For each of the load cases the maximum tensile force is given in Table 4.21

T	LC1	LC2	LC3
Maximum tensile force (kN)	375,56	1289	1051,6

Table 4.21: Maximum tensile force Cylindrical roof theoretical results

The compressive stresses do not have to be checked since they are generally not critical for ordinary situations. To determine the shear stresses the following approach will be followed. The free body of a cylindrical shell roof is shown in Illustration 4.19. It is apparent that at the neutral axis, the total horizontal shear  $V_h$  is equal to the axial tension or compression force, with  $V_h$  being the resultant of the triangular shear diagram for the shell beam under uniform load action.

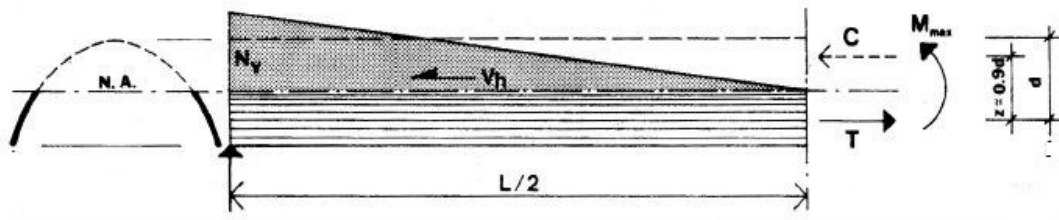


Illustration 4.19: Free body diagram of shell beam

From the picture,

$$V_h = T = N_v(L/2)/2$$

where  $N_v$  is the maximum unit shear force at the support. For every load case, Table 4.22 contains this value.

$N_v$	LC1	LC2	LC3
Max. unit shear force (kN/m)	72,23	247,88	202,23

Table 4.22: Maximum unit shear at support of cylindrical roof theoretical results

#### 4.6.3 FEA results

The results of the finite element analysis are presented here. The same quantities will be defined, and a comparison will follow. Due to the high refinement of the mesh, an average value for the bending moment will be calculated concerning the centre of the shell beam span. The smaller the region which is considered around this point, the closer the results of the finite element analysis to the theoretical analysis results. The larger the area, the greater the deviation. The averaged moments obtained from FEA are found in Table 4.23.

$M_{\max}$	LC1	LC2	LC3
Maximum moment (kNm)	19,2	73,35	52,67

Table 4.23: Moment at midspan Cylindrical roof FEA results

The axial forces provided by the finite element analysis are given in kN/m. Also due to the longitudinal curvature of the roof, larger forces are present in the longest side. For this reason an average is chosen for the whole tensile region and the value acquired is multiplied by the effective height of the section of the roof, which is equal to  $h=0,36$  m. After this procedure, the values are shown in the following table, with the percentages of deviation.

T	LC1	LC2	LC3
Maximum tensile force (kN)	361,03	1182,24	1013,76

Table 4.24: Maximum tensile force Cylindrical roof FEA results

The unit shear force at the support should be then taken from the FEA results. From Illustration 4.19, it is noticed that  $N_v$  is equal to the distributed shear force  $Q_{yz}$ . The average of this force at the region close to the supported is estimated for each load combination. Table 4.25 contains these values.

$N_v$	LC1	LC2	LC3
Max. unit shear force (kN/m)	68,96	263,77	189,27

Table 4.25: Maximum unit shear force at support Cylindrical roof FEA results

#### 4.6.4 Comparison

The percentages of deviation between theoretical and FEA results will be calculated and comments will follow. For the comparison of the bending moments, the values obtained from the theoretical calculations have to be divided with the chord width of the cylindrical roof, in order to facilitate the comparison with the FEA results. This produces the following values for the bending moment at the centre of the span of the beam per meter of width.

$M_{\max}$	LC1	LC2	LC3
Moment at midspan (kNm/m)	20,16	69,27	56,5

Table 4.26: Bending moment Cylindrical roof FEA results

	LC1	LC2	LC3
Maximum moment $\Delta M_{\max}$ [%]	3,8	-5,9	7,2
Maximum tensile force $\Delta T$ [%]	3,86	8,3	7
Max. unit shear force $\Delta N_v$ [%]	4,5	-6,41	6,4

Table 4.27: Deviation between theoretical and FEA results Cylindrical roof

The percentages of the deviation are acceptable, and they are mainly the result of the simplifications made during the hand calculations. The roof in the theoretical analysis was modeled as a shell beam without fulfilling strictly the criteria for this consideration. For the roof to be considered as a shell beam without edge beams or even with edge beams that are not too deep, the ratio of the longitudinal span to the radius of curvature should have been greater than 5 or 3 respectively. The resulting height of the roof would not comply with design criteria and the deviation from the original model would be significant.

Furthermore, shell beams are assumed not to distort under load action so that linear stress distribution can be used instead of a curvilinear one that is actually the case. However, in the case of long barrel shells, lateral thrust forces causes large deformations, which make the application of the beam theory questionable. Another simplification is the arch action in the transverse direction of the shell, that is neglected in the calculations though it does not affect the current results(longitudinal direction)

## 4.7 Spherical Side part

The analysis of the central part will be followed by the analysis of the remaining parts of the structure, i.e. the spherical side parts. This way the analysis using theoretical calculations will be completed, in order to proceed to the finite element analysis of the whole structure and its segmentation.

### 4.7.1 Side part-Dome

The two side parts on the left and right side of the structure have identical dimensions, and only one of the them will be representatively analysed. They comprise one quartile of an ellipsoid with  $R_1 = 5\text{m}$  and  $R_2 = 4\text{m}$ , and they are connected both to the side wall and the roof of the structure (Illustration 4.20).

For the connection of the side parts to the foundation, hinges are preferred over roll supports, as in the latter case large horizontal forces will cause great instability at the bottom of the shell where the rolls are applied. In addition, clamped supports are not selected as large mo-

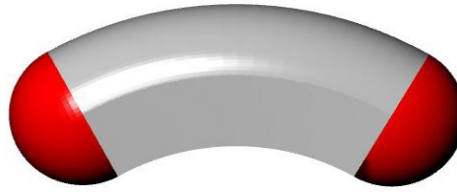


Illustration 4.20: Ellipsoid side parts

ments and forces emerge at the supports, and possible settlements provoke extra bending moments [14]. The dimensions are shown in Table 4.28.

Geometry Side part	Dimensions
Angle ( $\varphi$ )	90°
Sagitta (s)	4 m
Span (d)	10 m
Vertical radius of curvature ( $R_1$ )	4 m
Thickness (t)	0,1 m
d/s	2,5

Table 4.28: Geometrical dimensions Side part-Dome

Theoretical calculations will follow with certain quantities provided by analytical (FEA) calculations in order to examine whether the construction of the dome with the provided dimensions is feasible, satisfying strength and stability requirements.

The same loads are applied for the side parts as for the central part of the structure. The ultimate limit state combination will be checked for now, in order to obtain a first image of the strength requirements of the dome. Initially, the reaction forces of the dome will be calculated. Use of membrane theory is made in order to succeed this. No horizontal reaction forces are present due to angle of the structure at the supports( $\varphi=90^\circ$ ). For the vertical reaction forces, the following formula is used:

$$R_z = \frac{1}{2} \pi R_1 s p$$

from where  $R_z = 280,25$  kN.

Next, the internal forces and the membrane stresses will be calculated. Again, formulas from the membrane theory will be utilised, and specifically the equilibrium equations for the hemisphere. The radii of curvature for the case of the hemisphere are equal to each other. The forces and stresses will be calculated on the shell surface, for the meridional and radial direction. The forces in the two directions can be seen in Illustration 4.21

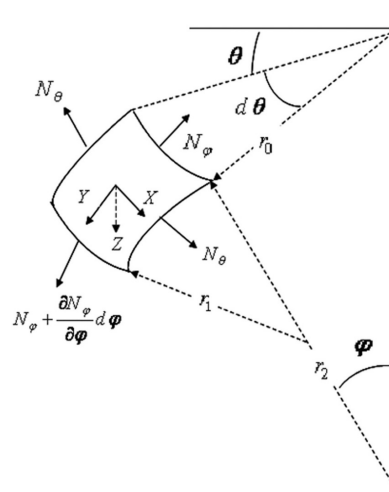


Illustration 4.21: Membrane forces on infinitesimal load element

The index  $\theta$  indicates the radial direction (hoop forces and stresses) and the index  $\varphi$  the meridional direction. With the equilibrium equations, the forces and stresses are defined for the base and the crown of the dome.

Forces in the meridional direction: 
$$n_{\varphi\varphi} = \frac{-pR}{1 + \cos\varphi}$$

Forces in the radial direction: 
$$n_{\theta\theta} = pR \left( \frac{1}{1 + \cos\varphi} - \cos\varphi \right)$$

The following table contains the forces and the stresses at the base and the crown of the dome.

	Top ( $\varphi=0^\circ$ )	Bottom ( $\varphi=68^\circ$ )
$n_{\varphi\varphi}$ [N/mm]	-22,31	-32,46
$n_{\theta\theta}$ [N/mm]	-22,13	15,75
$\sigma_{\varphi\varphi}$ [N/mm <sup>2</sup> ]	-0,22	-0,32
$\sigma_{\theta\theta}$ [N/mm <sup>2</sup> ]	-0,22	0,16

In the meridional direction, compression occurs throughout the whole length of the shell. In the radial direction however, a tensile force emerges at a specific point of the dome. For a sphere this point is located at an angle of  $52^\circ$  from the bottom of the shell, where a tensile hoop force appears.

The stress formulas produced from the membrane theory assume a perfect shell, and as a result do not take into account edge disturbances. As it was previously explained, the shell theory is extended with the bending theory for shells, in order to account for the non-estimated imperfections. These bending moments should firstly be calculated and then incorporated in the analysis of the structure. Due to the complexity of calculating these moments manually, the dome is analysed with a finite element software, which will provide these quantities. . The largest compatibility moments are required at the bottom of the shells, with their location

depending on the influence length. Contains the moments of the dome in meridional and circumferential direction.

	ULS
$m_{\varphi\varphi,\max}$ [kNm/m]	6,07
$m_{\theta\theta,\max}$ [kNm/m]	5,06

The large size of these moments, indicate that the dome of the design case building is an unfavourable structure, since the moments add a lot to the membrane forces. The geometry of the dome (half a dome) and the supporting conditions (hinge connection only to the foundation) can explain the large bending moments at the bottom of the structure. Their contribution is found with the following formulas:

$$\sigma_{\varphi\varphi} = \frac{n_{\varphi\varphi}}{t} + 0,5 \frac{t * 12m_{\varphi\varphi}}{t^3}$$

$$\sigma_{\theta\theta} = \frac{n_{\theta\theta}}{t} + 0,5 \frac{t * 12m_{\theta\theta}}{t^3}$$

Great attention should be drawn to the designing of this part of the structure, since large membrane forces finally occur, with the contribution of the bending moments. The final membrane forces are shown in

	<b>ULS</b>
$\sigma_{\varphi\varphi,\max}$ [N/mm <sup>2</sup> ]	2,71
$\sigma_{\theta\theta,\max}$ [N/mm <sup>2</sup> ]	2,89

# CHAPTER 5

## 5 Analysis of the Case Structure 'Bezoekerscentrum Waalbos'

This chapter commences the analysis of the design case building, which is the main topic of the thesis. Firstly, a description of the structure will be made and designs will be provided together with dimensions and features of the model. Then the supporting conditions will be defined and the applied loads and load cases will be determined. As far as the construction material is concerned, the grade of concrete will get modified with the progress of the analysis in order to satisfy strength requirements of the structure. The analysis of the building is conducted with a Finite Element Analysis software (DIANA FEA), with the model being originally designed with Rhinoceros 3D.

### 5.1 Description of the structure

A design case provided by Professor H.R. Schipper, concerning the concrete shell of the Rijsoordse Molen, is a great opportunity to investigate the scope of the thesis, guided also by the suggestion of the architect of the building. The shape of this shell structure is challenging and requires the production of many uniquely shaped double curved elements. This will be realized either by using prefabricated unique moulds or prefabricated concrete elements. The design case shell structure that will host the activities of the mills, the foundation 'Natuurbeheer Waalbos' and the Ice Association, is a building typical representative of organic architecture, a philosophy that promotes harmony between human beings, human constructions and the natural world [37]. Illustration 5.1 shows a model of the structure and Illustration 5.2 a depiction of the integration of the structure to its natural surroundings.

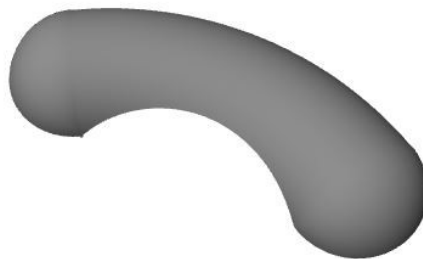


Illustration 5.1: Model of the structure



Illustration 5.2: Structure with its surroundings

The concept of the design case is its incorporation with the natural environment and the least disturbance to the surroundings of the site of the mills. Materials, motifs and basic ordering principles continue to repeat themselves throughout the building as a whole [38]. The design is inspired by the nature, and considers the building as a living organism. That justifies the soft curves, the partial integration of the shell in the ground of the site and its organic shape.

The current design of the structure differs in parts from the original design, provided by the architect. The main difference is located in the front part of the building, where instead of a continuous opening throughout the whole length of the facade, an arch opening has been positioned instead. The reason for this alteration was obliged by the lack of specified dimensions for the structure, which led to the previously mentioned simplification. Despite this, the structure still resembles to a great extent the original one, fulfilling strongly one of the set design criteria of the least deviation from the prototype.

The presence of the facade opening at the original design, was one of the most characteristic features of the structure. Since though its realisation was not possible, a different kind of opening should replace it. Different forms were investigated, concerning aesthetic and structural criteria, such as the occurring stresses and displacements. At last, an opening in the shape of an arch was selected, being supported by a concrete arch itself. The supporting arch can be seen in the following image.

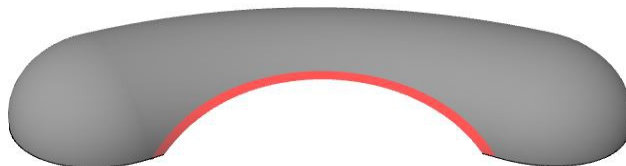


Illustration 5.3: Supporting arch at the facade opening

## 5.2 Verification of the final model

Before proceeding to the analysis of the structure, a verification process will be followed, similar to the one in Chapter 4. For this process the structure will be loaded solely by its self-weight. Certain quantities will be considered for the application of the checks. This process is conducted in order to confirm the rightness of the model before proceeding to the main analysis. As it was mentioned earlier, it is a common practice when using FEA software, as minor errors might produce significantly misleading results.

To begin with, an effortless check that is regularly conducted makes use of the sum of the reaction forces which has to be equal to the applied loads. Knowing that DIANA does not use the value of 2500 kg/m<sup>3</sup> for the mass density of the concrete, a smaller value will be used equal to 2400 kg/m<sup>3</sup>. The total surface area of the shell roof is calculated with the help of Rhinoceros, equal to 418,527 m<sup>2</sup>. Multiplying this value with the thickness of the shell, the total volume of the construction is obtained. Subsequently, the mass is the product of the volume and the concrete mass density, which for our case is equal to 104.448 kg or 1044 kN. The sum of the reaction forces produced by DIANA gives a value of 1026 kN.

Another quantity used for the verification process of the model and the structural analysis conducted, is the deflection at a certain point. Since the structure does not have a typical geometry for which formulas can be utilised for the calculation of deformations, parts of the structure will be isolated for this reason. The deflection of the stiffening arch obtained from DIANA will be compared with the one from numerical calculations. The following theoretical formula is used for the calculation of the deflection at the crown of the arch:

$$w = \frac{5\lambda^2/2}{1+8\lambda^2/5} \left( \frac{qR^2}{EA} \right) \quad [39]$$

where  $\lambda$  is the dimensionless arch rise parameter equal to the ratio of the arch rise to one-half of the arch thickness  $h$

$$\lambda = \frac{f}{h/2}$$

From the equation, the deflection is calculated equal to 12,13 mm. From DIANA a value of 13,48 mm is obtained for the deflection at the same point.

A final check is the one of the stresses, where a combination of data obtained from DIANA and numerical formulas will be used to verify results of analytical calculation. For this reason, initially the in-plane forces and moments will be calculated with DIANA. Then the total in-plane stress will be calculated using formulas, and the obtained result will be compared with the one from the finite element analysis. This process will be applied for all three layers of structural thickness (with the number three given as default by DIANA), so as to obtain the distribution of the stresses throughout the section of the shell. Illustration 5.4 shows the bending and normal stresses on a typical arbitrary cross-section.

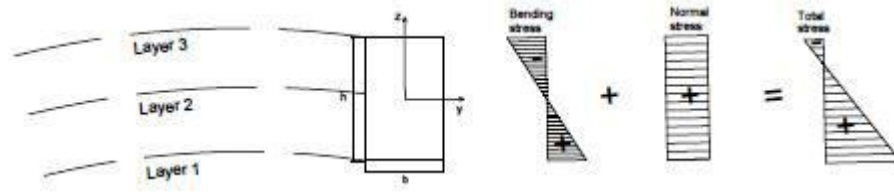


Illustration 5.4: Stresses on a cross section

An element will be chosen in DIANA model, so as to construct the distribution of the stresses. In order to calculate the stresses, first the normal forces and bending moments for the chosen element were taken from DIANA. For the normal stresses, the normal force was divided by the area of the cross section of the element (per meter), and for the bending stress, the bending moment was divided with the section modulus of the section to obtain the stress at its boundaries. The formulas are shown below

$$\sigma_n = N/A \quad \text{and} \quad \sigma_b = M/W$$

where

N is the normal force acting on the section

M is the bending moment acting on the section

A is the surface area of the section

W is the section modulus.

For the chosen element the bending, normal and total stress distribution can be seen in Illustration 5.5.

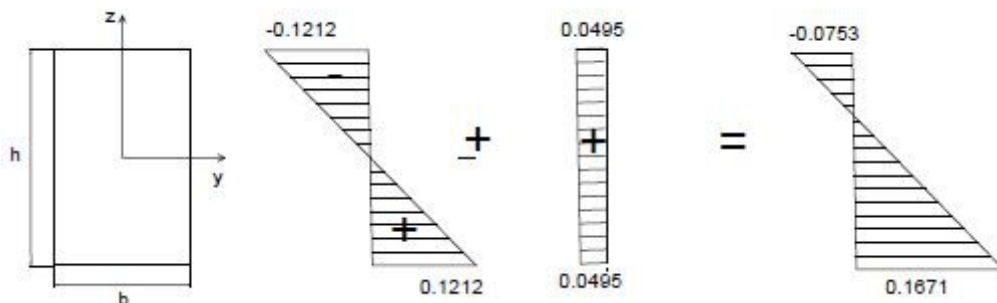


Illustration 5.5: Stresses of the chosen cross-section

The stresses at the middle point of the section are also calculated and are equal to 0,0459, since bending stresses do not contribute there ( $\sigma_b = 0 \text{ N/mm}^2$ ). The stresses refer to the local coordinate system of the element.

In the next step, the total stresses in the local axes system of the element are taken from DIANA, for each of the three layers. The local stresses for the chosen element from DIANA analysis are shown in Illustration 5.6.

For all the checked quantities the percentage of deviation between the analytical and numerical method will be given in Table 5.1 .

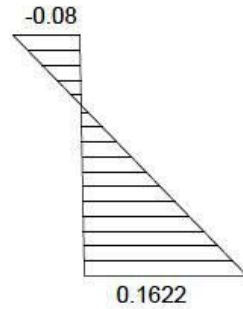


Illustration 5.6: Total stresses-DIANA

	Sum of reaction forces [kN]	Deflection of arch [mm]	Total stresses-Layers 1/2/3 [N/mm <sup>2</sup> ]
Theory	1044	12,13	-0,0753/0,0459/0,1671
FEA	1026	13,48	-0,08/0,04/0,1622
$\Delta$ [%]	1,75	-10	-6,5/-6,1/2,9

Table 5.1: Deviation of numerical and analytical calculation quantities

From the table above, it can be noticed that the percentages of deviation are quite small, with the exception of the deflection at the crown of the arch. This means that the model works as it is expected to work, and can be fully used for the determination of structural behavior of the structure and the structural analysis.

### 5.3 Supports

In order to analyse the structure, it is first necessary to define what forces can be resisted and transferred at each level of support throughout the whole structure. For this reason, the type of support of the structure-connection to its foundation-should be defined. Three kinds of supports comprise the options.

Firstly, a roll support is intrinsically excluded as it cannot support lateral forces. A structure on this kind of supports remains in place as long as it must only support itself and a perfectly vertical external load.

Fixed supports are restrained both against rotation and translation so they can resist any type of force or moment. Due to this, large forces and moments emerge at the supports. Fixed supports demand greater attention during construction and are often the source of building failures. Their rigidity though reduces substantially the deformation of the structure.

Pinned supports can resist both vertical and horizontal forces but not moments. They allow rotation in one direction, providing resistance to rotation in any other direction. For this reason, their construction is less complex than that of fixed supports, being able however to resist the same size of forces. Initially, an analysis of the structure taking into account only its self-weight will be conducted, in order to check whether the dimensions and supports of the

model are suitable for the structure, without any excessive deformations or stresses. Hinge supports are assumed throughout the perimeter of the structure with its connection to the foundation.

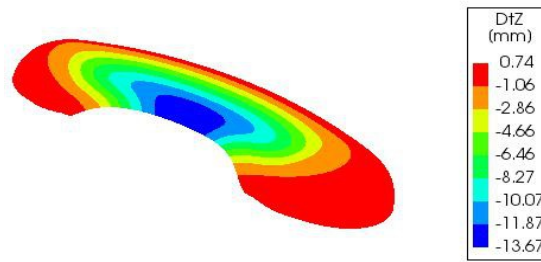


Illustration 5.7: Initial deformations of the structure

With this assumption, the analysis produces the deformations shown in Illustration 5.7, that seems quite significant. For this reason, it is decided to enhance the support of the part of the structure that presents excessive deformation by inserting the supporting arch. This support will transfer the forces from the curved roof to the foundation along the entrance of the building. On the one hand, the arch will take up the loads coming from the curved roof, and on the other hand the shell foundation will take up the thrust of the arch, and the shell will prevent its buckling. The results of this analysis are found in the following table.

Sum of reaction forces (z-axis)	$\Sigma R_z$ [kN]	1026
Membrane force meridional direction (max)	$n_{\varphi\varphi,\max}$ [N/mm]	350,59
Membrane force meridional direction (min)	$n_{\varphi\varphi,\min}$ [N/mm]	-1251,10
Membrane force circumferential direction (max)	$n_{\theta\theta,\max}$ [N/mm]	491,71
Membrane force circumferential direction (min)	$n_{\theta\theta,\min}$ [N/mm]	-976,07
Membrane stress local x-axis (max)	$\sigma_{xx,\max}$ [N/mm <sup>2</sup> ]	3,06
Membrane local x-axis (min)	$\sigma_{xx,\min}$ [N/mm <sup>2</sup> ]	-13,36
Membrane stress local y-axis (max)	$\sigma_{yy,\max}$ [N/mm <sup>2</sup> ]	4,28
Membrane stress local y-axis (min)	$\sigma_{yy,\min}$ [N/mm <sup>2</sup> ]	-9,98
Moment in the meridional direction (max)	$m_{\varphi\varphi,\max}$ [kNm/m]	11,27
Moment in the meridional direction (min)	$m_{\varphi\varphi,\min}$ [kNm/m]	-5,22
Moments in the circumferential direction (max)	$m_{\theta\theta,\max}$ [kNm/m]	8,95
Moments in the circumferential direction (min)	$m_{\theta\theta,\min}$ [kNm/m]	-7,72
Maximum vertical displacement (z-axis)	$u_{z,\max}$ [mm]	7,86

Table 5.2: Results of the analysis of the model due to its self-weight

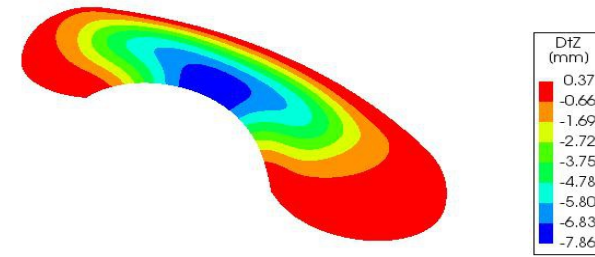


Illustration 5.8: Deformations due to self-weight in the z-axis – arch support

#### 5.4 Discussion on the results of the analysis

From Error: Reference source not found and Illustration 5.8 it can be seen that the maximum vertical displacement has decreased 44% with the introduction of the arch support on the front side of the roof, with the actual point of occurrence at the point where it is expected, at the crown of the arch. Furthermore, as it can be seen from the deformation diagram, the shell behavior of the structure is working in favor of reducing the deflections, pointing the efficiency of shell structures. The size of the reaction forces is small due to the spreading of the supports along the perimeter of the structure. For the membrane and bending stresses the extreme values are presented in the table. From Illustration 5.9 showing the membrane forces in the circumferential direction (hoop forces), the maximum compressive stresses occur at the highest point of the shell, where they are needed in order to produce the 'outward horizontal force', which in combination with 'inward horizontal force' at the base of the shell will make equilibrium with the applied loads.

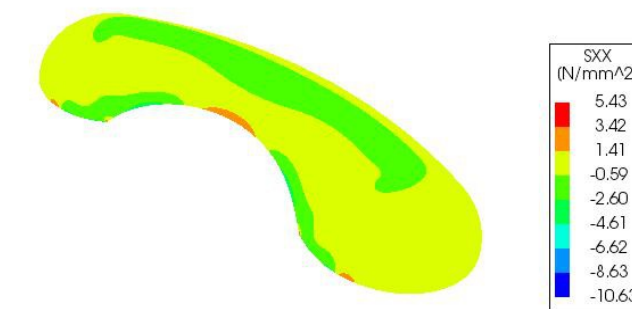


Illustration 5.9: Hoop stresses-self weight

As far as the membrane stresses in the meridional direction are concerned, they are tensional close to the arch ring until the highest point, transferring the applied loads there, and then compressive transferring the forces to the foundation. The following image with the membrane meridional forces confirms the theory,

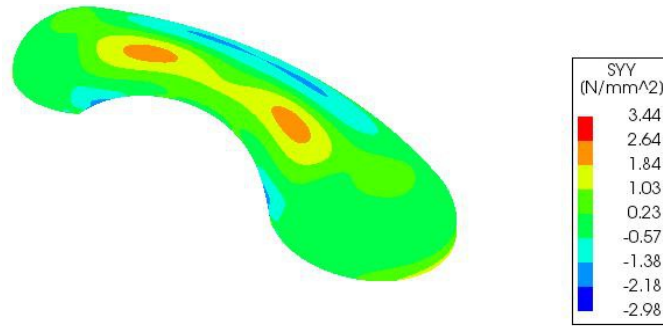


Illustration 5.10: Meridional stresses-self weight

The compressive meridional and circumferential membrane stress is sufficiently smaller than the design compressive strength of C 25/30 which is equal to 17 N/mm<sup>2</sup>. However, tensile forces of large magnitude emerge both in the meridional and the circumferential direction. The magnitude is justified by the discontinuity of the shell on the front side, which causes the emergence of bending stresses. The tensile strength of C25/30 is limited to 2.6 N/mm<sup>2</sup> which cannot compensate for the larger tensile membrane stresses. Reinforcement is thus necessary to take up the occurring tension on the shell, or the use of concrete with higher strength.

## 5.5 Analysis with service loads

In this part, the structure will be analysed with the actual service loads, and governing parameters such as the thickness of the shell and the concrete grade will be determined. This way, the final model will be of an optimal design and will contribute to the next step, which concerns the design of a segmented prefabricated shell.

The main differentiating feature of this part is the loading and the load cases of the structure, through which strength and stiffness requirements will be made clear. The supporting conditions do not deviate from the ones mentioned in the previous analysis (hinged connections throughout the perimeter of the structure)

### 5.5.1 Permanent Loads

As it was already mentioned in 4.3.1, permanent loads consist of the self-weight of the structure, plus any additional finishing. A thickness of 0,1 m is assumed for the concrete shell, producing a self-weight load of 2,5 kN/m<sup>2</sup>, and a soil layer as a finishing layer, of 0,2 m with a specific weight of 15 kN/m<sup>3</sup>, producing a load of 3 kN/m<sup>2</sup>. Consequently, the total dead load acting on the shell is 5,5 kN/m<sup>2</sup>.

### 5.5.2 Variable Loads

The variable loading on the shell consist of the live load, the snow load and the wind load.

### 5.5.2.1 Live load

According to EN 1991-1-1 a live load  $q_k$  may be selected for the roof of category H (roofs not accessible except for normal maintenance and repair) within the range of 0,0 to 1,0 kN/m<sup>2</sup> and a point load  $Q_k$  value ranging from 0,9 to 1,5 kN. The recommended values are  $q_k = 0,4$  kN/m<sup>2</sup> and  $Q_k = 1$  kN. Because of the soil covering and the vegetation on top of the shell roof, the effect of point load becomes distributed on the roof surface. For this reason, a uniform distributed live load of 1,0 kN/m<sup>2</sup> is assumed for the construction instead.

### 5.5.2.2 Snow Load

To begin with, snow load is assumed to act vertically and refers to the horizontal projection of the roof. The calculation of the snow load on ground should proceed the calculation of the snow load on the roof. This reference value depends on the geographical location and the altitude of the building. EN1991-1-3 Annex C provides the characteristic values for the snow load on ground for European countries. For the location of Waalbos, a value of 0,4 kN/m<sup>2</sup> is taken from figure C.7 ( EN1991-1-3 Annex C).

The snow load on the roof surface is given by :

$$s = \mu_i * C_e * C_t * s_k$$

where  $\mu_i$  is the roof shape coefficient,  $C_e$  the exposure coefficient,  $C_t$  the thermal coefficient, and  $s_k$  the characteristic value of snow load at the ground.

The shape coefficients for a cylindrical roof are given by the following expressions:

$$\begin{aligned} \text{For } \beta > 60^\circ & \quad \mu = 0 \\ \text{For } \beta < 60^\circ & \quad \mu = 0,2 + 10h/b \end{aligned}$$

where  $\beta$  is the angle of the roof inclination,  $h$  is the height of the roof, and  $b$  is the width. Illustration 5.11. For the roof of the design case building with  $\beta < 60^\circ$ ,  $\mu = 4,2$ . The upper limit of this coefficient is 2, so  $\mu = 2$ .

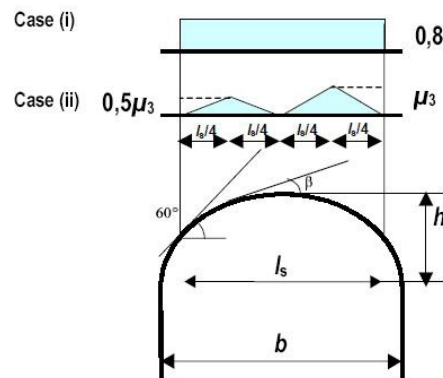


Illustration 5.11: Snow load shape coefficients for cylindrical roof

.Furthermore, for a cylindrical roof two load arrangements should be taken into account according to the Eurocode. Both arrangements are shown in Illustration 5.11. Case (i) represents the undrifted load arrangement, and case (ii), the drifted load arrangement. The roof shape coefficient for case (i) is 0,8, and for case (ii) 2.

For every climatic region Annex C contains a relation for the characteristic value of snow on the ground. The Netherlands belong to the central west climatic region, where the following relationship between the snow load and the altitude is valid:

$$s_k = 0,164 Z - 0,082 + \frac{A}{966}$$

where

A is the site altitude above sea level[m]

Z is the zone number given on the map

In this case, A=0 and Z=3, which at last gives  $s_k = 0,4 \text{ kN/m}^2$ .

$C_t$  is equal to 1 for normal situations, and  $C_e$  is obtained from the following table, equal to 0,8 for windswept topographies.

Topography	$C_e$
Windswept <sup>a</sup>	0,8
Normal <sup>b</sup>	1,0
Sheltered <sup>c</sup>	1,2

<sup>a</sup> *Windswept topography*: flat unobstructed areas exposed on all sides without, or little shelter afforded by terrain, higher construction works or trees.  
<sup>b</sup> *Normal topography*: areas where there is no significant removal of snow by wind on construction work, because of terrain, other construction works or trees.  
<sup>c</sup> *Sheltered topography*: areas in which the construction work being considered is considerably lower than the surrounding terrain or surrounded by high trees and/or surrounded by higher construction works.

Illustration 5.12: Recommended values of  $C_e$  for different topographies

The following table contains the snow load for each of these cases

Load case	Magnitude [ $\text{kN/m}^2$ ]
Case (i) undrifted	0,256
Case (ii) drifted-min	0,32
Case (ii) drifted-max	0,64

Table 5.2: Snow load values

### 5.5.3 Wind Load

The wind action is represented by a set of forces whose effects are equivalent to the extreme effects of the turbulent wind. Basis for the calculation is the wind velocity. The basic wind velocity  $v_b$  should be determined by the fundamental value of the basic wind velocity  $v_{b,0}$ . For

the region of Waalbos, a fundamental wind velocity of 27,0 m/s is provided. The following relation is provided by the Eurocode:

$$v_b = c_{dir} \cdot c_{season} \cdot v_{bo}$$

where

$c_{dir}$  is the direction factor with recommended value equal to 1,0 and

$c_{season}$  is the season factor with recommended value equal to 1,0

To determine the peak velocity pressure, Eurocode 2 1991-4-5 provides the following formula:

$$q_p(z_e) = \frac{1}{2} \cdot c_e \cdot \rho \cdot v_b^2$$

where:

$\rho$  is the air density equal to 1,25 kg/m<sup>3</sup> and

$c_e$  is the exposure factor depending on the height and terrain roughness, determined according to Illustration 5.13. for the region of Waalbos, a terrain category II is chosen, which refers to areas with low vegetation and isolated obstacles. With a height of 4 m, the exposure factor is approximately equal to 1,8.

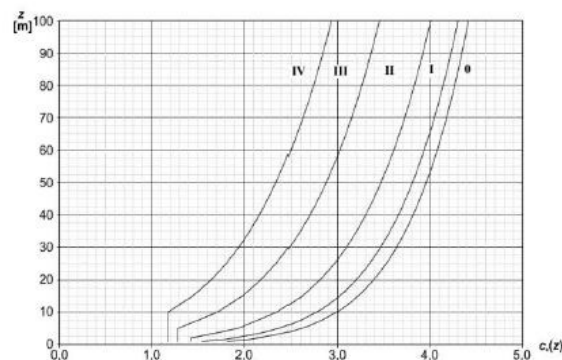


Illustration 5.13: Exposure factor according to Eurocode

As a result, the peak velocity is equal to 820,125 kg/m<sup>2</sup>s = 0,82 kN/m<sup>2</sup>

The last step would be to calculate the wind pressures on the structure. Both internal and external actions should be taken into account. However, the inside of the building is not accessible to wind, and for this reason, internal actions will not be estimated. The wind pressure,  $w_e$  acting on the external surfaces is derived from the following expression, according to the Eurocode:

$$w_e = q_p(z_e) \cdot c_{pe}$$

where:

$q_p(z_e)$  is the peak velocity pressure

$z_e$  is the reference height for the external pressure

$c_{pe}$  is the pressure coefficient for the external pressure

For domes with circular base, external pressure coefficients are given by Figure 7.12 of the Eurocode 1991-1-4.6, which can be seen in the following image.

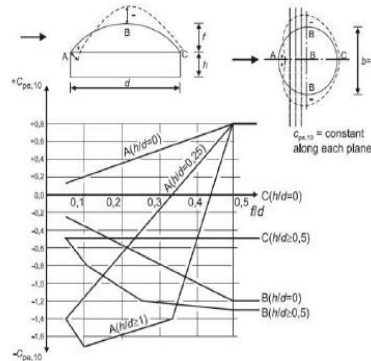


Illustration 5.14: Illustration 5.11:  
External pressure coefficients  $c_{pe,10}$  for  
domes with circular base

In the previous figure, the value of  $c_{pe,10}$  is provided, which refers to the overall coefficients. These coefficients concern loaded areas larger than  $10\text{m}^2$ , in contrast to local coefficients which refer to loaded areas of  $1\text{m}^2$  or smaller. Three different regions are distinguished for the structure. For each of these regions the coefficient is calculated.

	$c_{pe,10}$	$w_e$ [ $\text{kN/m}^2$ ]
Zone A	+0,62	0,51
Zone B	-1,0	-0,82
Zone C	0	0

Table 5.3: External pressure on the shell

The regions A, B and C have to be defined on the shell structure. And for this reason the distribution as suggested for vaulted roofs will be followed. The following picture demonstrates this distribution.

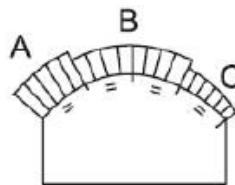


Illustration 5.15: Distribution  
for vaulted roofs

For the distribution in the circumferential direction, an opening of  $60^\circ$  is chosen, as in

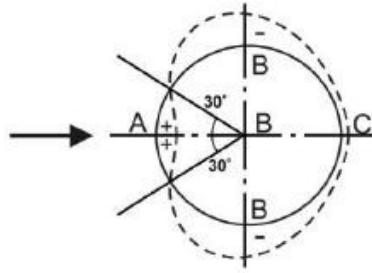


Illustration 5.16: Wind distribution in the circumferential direction

#### 5.5.4 Load combinations

Different load combinations should be considered in order to define extreme structural quantities. ultimate limit states and serviceability limit states should be considered. The Eurocode though states that verification using only one of the two categories of limit states is permitted, provided that there is sufficient information to prove that it covers the omitted one. Taking this statement into account and assuming safely that SLS load combination will lead to loads of smaller magnitudes, it is decided that all combinations will be calculated in the ULS. The following formula is used for the ULS combinations:

$$\sum_j \gamma_{G,j} \cdot G_{k,i} + \gamma_{Q,1} \cdot Q_{k,1} + \sum_{i>1} \gamma_{Q,i} \cdot \psi_{0,i} \cdot Q_{k,i}$$

where

$G_{k,j}$  is the permanent load

$Q_{k,1}$  is the dominant variable load and

$Q_{k,i}$  are other variable loads.

Load factors take the following values:

$\gamma_G = 1,35$  (or 1,00 where unfavourable)

$\gamma_{Q,1} = 1,50$  (or 0,00 where unfavourable)

$\gamma_{Q,i} = -1,50$  (or 0,00 where unfavourable)

The roof live load, the snow load and the wind load comprise the variable loads. The following table contains the load combinations that are applied to the model of the design case building.

Load combination	Magnitude of load [kNm/m]
Main variable: Live load (wind zone A)	9,86
Main variable: Live load (wind zone B)	8,67
Main variable: Wind load (wind zone A)	8,67
Main variable: Wind load (wind zone B)	6,60
Main variable: Snow load (wind zone A)	8,84
Main variable: Snow load (wind zone B)	7,65

Table 5.4: ULS load combinations

For the snow load only the maximum calculated load value is considered. For wind zone C, half of the load of wind zone B is applied. It is concluded from the table that the combination in which the live load is the dominant variable action, has the largest magnitude. In fact the negative value of the wind load for zone B is favourable since it acts in the opposite direction to the rest of the applied loads, reducing this way the magnitude of the combinations it is contained. To sum up, the load combinations in which the live load is the dominant load are the governing ones, and they will be applied on the structure. Another load case that is wise to be applied is the maximum load of the first combination throughout the whole structure. The application of this load case is unrealistic as it is not predicted by the codes, it is applied though conservatively in order to obtain maximum values of structural quantities. Two other load cases are defined, for reasons of comparison of results. The third load case concerns the loading only of the central part of the structure, with the side parts loaded by their self-weight, and another load case where the opposite happens. Four load cases will be applied and examined as a result, and they can be found in the following table.

Case	Loaded part
Load Case 1	Loading each wind zone with its specific load
Load Case 2	Loading the whole structure with the maximum load
Load Case 3	Loading the central part(cylindrical roof) of the structure
Load Case 4	Loading the side parts

Table 5.5: Applied load cases

## 5.6 Results of linear static analysis

The most frequently used form of analysis in FEA software is the linear static analysis. In this kind of analysis, the relation between a force vector and a displacement vector is linear, idealising this way the nonlinear reality.

The roof of the structure is analysed with the applied load combinations. No serviceability limit state design is taken into account, for reason of simplification, and the measured deformations are produced for the ultimate limit state design combinations. The calculations are based on an ideal shell without any imperfections assuming infinite linear elastic material behaviour. As previously, certain quantities are defined and compared, as the most representative for the design of the structure. Initially, the reaction forces are measured, as they indicate the force that has to be resisted by the foundation. Then the membrane stresses are checked, because they will define the strength requirements that the structure must fulfil. Shells may fail due to failure of the material, the so-called strength failure, where a loss of the load carrying capacity takes place, due to material deterioration. For thin concrete shells, the tensile forces may cause the concrete to crack, and compressive forces may lead to loss of concrete strength.

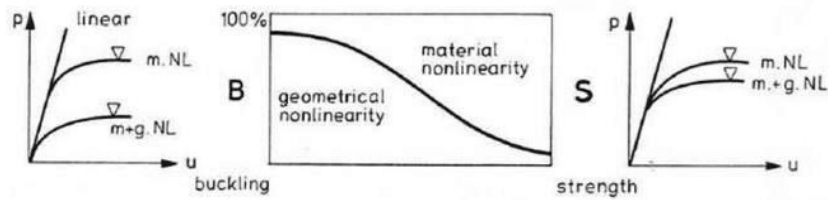


Illustration 5.17: Structural failure modes for shells

The bending stresses are additionally examined, in order to define the regions of edge disturbances. The small regions where these disturbances occur are determined by the influence length (Illustration 5.18).

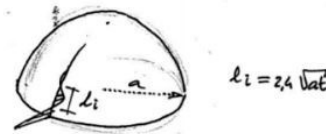


Illustration 5.18: Influence length of edge disturbances in a spherical dome

One of the last checked quantities produced from the analysis of the structure are the maximum vertical deformations. Excessive deformations should be avoided, as they can lead to failure of the structure. There is no standard value of accepted deformation or a formula prescribing it. For this reason, the deformations of the applied load combinations are compared relatively to each other.

## 5.7 Mesh size study

Before proceeding to the analysis of the structure, a mesh size study should be conducted, in order to obtain accuracy in the results. Mesh size is one of the most common problems in FEA software. Bigger elements provide inaccurate results, but smaller elements require computational time and cost. The reason for this study is to choose the correct size of mesh and estimate at which mesh size, accuracy of the solution is acceptable.

### 5.7.1 Process

Initially, an outcome of the analysis will be considered as a representative checking quantity for the current project. the buckling load factor of the first eigenvalue will be chosen, since its computation is fast and simple. Subsequently, different mesh sizes will be applied on the shell, and the value of the checking quantity will be obtained from the analysis. A chart will be built showing the outcome dependence on node count (or on mesh size). The chart will be asymptotically reaching for the correct answer.

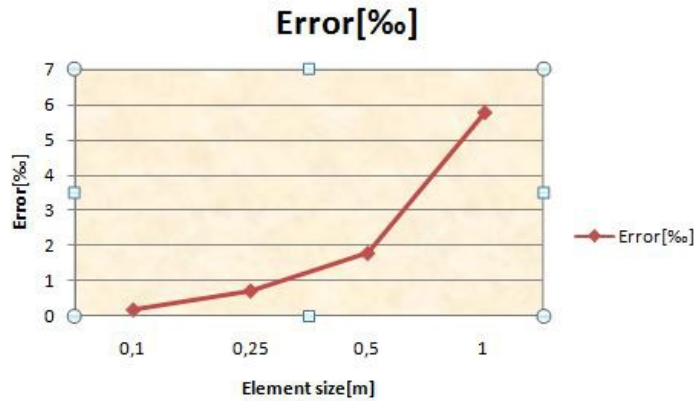


Illustration 5.19: Error function of displacement in relation to mesh size

The error function of the displacement at the crown of the stiffening arch was created, and a mesh of 0,25 m is sufficient enough to describe the structural quantities. For the analysis of the shell, a mesh of 0,2 m was applied finally.

.For each load combination, the following quantities are produced.

	C1	LC2	LC3	LC4
$\Sigma R$ [kN]	3622	4130	3454	3276
$n_{\varphi\varphi,max}$ [N/mm]	1237,72	1410,93	1223,08	1071,05
$n_{\varphi\varphi,min}$ [N/mm]	-4400,84	-5035,05	-4364,65	-3823,94
$n_{\theta\theta,max}$ [N/mm]	1236,40	1978,86	1726,61	1498,45
$n_{\theta\theta,min}$ [N/mm]	-3654,44	-3928,18	-3405,80	-3014,74
$\sigma_{\varphi\varphi,max}$ [N/mm <sup>2</sup> ]	11,91	13,60	11,82	10,32
$\sigma_{\varphi\varphi,min}$ [N/mm <sup>2</sup> ]	-50,63	-58,00	-50,28	-44,04
$\sigma_{\theta\theta,max}$ [N/mm <sup>2</sup> ]	16,90	19,25	16,78	14,60
$\sigma_{\theta\theta,min}$ [N/mm <sup>2</sup> ]	-40,55	-46,40	-40,22	-35,24
$m_{\varphi\varphi,max}$ [kNm/m]	40,04	45,34	39,30	34,90
$m_{\varphi\varphi,min}$ [kNm/m]	-18,52	-21,05	-18,20	-15,90
$m_{\theta\theta,max}$ [kNm/m]	31,80	38,00	31,20	27,70
$m_{\theta\theta,min}$ [kNm/m]	-27,11	-31,08	-26,90	-23,60
$u_{z,max}$ [mm]	27,77	31,63	27,48	24,09
$\lambda_1$	3,58	3,28	3,68	4,04
$\lambda_2$	3,79	3,50	3,99	4,22
$\Delta\lambda/\Delta p_{crit}$ [%]	5,9	6,7	8,4	4,5

Table 5.6: Results of applied load cases-Linear static analysis

From the table, it is clearly seen that the maximum quantities appear only for LC2 (except buckling factors which will be commented later). On the one hand this is expected since the

maximum load is applied throughout the whole structure. On the other hand, the application of different loads on each part of the structure, which happens in LC1, might have produced greater quantities due to the asymmetric loading. It has to be mentioned here, that the table contains the extreme value for stress and force quantities.

The sum of the reaction forces, indicates that the shell structure is a light construction, and due to its continuous connection of its perimeter to the foundation, the distributed reaction foundation loading will be low.

The maximum stress and force quantities as well as deformations appear on the cylindrical part of the roof. Comparing the deformations at a point of the cylindrical roof and at the 'spherical side part', the structural efficiency of a dome structure is made obvious. In LC1, where the whole structure is loaded with the same load, a reduction of 92% in the average deformation occurs between the displacement in the two afore mentioned points. What is also observed at the side parts, is a positive deflection (upward) due to the loading of the central cylindrical part.

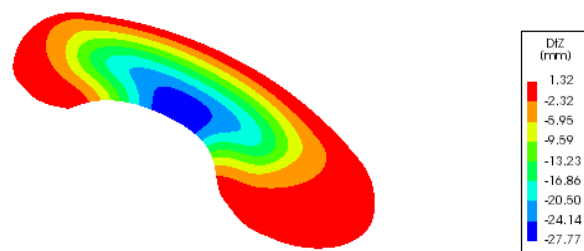


Illustration 5.20: Vertical deformation diagram-LC1

The latter functions as a beam supported on the two sides by the domes. When the load is applied, the iconic supports are deflected upwards. An analogy of the phenomenon can be seen in the following image.

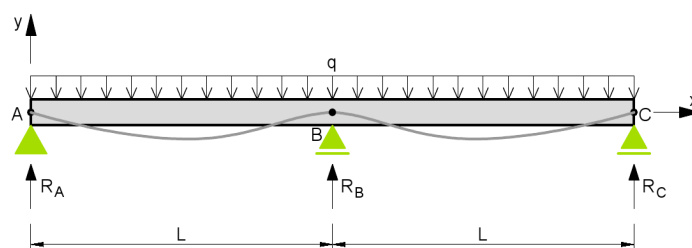


Illustration 5.21: Deflection diagram of two-span beam with uniformly distributed load

If an alternative of LC4 is considered, without any load on the central part, then a very small vertical deflection is observed (1,62 mm), realising once more the structural efficiency of the domes. Furthermore concerning the deformation of the structure, the small difference

between the LC1 and LC3 has to be spotted. This means that the extra deformation produced at the edge of the cylindrical roof due to the loading of the side parts is only minor.

The table contains the local axes system stresses. Since the geometry of the structure is not clearly developed in a discrete global axes system, local stresses are preferred as an analysis outcome, facilitating the design of the shell. Both tensile and compressive membrane stresses are quite large, which demonstrates the unsuitability of C25/30 for this case. The compressive stresses both in x- and y-direction could be resisted by concrete of higher strength (at least C50/60). The same holds for the tensile stresses, which have to be taken up by some kind of reinforcement. The design of the structure will be realised using LC1, since LC2 describes an extreme situation that is not prescribed by the codes. Another option to account for the large compressive membrane stresses, is to increase the thickness of the structure, which will be examined later.

As far as the global axes stresses in the cylindrical roof are concerned, they resemble the stresses in a doughnut like shell. The circumferential compressive forces occur at the highest point of the shell, in between tensile circumferential forces for equilibrium. On the other hand, the meridional forces are tensile close to the edge to the highest point of the shell, in

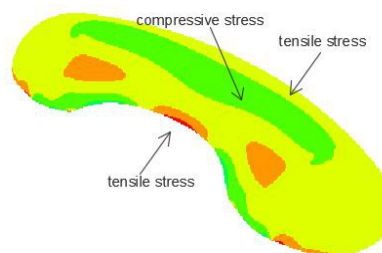


Illustration 5.22: Global stresses in the circumferential direction-LC2

order to carry the loads to that point, and then compressive carrying the loads to the foundation. This is the case for LC1, LC2, LC3 (Illustration 5.23, Illustration 5.22).

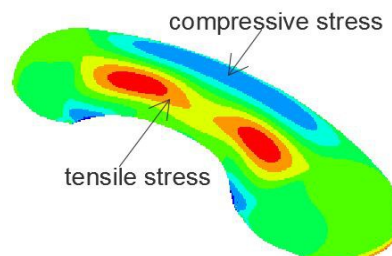


Illustration 5.23: Global stresses in the meridional direction-LC2

Bending stresses are also obtained from the linear static analysis of the structure. Due to the hinge supports being unable to transfer bending moments, quite large bending stresses occur at the structure. These appear mainly at regions where the membrane stresses are insufficient to carry the applied loads.

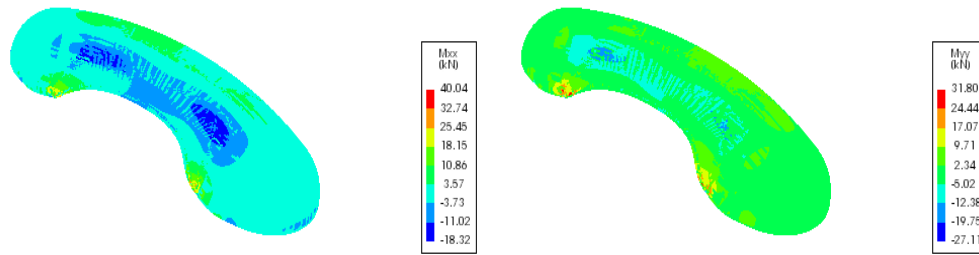


Illustration 5.24: Moments in the x-axis (left) and y-axis (right)

The occurring bending stresses do not carry any loads, but only compensate for the inadequacy of membrane behavior. For the design case shell, these disturbed zones are located close to the supports and at the cylindrical roof part supported by the arch. The bending stresses influence greatly the membrane stresses in both directions. Reinforcement is placed in both directions as well at the top and the bottom of the section due to the positive and negative bending moments. Concrete covering of at least 30mm must be provided.

For LC4, bending stresses of low magnitude occur mainly around the support points of the arch indicating that the structure is at a state of pure membrane action.

Yielding is not the only failure mode. Last but not least, the buckling load which is the lowest value of the load at which buckling commences, should be defined. Buckling happens suddenly and leaves no allowance for corrective action. Although in most cases, determining only the first buckling load is sufficient to describe the structural behavior of a building, in shells it might be necessary to investigate the post-buckling behavior, because it has an important bearing on the magnitude of the failure load [40]. After the initial buckling, the shell can only transfer loads smaller than the initial buckling load, particularly for the cases of concrete shells because of creep and imperfection of the shell shape, which are not taken into account in the theoretical model. In general, the value of the buckling load depends on the shell geometry, type of support, material properties and type of load.

In order to define the critical buckling loads from DIANA, the first and second buckling load factors are calculated. These factors are expressed by a number, which the applied load must be multiplied by in order to obtain the buckling load magnitude. However, the FEA software overestimates these buckling load factors and provides non-conservative results. The model of FEA represents a geometry with no imperfections, where loads and supports are applied with perfect accuracy. This is not the case in reality though, where the shell surfaces are not perfectly smooth and loads are applied with offsets. Considering the combined effect of discretisation error and modeling error, the buckling load factors should be treated with caution and for this reason modified. The modification is realised through a 'knock-down factor', by which the obtained values from the FEA software buckling values are divided. This factor is experimentally determined, having a value of 1/6.

An interesting point has to be mentioned here. For LC1, LC3 and LC4, a load of different value is applied on each part of the structure. This means that the first buckling factor for the whole structure coincides with the first buckling factor of each of the different loaded parts of the structure. Thus in order to obtain the critical buckling load for these load cases, the buckling factor should be multiplied

with the load of this part of the structure that buckles first. Summing up, Table 5.6 contains the first and the second buckling load factors, produced from the previously mentioned procedure. As it is noticed, no buckling value is below 1. This means, that under no load case the applied load causes buckling of the structure. Moreover, the difference of the first and second buckling load factor is of crucial importance since in the case that these values are close, the structure is expected to be highly sensitive to imperfections. The smallest difference is noticed for the LC4. However, this difference is not sufficiently enough to declare the shell sensitive to imperfections. In the opposite case, nonlinear buckling analysis would be necessary. Furthermore, it has to be mentioned that the buckling modes of DIANA present the shape the structure assumes when it buckles but do not provide any information about the resulting displacements or stresses.

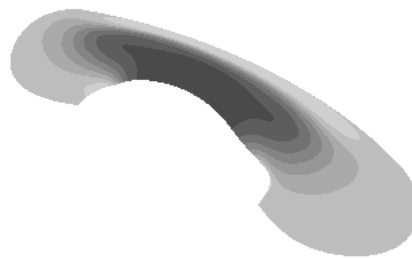


Illustration 5.25: First buckling mode-LC2



Illustration 5.26: Second buckling mode-LC2

## 5.8 Investigation of the thickness of the shell

The thickness of 100 mm for the shell was chosen semi-arbitrarily, since the conditions that were used for its definition provided not strict results. For this reason and because the thickness affects the occurring stresses and forces (inertia and self-weight are affected), it is considered wise to investigate whether a different thickness would have positive results on the structural behaviour or the cost efficiency of the shell. The following table contains the extreme values produced by the analysis for the shell with three more different values of thickness.

	70mm	120 mm	150 mm	100 mm
$\Sigma R$ [kN]	3138	3831	4146	3622
Reaction/meter [kN/m]	53,12	64,85	70,18	61,31
$n_{\varphi, \max}$ [N/mm]	1131,60	1265,19	1322,86	1237,72

$n_{\varphi\varphi,\min}$ [N/mm]	-3842,34	-4656,02	-5071,51	-4400,84
$n_{\theta\theta,\max}$ [N/mm]	1643,98	1816,23	2025,34	1236,40
$n_{\theta\theta,\min}$ [N/mm]	-3329,65	-3461,23	-3482,58	-3654,44
$\sigma_{\varphi\varphi,\max}$ [N/mm <sup>2</sup> ]	17,94	9,74	8,51	11,91
$\sigma_{\varphi\varphi,\min}$ [N/mm <sup>2</sup> ]	-67,60	-43,47	-36,29	-50,63
$\sigma_{\theta\theta,\max}$ [N/mm <sup>2</sup> ]	24,20	14,17	11,93	16,90
$\sigma_{\theta\theta,\min}$ [N/mm <sup>2</sup> ]	-56,30	-33,82	-27,56	-40,55
$m_{\varphi\varphi,\max}$ [kNm/m]	31,06	44,47	50,38	40,04
$m_{\varphi\varphi,\min}$ [kNm/m]	-14,70	-20,59	-23,19	-18,52
$m_{\theta\theta,\max}$ [kNm/m]	24,22	36,02	42,95	31,80
$m_{\theta\theta,\min}$ [kNm/m]	-24,91	-28,99	-30,39	-27,11
$u_{z,\max}$ [ mm]	48,85	21,51	16,20	27,77
$\lambda_1$	1,30	5,26	9,464\]]	3,58

Table 5.7: Results of analysis for different shell thickness

From Table 5.7, the change in the reactions forces is initially noticed due to the change in the thickness and subsequently on the self-weight of the structure. This change though is more useful to be compared when the sum of the reaction forces is divided by the perimeter of the structure equal to 59,074m. There is a substantial decrease on the foundation load with the decrease of the thickness to 70mm. The opposite holds for the thickness of 150mm. When the thickness is increased, a decrease in membrane stresses of both directions occurs, with the one of compressive stresses more prominent. As a result, a concrete of lower strength might be used with the necessary reinforcement. The increase in the component of bending stresses is also noticeable with the increase of the thickness. Deformations are moreover affected, with the one of 70mm large enough to exclude the reduction of the thickness as an option. The low buckling load factor supports this strongly as well. The thickness of 120mm is accompanied by a reduction of membrane stresses with the disadvantage of bending stress increase. The increase also in the reaction forces is important but not to the extent of making the solution unsuitable. As a conclusion the current thickness of the shell is considered proper for the construction, with a possible increase producing a more favourable structural behavior.

## 5.9 Investigation of concrete grade

From the results of the linear static analysis, the existence of large tensile stresses is obvious. The use of a higher concrete grade that would take up the a part of the large tensile stresses might be necessary. The E-modulus of concrete changes with the change of the concrete grade, affecting subsequently the stiffness of the structure. The

study proved that only the maximum deflections and the buckling load is affected by the change of the concrete strength, a fact that can be justified by the change of the Young's modulus.

As a conclusion, It is made obvious that an increase in the shell thickness by 20mm together with a use of concrete of higher strength will enhance the structural behaviour of the structure decreasing the stresses and deformations and increasing the critical buckling load. These improvements are accompanied by an increase in the construction costs which have to be taken into account.

# CHAPTER 6

## 6 Analysis of the Prefabricated Concrete Shell

This chapter contains the process of segmentation of the concrete shell of 'Bezoekerscentrum Waalbos'. Practices used for the segmentation process will be described together with criteria that this process should fulfill, and subsequently the process will take place, producing the prefabricated elements, of which the shell will consist.

### 6.1 Segmentation of the shell

Since the concrete shell will consist of the flexible mould prefabricated elements, its surface has to be segmented. A grid has to be generated on the surface of the shell, representing the panels which will consist of. Generally, grid generation techniques are applied to facilitate numerical solutions of physical problems, where partial differential equations are solved using e.g. finite element methods. In this case though, the grid generation is used to describe a complex free-form shell surface into discrete pieces, in such a way that accurately represents the original surface.

Various techniques have been developed for the generation of a grid on a surface, the most representative of which will be mentioned briefly in this chapter. Furthermore, the procedure of segmentation for the design case shell will be explained and realised.

The grid which we need to segment the shell surface in, must generate double curved elements and not flat elements. There are three types of grids on surfaces, with the assumption of zero shell thickness.

#### 6.1.1 Boundary-Conforming Grids

These grids comprise the most popular and efficient method for grid generation and are based on a mapping concept. According to this concept, the nodes and cells of the grid in an  $n$ -dimensional region  $X^n$  are defined by mapping the nodes and nodes of a reference grid in a standard  $n$ -dimensional domain  $\Xi^n$ , to which a transformation process will lead. The domain  $X^n$  is referred to as the physical domain, whereas the domain  $\Xi^n$  as the logical or computational domain. A transformation from  $X^n$  to  $\Xi^n$  is realised by choosing a proper transformation  $x(\xi)$  [3]. Choosing a logical domain with a simpler geometry than that of the physical domain is the driving idea of this grid generation process. If the logical domain and the transformation are properly selected, the transformed domain should be accurately represented by a small number of equally spaced mesh points. A boundary fitted coordinate grid is first generated on the boundary of  $X^n$  and then extended to the interior.

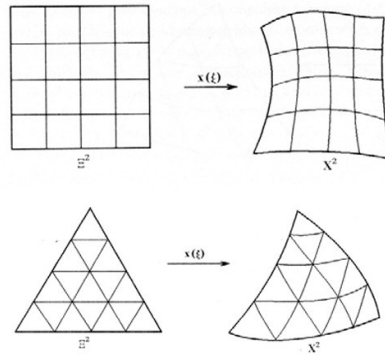


Illustration 6.1: Boundary conforming quadrangular and triangular grid [3]

Their advantage lies on the fact that they can be easily applied with a good level of accuracy. The challenging point of defining a correct transformation by the minimisation of uniformly spaced points required to determine the solution with a certain accuracy and element size.

### 6.1.2 Structured grids

In this type of grids, the local organisation of the grid points and the form of the grid shells do not depend on their position but are defined by a general rule [3]. They are the most commonly used type of grid in structural engineering due to their simplicity in grid generation and their flexibility in mesh size, element size and element organisation. Two forms of structured grids are the ones most frequently applied and will be discussed briefly, as they might find application in the segmentation of the design case structure.

### 6.1.3 Block-Structured Grids

In order to create a grid that fits most properly on a surface, these grids make use of a number of different grid systems with different coordinate systems which are combined and placed on the field of interest [3]. They can be applied on any shape, and expanded or compressed to fill any region (geometrically defined, free-form or form-finding shape), creating a curvilinear grid, having the same correspondence to a logically rectangular grid. The coordinate lines defining the grid nodes of two adjacent grid systems(blocks), can join smoothly or non-smoothly, creating the patterns of Illustration 6.2. If the coordinates do not join smoothly, which is more efficient for load transfer and element connection, then during calculation the solution values of one block must be transferred to these of the adjacent block at the location of the intersection, something achieved by an interpolation process.

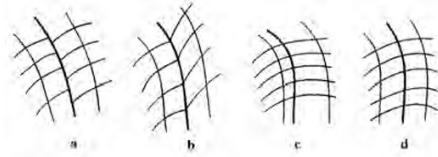


Illustration 6.2: Types of interface between contiguous blocks: (a) discontinuous, (b and c) non-smooth, (d) smooth [3]

Although its universal application, a time-consuming generating process is required. The possibility of using these grids for both developable and non-developable surfaces produces both smooth grids but also in certain parts, strangely stretched and deformed patterns.

#### 6.1.4 Translational grids

Translational surfaces are obtained from two curves by translation of either of them parallel to itself in such a way that each of its points describes a curve that is the translation of the other curve. They allow the generation of surfaces of quadrangular planar mesh, like shown in Illustration 6.3.

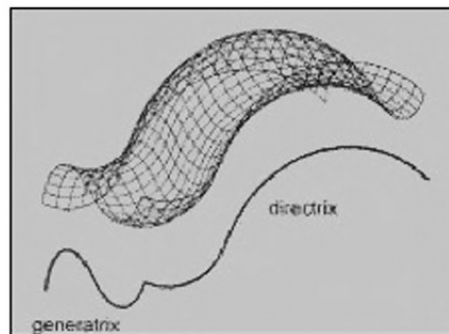


Illustration 6.3: Segmentation of translational surface [3]

As it is noticed from the previous image, the prefabricated elements produced have the same shape and weight, creating a great benefit if the flexible mould method is implemented. However, the shape of the design case building does not allow for application of the translational grid on the shell, and the method is simply mentioned for reference purpose.

A sub-type of block-structured grids, these grids consist of two sets of line segments that run parallel to the boundary lines. Different patterns of translational grids can be seen in Illustration 6.4.

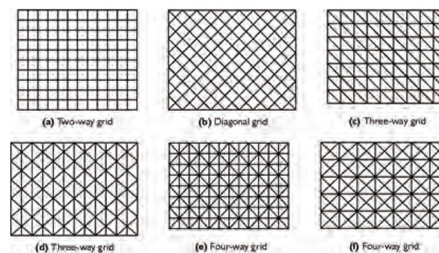


Illustration 6.4: Basic grid patterns [2]

These grids are composed by sliding one, two or three curves over another curve. Furthermore, many other patterns can be generated from the basic ones by removal of some elements from the basic patterns that were presented above.

### 6.1.5 Grid generation for dome structures

Once the side parts of the design case shell consist of domes, it is considered wise to mention the process of grid generation on these kind of shapes. Six types of grid configurations for domes can be distinguished and will be briefly mentioned in this section.

A ribbed dome is generated by the rotation of a curve around an axis and by translation of a ring over the same axis. A Schwedler dome is a modified version of a ribbed dome obtained by bracing the quadrilateral panels of the dome. Trimming at the upper part of the dome is possible to avoid overcrowding of the elements. A lamella dome has a diagonal pattern and may involve one or more rings. Diamatic domes are shown in Illustration 6.5(g) and Illustration 6.5(h). Illustration 6.5(g) shows a basic diamatic dome with triangulated patterns and the diamatic dome of Illustration 6.5(h) is obtained from a denser version of the Illustration 6.5(g) by removing every other line of elements. Grid domes are obtained by projecting a plane grid pattern onto a curved surface. Finally geodesic domes are obtained by mapping patterns on the faces of a polyhedron and projecting the resulting configuration onto a curved surface.

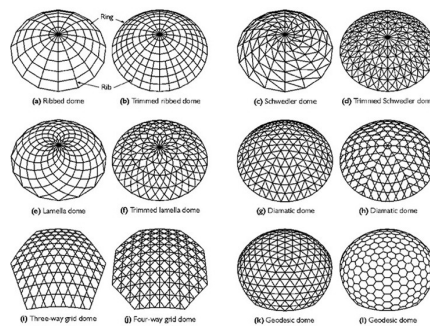


Illustration 6.5: Grid configuration for some shapes [3]

Since the amount of repetitive elements comprising the grid only depends on the amount of total elements and the shape of the structure, no preference between different grid configurations on a dome exists. Furthermore, the amount of elements segmenting the surface can vary by adjusting the mesh width and so the curve distances generating the mesh.

## 6.2 Segmentation of 'Bezoekerscentrum Waalbos'

Considering the above techniques and with the help of a parametric software (Grasshopper), the segmentation of the shell into elements will be executed. However, this segmentation process will have to take into account restrictions posed by the process of element production and building construction. These restrictions will influence the design of the elements. Subse-

quently, the elements have to be transported to the site, by means of a truck, a train or a boat. To this transport extra limitations are given for the size and weight of the elements.

The main limitation of the flexible mould method concerns the maximum curvature of the elements. The current data give this value equal to  $1/1,2 = 0,666$ , where 1,2 m is the minimum radius tested [41]. However, the whole system can be scaled to realise smaller radii. The value of 0,666 is provided for double curved elements, whereas for single elements smaller radii might be possible.

Another limitation is set for the dimensions of the elements. Experiments were conducted (REFERENCE) using a mould of 1,2 m x 1,2 m. However, this value was restricted by the size of the mould, with this meaning that moulds with larger dimensions would provide larger elements. A limit though, for the maximum dimensions should be set in order to achieve comfortable and safe handling of the elements and facilitate transportation, if the elements are not produced on site. Larger elements require typically more care during transport than smaller ones of the same thickness and curvature. Similarly, thinner pieces should be treated with more care than thicker pieces. Moreover, in the Netherlands, there are restrictions for the sizes of elements and the transported load on a vehicle [42]. When these limits are exceeded a special transport license is necessary.

The size of the elements influence furthermore their weight a matter which may obstruct the installation of the elements in the case that they will be hand set in their position. Restrictions concerning the weight of the vehicle, including the transferred load, also exist and should be taken into consideration.

The innovation of the flexible mould method lies in the fact that a single mould is able to produce multiple concrete elements with different shape, curvature and dimensions, by simply reconfiguring the mould. However, it is desired that the least mould reconfigurations take place, since this is a time-consuming process conducted by specialised personnel. The least the different elements are, the most convenient also their storage is. Generally, the curvature of the elements makes it more difficult to store the elements. In the case of elements with different curvature, they cannot be stored in the same way as flat floor elements on top of each other. In the case though, of elements with the same curvature, the storage is greatly facilitated still with certain provisions like frames with adjustable pins [42].

For the segmentation of the structure, a simple procedure was followed. Initially, the structure was segmented into three main parts: two side domes and the central cylindrical part. The segmentation technique was common, although the shapes were totally different. The technique involved the segmentation of the shapes in a specific number of parts, so as to create elements, the dimensions and curvature of which would comply the most with the aforementioned boundary conditions. Iterations were conducted until the point that the elements had feasible geometrical characteristics. The requirement of the least mould adjustments

(smallest number of different elements) was not strictly considered, although a very good result was finally achieved.

Finally, the cylindrical part was radially segmented in twelve parts and circumferentially into 6 parts. This led to elements of edge dimensions varying from 1,47m to 2,26 m in the circumferential direction and 2,23m to 2,36 m in the radial direction. In the location of the arch, where the segmentation produced odd and small shapes, these were incorporated with their neighboring elements. In a different case, curved quadrilateral elements were created.

For the side domes, the technique of the ribbed dome as it was mentioned in 6.1.5 is applied, where the curve at the base of the dome is rotated around the diameter at the same place, and the ring starting from the highest point of the dome to the base is translated over the same diameter. This segmentation produces elements with edge dimensions varying 2,36m to 2,63m in the circumferential direction and from 0,97m to 1,97m. The technique followed for the segmentation of the dome leads to the creation of triangular elements like in Illustration 6.6 along the sides of the domes. In order to avoid as much as possible elements of this configuration, a different segmentation of this part is followed, resulting in Illustration 6.7.

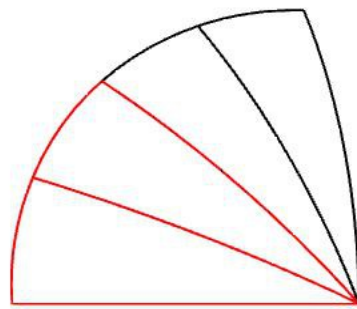


Illustration 6.6: Triangular elements at the sides of the domes

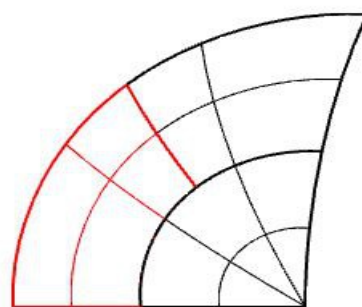


Illustration 6.7: Final segmentation at the sides of the dome

The result of the segmentation of the shell roof into elements can be seen in Illustration 6.8 and Illustration 6.9.

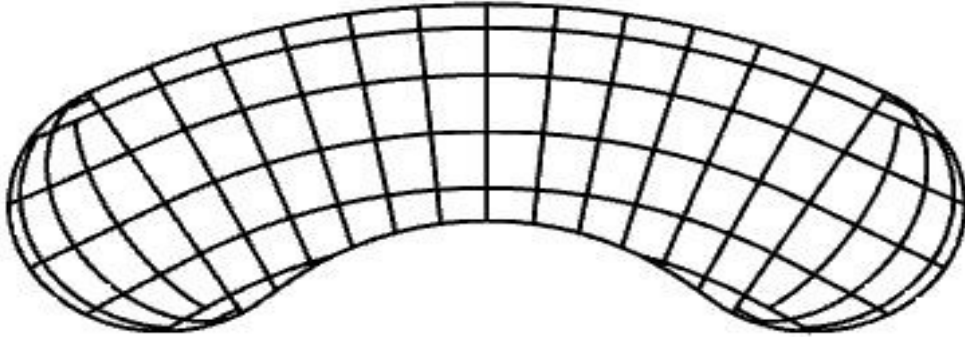


Illustration 6.8: Segmented shell-top view

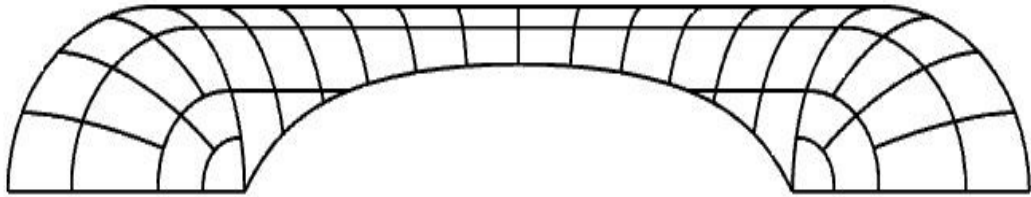


Illustration 6.9: Segmented shell-front view

# CHAPTER 7

## 7 Analysis of the segmented structure

The construction process of the segmented shell should be initially presented since it affects the structural behavior and the analysis of the shell.

### 7.1 Construction method-Connections between elements

In this chapter we are particularly interested in the way the elements are assembled together in order to form a shell structure. Connections are one of the most essential parts in prefabricated structures. They are responsible for taking up all service, environmental and ultimate load conditions. Free-form prefabricated structures are composed of concrete elements that are joined together in a mechanical way, for example using bolts, welds, pretensioning steel, adhesives or grout and concrete in the joints. However, connecting the elements together is not just a question of fixing the elements to each other, but ensuring the structural integrity of the whole structure. The structural response will depend on the behavior and the characteristics of the connections. Moreover, connections are entitled to transfer forces between the prefabricated elements in order to enable the intended structural interaction when the structure is loaded [43]. They are closely related and interfere with the adjacent structural elements. The design and detailing of a connection is influenced by the design and detailing of the prefabricated elements that are to be connected.

### 7.2 Types of connections

For prefabricated elements, certain types of connections have been proposed and implemented, the most important of which, will be mentioned in the following paragraph.

#### 7.2.1 *Wet connection*

In this case, two prefabricated elements are placed close to each other separated by a gap, at a specific distance. The gap is filled with mortar and might be reinforced or not, to strengthen the connection. Instead of reinforcing bars, fibres can be added to the grout mix. The use of fibres like the ones in UHPFRC is not appropriate, due to their small size. Instead, fibres with a diameter of 0,7 mm, length of approximately 60 mm and a hooked end are utilised [42].

### 7.2.2 Bolted connection/welded connection

For both of these connection types, certain provisions are required on the elements. For bolted connections, these provisions can be steel plates with holes for bolts and for welded connections the same steel plates are welded to each other to form a permanent connection.

### 7.2.3 Post-tensioning connection

In order to apply this type of connection, ducts should be predicted passing through the prefabricated elements, where continuous tendons are placed. After the placement of the elements, the tendons are tensioned and fixed at the edges of the shell surface. Epoxy resin is used to temporarily connect the elements, before the tendons are stressed.

### 7.2.4 Glued connection

Gluing is used as a practice in civil engineering to temporarily fix prefabricated elements that are subsequently fastened with mechanical means. The strength of this type of connection is caused by adhesive and cohesive forces. The glue in this case functions more as a seal and less as a point of bearing loads. Ultra High Performance Concrete (UHPC) is specifically suitable for this kind of connection, due to the property homogeneity throughout its thickness.

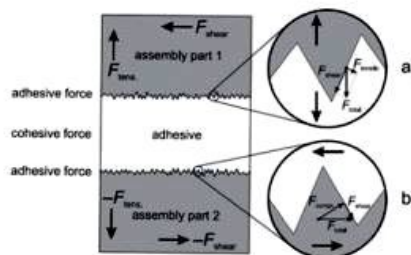


Illustration 7.1: Glued connection [42]

### 7.2.5 Prefabricated connection

This kind of connection, proposed by ter Maten is an alternative of a post tensioning connection either continuous over multiple elements or localised between two elements. In order to simplify the post-tensioning and bolted connection, ter Maten replaced the tensioning at the edges of the shell with local tensioning or even on multiple elements and simpler connecting bolts. Local force introduction is possible using

UHPC, and this is the case also with the specific connection type. Of course, an increase of the element thickness was obliged in order to accommodate the tendons. Some proposed ideas are presented in

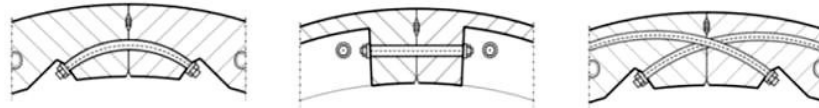


Illustration 7.2: Different versions of prefabricated connection [44]

### 7.3 Proposed construction method for 'Bezoekerscentrum Waalbos'

A construction method that could combine the advantages of the cast in-situ and a prefabricated structure would be ideal. The semi-precast construction method was proposed as a solution by Moiralis in his Master Thesis. In this method prefabricated elements collaborate with cast in-situ concrete to form the final structure.

#### 7.3.1 Description of construction method

An essential part of the total cost for the construction of a cast in-situ concrete shell is produced by the required formwork. Their complex shape makes their construction a time-consuming process executed by highly trained workers. The proposed connection model copes with the problem, by utilising the concrete prefabricated elements as formwork, which will later be incorporated into the structure.

Initially the site that will host the construction should be prepared. The prefabricated elements should be positioned in place, the same way it happens with other types of formwork. The panels have to be set in the right height and the right position by means of a scaffolding system or other type of temporary support. This system should be able to withstand movement and loading, and be lowered and removed after the shell is completed [42]. The loads that emerge during the construction process are usually larger than service loads. For this reason, measures have to be taken to account for these loads, like strengthening of the connection or placing temporary structures.

After the setting of the temporary structure, the prefabricated elements are lifted by crane and are subsequently lowered and placed at their final position, a process that requires manual labour. The elements have to be fastened on the supporting structure with a temporary connection. The final fastening is made after the positioning of several elements in order for the connection to gain its final strength.

The connection between the elements that have been placed to a certain distance from each other, can be realised with the use of mortar or glue [42]. In the first case, reinforcing bars can be placed in the gap to strengthen the connection or special fibres for the same reason. In the case of a glued connection, treatment should be applied on the edges of the elements for roughening. Moreover, loose particles should be removed before the application of the epoxy resin, in order to ensure a proper bonding of the adhesive on the element surface [42].

After the positioning of the prefabricated elements, the reinforcing bars of the cast in-situ concrete are placed. Wet concrete is subsequently cast on top of the prefabricated elements to form the final surface of the shell.

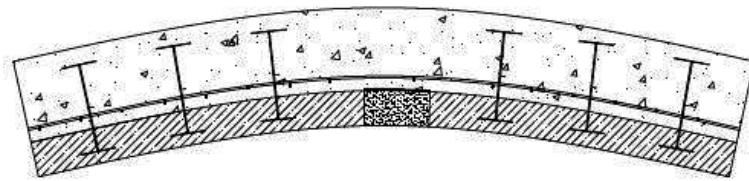


Illustration 7.3: Prefabricated connection model design

### 7.3.2 Evaluation of the method

One of the main disadvantages of the cast in-situ construction method, which is the high formwork cost, is excluded this way, reducing subsequently the total construction cost. The prefabricated elements which function as formwork are incorporated into the final structure. The wet connection between the elements allows for imperfections and deficiencies in the size and shape of the edge can be taken by the cast in-situ concrete. The required reinforcement does not need to be applied in the prefabricated elements, but similarly to the cast in-situ construction method in the form of reinforcing bars inside the wet concrete. On the one hand this facilitates the production of the prefabricated elements, on the other hand it requires bending of the bars, an arduous and time-consuming procedure.

In addition, disadvantages concerning the mortar between the elements can be noticed. The introduction of the mortar and the necessary reinforcement in the seam between the elements is a labour intensive process. The use of fibres instead of reinforcing bars might increase the construction speed, although the properties of a fibre reinforced connection between prefabricated elements are not fully known [42] and further inves-

tigation is required. Last but not least, weather conditions might affect the properties of the mortar and its application.

#### **7.4 Segmented shell characteristics and analysis**

For the case of the segmented shell, a similar procedure will be followed as the one for the cast in-situ shell. Initially, the thickness of the complete structure, the prefabricated elements and the wet concrete will be chosen. The structural analysis will be based on these values.

##### *7.4.1 Introduction*

The connection model proposed previously resembles quite significantly the properties of a cast in-situ shell. The introduction of the mortar between the prefabricated elements and the wet concrete topping, might ensure that the loads are introduced equally spread over the edges of the elements and throughout the whole shell thickness. For this, investigation is necessary. A conservative assumption will be also to consider that the concrete elements do not participating in undertaking the applied loads. And this will be the axis around which it will be investigated whether the construction of the concrete shell using the flexible mould prefabricate elements is possible and under what cost. The elements will function mainly as a lost formwork and this process already decreases the complexity of the traditional shell construction method. First the production of the formwork is facilitated, becoming faster and less painstaking, as now the formwork elements are produced using flexible moulds. Another point of improvement concerns the fact that the formwork do not have to be removed after the completion of the construction process since they get integrated into the final structure. Finally, with further investigation that is demanded on this topic, it can be possible proved that the connection has properties that allow for transfer of actions, then the thickness of the wet concrete is decreased and consequently the construction costs.

##### *7.4.2 Dimensions of the elements-Transportation to the building site*

As it was described in 6.2, certain aspects like the dimensions of the flexible mould or the restrictions posed by Dutch regulation concerning transportation of elements, were taken into account in order to determine the way the shell will be segmented. In this paragraph, the thickness of the elements will be examined in different stages of the construction process.

After the fabrication the elements have to be transported to the building site. This process requires first the loading of the elements on the truck, and then the unloading of the truck at the building site. During this process the elements are posed to loading by their own weight. This is a process studied by the static analysis, where the load is applied slowly on the element, and consequently the inertial effect on the basis of Newton's first law of motion is neglected [45]. However, during the transportation of the elements in the truck, they are imposed to time-varying loads, inducing time-varying responses (displacements, reaction forces, stresses).

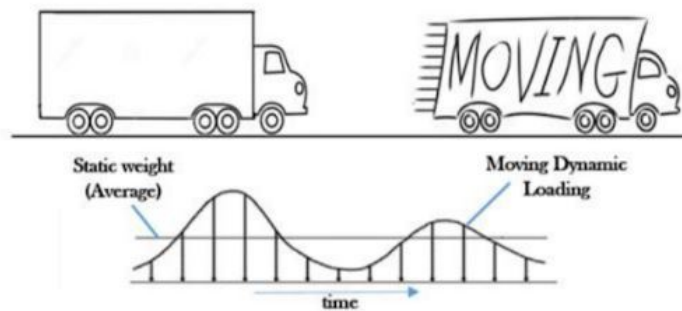


Illustration 7.4: Representation of static and dynamic loads [45]

The study of this kind of phenomena is a subject of dynamic analysis, with the difference of the explicit consideration of inertial forces developed during the time varying loads. In order though to avoid conducting a time-consuming dynamic analysis, amplification factors can be applied to the results of the exerted loads of static analysis, corresponding to the time variation of the loads. These artificial amplification factors are suggested in the range between 1,5 and 2,0 [45]. Subsequently, each element has to be lifted by a crane individually. Certain provisions are introduced on the elements in order to facilitate the carrying process by the crane. Three supports are sufficient to create a statically determinate structure. However, in order to ensure safety during lifting, four points of support are introduced on the element, despite the larger stresses that might appear due to indeterminacy of the system. While the prefabricated element is lifted by the crane, it has to be able to withstand its own weight (Illustration 7.5).

A prefabricated element out of the segmented shell will be examined under the influence of its own weight while transported by the truck and lifted by the crane. For the case of the prefabricated shell, the total shell thickness was chosen equal to 12 cm, and the reasons for these are two. In the previous chapter it was proved that a shell thickness of 12cm provides beneficial structural results with only a small additional cost, in the case that the connection provides transfer of axial tension and compression forces but also bending and torsion. On the other hand in case the connection between the prefabricated elements does not function properly, and subsequently the thickness of 2cm of the elements (chosen as a starting point) can-

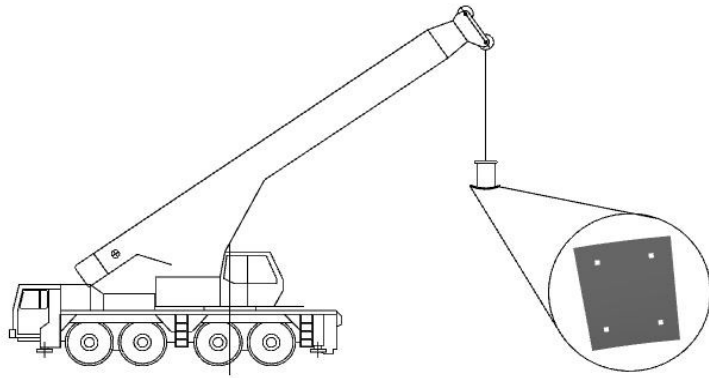


Illustration 7.5: Crane lifting element

not be taken into account, the remaining thickness of 10 cm has been proved adequate to take up the applied loads That is how the analysis will proceed.

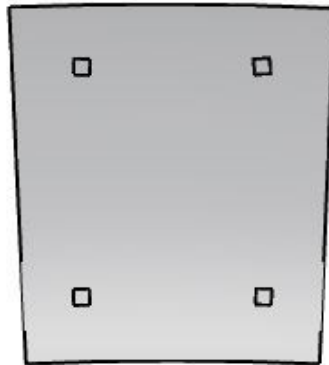


Illustration 7.6: Element to be examined under its own weight

From the above, it is obvious that the flexible mould prefabricated elements are considered conservatively to work solely as a lost formwork, on top of which the in-situ concrete will be cast and form the complete shell. We are thus interested in whether the elements can support their own weight and the weight of the wet concrete and reinforcement. C90/105 is applied for the prefabricated elements. High performance concrete offers a fast and high strength development, with good homogeneity. In combination with fibres, the result is a concrete with high tensile and compressive resistance and long term performance.

	C90/105
Ult. Tensile Strength 0° [N/mm <sup>2</sup> ]	90
Ult. Comp. Strength 0° [N/mm <sup>2</sup> ]	3,5
Modulus of Elasticity [N/mm <sup>2</sup> ]	36667

Table 7.1: Properties of C90/105

The element is supported at the faces where it is connected to the crane cables. The same points are considered for the transportation of the elements in the truck. From the analysis of the prefabricated element, the following results are obtained. The de-

flections of the element are given in Illustration 7.7 and the stresses in the local x and y axis in Illustration 7.8 and Illustration 7.9 respectively.

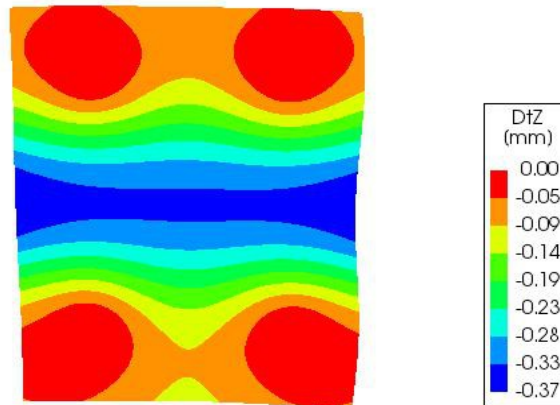


**Illustration 7.7: Displacements in the vertical axis**

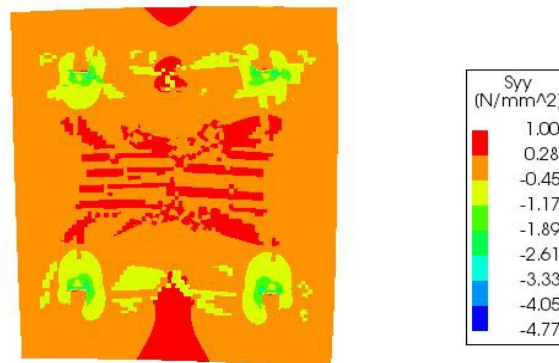


Illustration 7.8: Local stresses y-axis

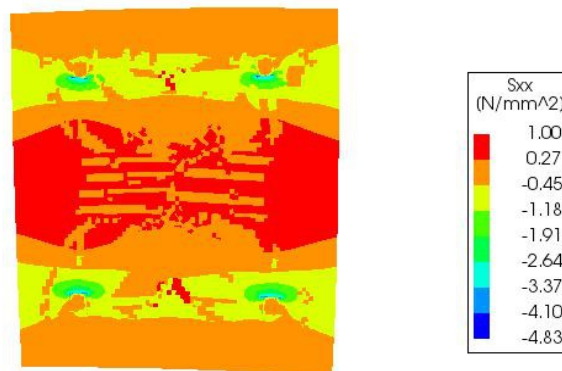


Illustration 7.9: Illustration 7.8: Local stresses x-axis

An amplification factor of 2 is chosen to take into account the dynamic loading during transportation. The following table contains the amplified values.

Quantity	Displacement [mm]	Compressive stress x-axis [N/mm <sup>2</sup> ]	Compressive stress y-axis [N/mm <sup>2</sup> ]	Tensile stress x-axis [N/mm <sup>2</sup> ]	Tensile stress y-axis [N/mm <sup>2</sup> ]
Value	0,74	9,46	9,54	2,00	2,00

Table 7.2: Analysis results multiplied by amplification factor

The deflection of the element is greater at its centre, at the region of the maximum distance from the supports. The amplified value of the deflection, calculated at 0,74 is still smaller than the maximum allowable deflection of a slab equal to  $l/250$ , where  $l$  is the span of the slab. In this case, the smallest dimension of the element is considered conservatively the span of the slab. Thus  $l/250=1833/250 \rightarrow l/250=7,33$  mm.

Moreover, the stresses are checked. As far as the compressive stresses are concerned, it was not expected to deal with a problem there. Indeed, the maximum compressive stresses in both directions are much smaller than the resistance in compression of 90 N/mm<sup>2</sup> of C90/105, which is used for now for the prefabricated elements

The tensile stresses in both directions have a value of 2 N/mm<sup>2</sup> with the mean axial tensile strength of C90/105 equal to 5N/mm<sup>2</sup> and the characteristic axial tensile strength of the lowest 5% equal to 3,5 N/mm<sup>2</sup>. This means that the integrity of the element during transportation might be at risk due to the tensile stresses, and for this reason the placement of reinforcement inside the prefabricated element should be considered. Reinforcement is also necessary to avoid brittle failure of the element. Thickening of the element or decreasing the dimensions will decrease the slenderness and the high tensile stresses.

Another stage of the construction that governs the thickness and consequently the strength of the elements is the point where the elements are temporarily supported by a scaffolding system, followed by the placing of the reinforcement and the casting of the wet concrete. During this stage, the elements are fixed by props or other kind of substructure (illustration 7.6). The fixation might be temporary or permanent depending on the type of the element connection. The loads that are introduced on the elements during construction are often greater than the final service loads. In order to define the thickness of the elements as it was mentioned previously, these loads have to be taken into consideration and the elements have to be checked under their application. Extra care must be taken to prevent damage to the elements because of the constructions loads, and measures like strengthening the connection or placing additional supports might be necessary.

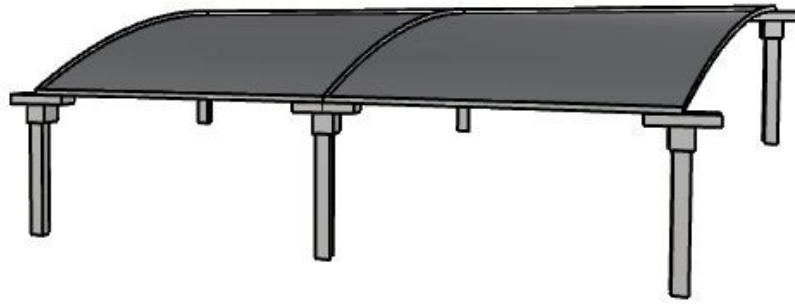


Illustration 7.10: Prefabricated elements supported by props

The analysis of the an element supported by props follows. The support is facilitated by the application of a square support block on the top of the prop in order to spread the weight of the element. Square supporting plates 300mm x 300mm are chosen. The elements are fixed for displacement on the axis perpendicular to their plane and for rotation in their plane. A more realistic approach for the same construction stage, is to consider that the element due to deflection from the weight of the wet concrete and the reinforcement, is line-supported On the edges of the supporting plates. However, if the current supporting conditions are applied in DIANA, the elements would behave as if they are clamped at the four corners. This situation is not representative of the existing supporting condition, and for this reason a different approach will be followed. A simplified and rational approach would be to replace the face or line support in DIANA with point supports at the element corners. From this calculation the displacement and the reaction forces would be received, but not the stresses. As far as the analysis of the element in DIANA is concerned, the loads that are applied apart from the self-weight, include the weight of the wet concrete and the reinforcement. The weight of the reinforcement was calculated using the results of paragraph 4.4, equal to 1279 mm<sup>2</sup>/m or 0,122 kN/m<sup>2</sup>. A live load due to labour during construction is also considered in the form of a point load of 1,0 kN. The load case that is applied uses the ULS load factors of 1,35 for the dead load and 1,5 for the live load. For the calculations that will follow it is assumed that concrete C90/105 is utilised for the prefabricated elements. Furthermore, loads that were considered during the analysis of the monolithic shell, such as soil or wind load, are not taken into account in this stage, as they act after the completion of the shell, where a different structural thickness takes up the applied loads.

With the results of the previous analysis it was found out that increased tensile stresses appear during the lifting of the element by the crane. For this reason an increased

element thickness will be examined, equal to 40mm, since this thickness has been experimentally applied to similar projects.

Shell thickness	20 mm	40 mm
$R_z$ [kN] at each support	4,245	4,89
$u_z$ [mm]	63,27	9,32

Table 7.3: Element on props-Construction loads

As it is seen from the table above, extremely large deformations appear for the case of 20mm. The main reason for this, is the nature of the supports, where only points are supported instead of a face or a line. Obviously, the simplification made, describes the most unfavourable circumstances, provides though an indicative image of how the element behaves. An increase of the thickness to 40mm provides a great reduction in the deflections, and for this reason it is considered suitable, for the formwork elements. The deflections are checked using the limit of 1/250 of maximum allowable deformation of a slab, which is equal to 7,30 mm. The occurring values are greater than this value. In order to limit the deflections, intermediate supports could be inserted.

Shell thickness	20 mm	40 mm
$R_z$ [kN] at each support	2,83	3,24
$u_z$ [mm]	32,12	4,76

Table 7.4: Element on props-Three prop supports per side

With an insertion of a middle support, the deflections are significantly decreased (Table 7.4). For the case of 20mm the value of the thickness is still higher than the maximum allowable limit. For the case of 40mm, the deflections are acceptable.

The element should be also checked to punching shear at the regions of the supports. For this reason the support reaction force or the internal shear force will be used. Both cases will be examined.

- Thickness 20 mm

Due to the nature of the support, the method that will be followed differs from the typical procedure of punching shear check. The shear stress at the support is equal to:

$$\tau = V / (u d) < v_{Rd,max}$$

The perimeter of the corner support is  $u_0 = 2 * 0,15 = 0,3 \text{ m} = 300 \text{ mm}$ . The thickness of the element is  $d = 20 \text{ mm}$ . Thus  $\tau = 0,471 \text{ N/mm}^2$ .

$$v_{Rd,max} = 0,5 v_{f_{cd}} \rightarrow v_{Rd,max} = 0,5 * 0,6 (1 - f_{ck} / 250) * \alpha_{cc} f_{ck} / \gamma_m \rightarrow v_{Rd,max} = 11,52 \text{ N/mm}^2$$

$$\tau < v_{Rd,max} \quad \text{OK}$$

Check shear at basic control perimeter

$$\tau_{ul} = V_{Ed} / (u_1 d) < v_{Rd,c}$$

The basic control perimeter  $u_1$  for a corner support can be seen in Illustration 7.11.

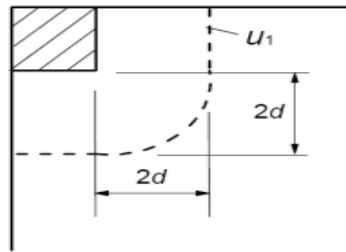


Illustration 7.11: Basic control (critical) perimeter for corner support

For the support of 150 mm, this perimeter is equal to 362,8 mm. Thus  $v_{ed} = 0,39$  N/mm<sup>2</sup>.

$v_{Rd,c} = 0,12 k (100 \rho_l f_{ck})^{1/3}$  For  $\rho_l$  which is the ratio of the reinforcement area over the cross section area, the lowest allowable value of 0,0025 is assumed for both directions.  $v_{Rd,c} = 0,68$  N/mm<sup>2</sup>. The check  $v_{Ed} < v_{Rd,c}$  is valid, which means that punching does not occur.

The same checks are conducted for the thickness of 30mm.

- Thickness 0 mm

At the perimeter of the support

$$\tau = 0,34 \text{ N/mm}^2 < v_{Rd,max} = 8 \text{ N/mm}^2 \quad \text{OK}$$

At the basic control perimeter

$$\tau = 0,31 \text{ N/mm}^2 < v_{Rd,c} = 0,56 \text{ N/mm}^2 \quad \text{OK}$$

Although the occurring displacements exceed the maximum allowable limit due to the assumed supporting conditions, the punching shear check is satisfied, meaning that the slab of both thicknesses does not suffer from punching shear. If this was not the case, then an increase of the element thickness would have been a solution. Moreover, a beneficial way to deal with punching shear would be the increase of the supporting plate width in order to achieve more favourable distribution of the load at the supports. For safety reasons, the plate width is increased to 450 mm for the analyses that will follow.

In a final stage, the connection between the elements should be examined. It was previously mentioned that wet concrete will be placed between the elements with a certain type of reinforcement. The main problem of the connection between the prefabricated elements is not the compression forces, since these can be taken up by a high

strength mortar, but the tensional forces. The first thought that comes to mind in order to account for the tension at the connection is the introduction of reinforcing bars. At a first glance, this might sound simple but there are issues that have not been studied or researched which influence the tensional resistance of the connection. The placement of the rebars entails the existence of sockets in which the bars will be placed, get concreted and cooperate with the elements.

The use of fibres instead of rebars have been proposed and researched. Fibres used as concrete reinforcement are not appropriate for use in the connection, due to their small dimension [42]. Instead fibres of larger length and diameter with a hooked end have been used. Tests have been conducted [46] which indicate that fibres can work, however further investigation is required to gain confidence in the properties of the connection.

#### *7.4.3 FRP reinforcement of concrete structures*

The idea of using Fibre Reinforced Polymers (FRP) as a means of reinforcement for the connection between the prefabricated elements came up during a discussion with Pr. Schipper. FRP reinforcement is one of the most promising new developments for concrete structures. FRP laminates have been used to strengthen, repair or add ductility to existing and new structures. The practice of strengthening concrete structures with externally bonded FRP system had been widely investigated and applied. FRP laminate bonding involves adhering thin flexible fibre plies on the concrete surface using an epoxy resin. The method known as manual lay-up increases the shear and flexural resistance of concrete beams and slabs and offers the benefits of fast and easy construction with a durable, high performance and light-weight connection.

No application has been found though using FRP laminates for a connection between prefabricated double-curved concrete elements. However an attempt will be made in order to examine whether the application of the FRP laminates can be proved beneficial for this connection. Assumptions and simplifications will be made in order to arrive to results, and thus further extensive investigation is necessary, as only a proposal is made in this chapter.

The idea of FRP reinforcement for the connection uses the same principles with the application of strips of FRP laminates on concrete slabs, as mentioned previously. FRP systems restore the structural capacity both in reinforced and unreinforced concrete slabs. For the latter case, a substantial increase of the structural capacity is also

present [47]. Fabrics might be also used to increase the flexural capacity in slabs. For the connection reinforcement rigid FRP strips were assumed. They are produced in standard sizes of 60-120mm width and thicknesses varying around 1,6mm, and they are adhesively bonded to the concrete surface with epoxy resins [48]. Usually the laminates are fabricated by unidirectional pultruded Carbon or Glass FRP (CFRP or GFRP). The application on slabs can be seen in Illustration 7.15.

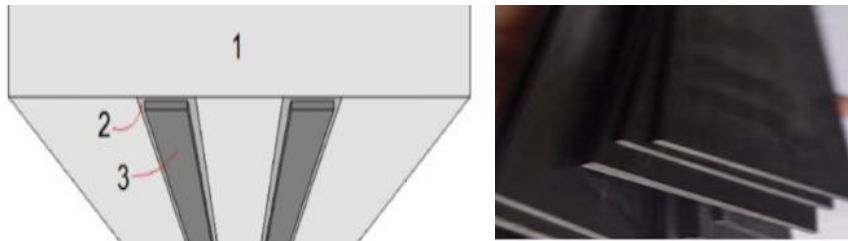


Illustration 7.12: Rigid FRP strips [48]

The manual or hand layup forms the FRP strips on the site, with similar properties with the rigid FRP strips, and widths varying from 100-1500mm [48]. The manual layup laminates can be seen in Illustration 7.13

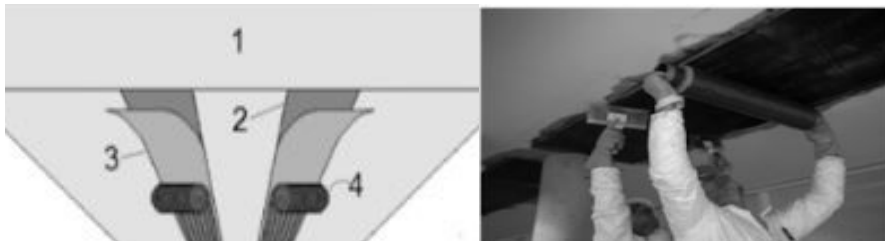


Illustration 7.13: Hand layup FRP laminates [48]

For the reinforcing of the connection FRP strips are positioned along the joint. Since no practical application or similar study on the application of FRP for prefabricated element connection exists, a width for the strip is assumed. Studies [47] conducted on two-way slabs of 2,46m x 2,46m, proved that a total of two unidirectional layers of CFRP strips of 457mm width spaced at 457mm from each other were sufficient to fully restore the structural capacity in applications of repair, and upgrade it greatly in applications of strengthening. In the case of the connection between two elements of 1,89m x 2,27m, a CFRP of 300 mm will be applied in order to check how the connection works. The following image demonstrates the different parts of the connection.

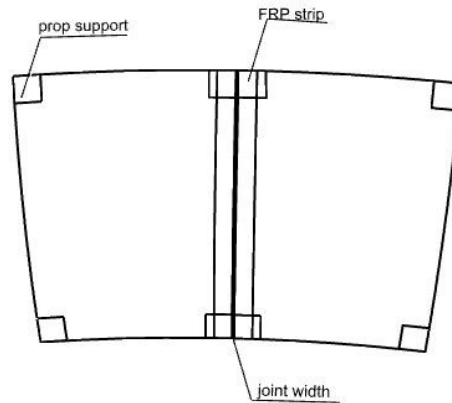


Illustration 7.14: Model of the connection

The elements are supported as already mentioned on props, and a joint of 10 mm width is applied. The FRP strip is positioned on the bottom side of the elements, in order to facilitate the concrete penetrate through the joint width, and take up the tension on the bottom side of the element. The connection will be checked and analysed using the weight of the wet concrete and the reinforcement as an applied load. No structural participation of the hardened concrete will take place, in order to determine whether the connection resistance is sufficient during the casting of the in-situ layer. Thus, the applied loads will coincide with the ones of the previous analysis, where the structural behavior of a single element was investigated.

The analysis of the influence of the applied loads on the connection will take place in DIANA as well. As seen from the previous image, the FRP strip covers the bottom surface of the elements along the joint length and the joint itself. However, DIANA cannot recognise two different meshes, one on the top of the other, and for this reason a certain approach will be followed to account for this issue.

Initially the properties of the FRP composite laminates will be presented, as the concrete properties are already known. The mechanical behavior of the FRP composites, is, as the name suggests, the result of the synergy between the fibres and the matrix. For the material of the connection, both stiffness and tensile strength are required. Stiffness is mainly a function of the reinforcing material, in other words the fibres, whereas the tensile strength is a product of the cooperation of the resins and the fibres [48]. High Modulus (HM) fibres are chosen with the properties found in Illustration 7.15. For the matrix of the FRP composite, an epoxy resin is chosen with properties found in Illustration 7.16.

		Glass		Carbon		
		E glass	R glass	HS	IM	HM
		Characteristic values	Characteristic values	Characteristic values	Indicative values	Indicative values
Density (kg/m <sup>3</sup> )		2570	2520	1790	1750	1880
Tension in fibre direction	Poisson's ratio $\nu_f$	0.238	0.2	0.3	0.32	0.35
	Young modulus $E_{f1}$ (MPa)	73100	86000	238000	350000	410000
	Strain limit $\epsilon_{f1}$ (%)	3.8	4	1.5	1.3	0.6
	Strength $\sigma_{f1}$ (MPa)	2750	3450	3600	4500	4700
Tension perpendicular to fibre direction	Poisson's ratio $\nu_t$	0.238	0.26	0.02	0.01	0.01
	Young modulus $E_{t2}$ (MPa)	73100	86000	15000	10000	13800
	Strain limit $\epsilon_{t2}$ (%)	2.4	2.4	0.9	0.7	0.45
	Strength $\sigma_{t2}$ (MPa)	1750	2000	135	70	60
Compression in fibre direction	Strain limit $\epsilon_{c1}$ (%)	2.4	2.4	0.9	0.6	0.45
	Strength $\sigma_{c1}$ (MPa)	1750	2000	2140	2100	1850
Shear	Modulus $G_{f1}$ (MPa)	3000	34600	50000	35000	27000
	Strain limit $\gamma_{f12}$ (%)	5.6	5.6	2.4	3	3.8
	Strength $\sigma_{f12}$ (MPa)	1700	1950	1200	1100	1000
Thermal expansion	$\alpha (10^{-6} K^{-1})$	5 - 0	3	-0.4	-0.6	-0.5

Illustration 7.15: Indicative fibre properties given in JRC2016

	Polyester	Vinyl ester	Epoxy
Density (kg/l)	1.2	1.1	1.25
Poisson's ratio ( $\nu_{12, resin}$ )	0.38	0.26	0.39
$T_g$ (°C)	approx. 60 <sup>(1)</sup>	approx. 100 <sup>(1)</sup>	80 - 150 <sup>(1)</sup>
Tensile or compression strength (MPa)	55 <sup>(2)</sup>	75 <sup>(2)</sup>	75 <sup>(2)</sup>
Young modulus in tension (MPa)	3550	3350	3100
Strain limit in tension or compression (%)	1.8	2.2	2.5
In-plane shear modulus (MPa)	1350	1400	1500
Shear strength (MPa)	approx. 50	approx. 65	approx. 80
Shear strain limit (%)	3.8	3.7	5
Expansion coefficient ( $10^{-6} K^{-1}$ ) <sup>(3)</sup>	50 - 120	50 - 75	45 - 65

Illustration 7.16: Indicative resin properties given in JRC2016

In order to predict the mechanical properties of the laminate, the simple rule of mixture is applied, according to which:

$$E = \beta E_f V_f + E_m V_m$$

where

$\beta$  is a factor based on the classical laminate theory depending on the direction of the fibres in the laminate

$E_f$  and  $E_m$  is the modulus of elasticity of the fibres and the matrix respectively, and

$V_f$  and  $V_m$  is the volume ratio of the fibres and the matrix respectively.

The previous formula is applied to derive the properties of the FRP laminate along the axis of the development of fibres. For the mechanical properties in the transverse direction, the following formula should be used:

$$E_{trans} = E_m / (1 - \sqrt{V_f * (1 - E_m / E_{(f, trans)})})$$

where

$E_{trans}$  is the modulus of elasticity in the transverse direction.

These formulas provide the modulus of elasticity for the FRP laminate. In order to define the rest of the material properties like Poisson's ratio or the shear modulus, the same rule is applied. The following table contains the properties of the FRP laminate of carbon fibres and epoxy resin. A thickness of 2mm is chosen for the FRP strip

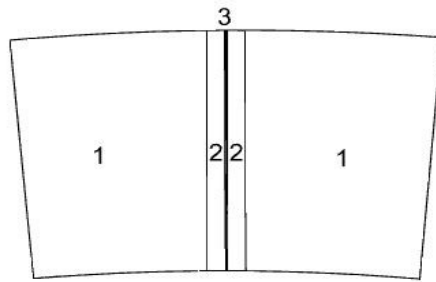
$E_x$ [MPa]	5970
$E_y$ [MPa]	267600
$\nu_x$	0,143
$\nu_y$	0,2
$G_x$ [MPa]	10450
$G_y$ [MPa]	10450

Table 7.5: Properties of FRP laminate

There are parts of the connection where the FRP strip covers the concrete surface, meaning that in a cross-section at this region two materials exist. Since two different material meshes cannot overlay one another, a new 'composite' material is introduced combining the properties of concrete C90/105 and the underlying FRP strip cover. The new material has a thickness equal to the sum of the concrete and FRP thickness (22mm in total) and properties derived from the rule of mixture as well. The following table contains the properties of the 'composite' material. To sum up, DIANA model will consist of three different materials, distributed symmetrically in five regions (Illustration 7.17).

$E_x$ [MPa]	40542
$E_y$ [MPa]	64327
$\nu_x$	0,1886
$\nu_y$	0,2
$G_x$ [MPa]	4950
$G_y$ [MPa]	4950

Table 7.6: Properties of the composite material (C90/105 and FRP)



1. Concrete C90/105
2. Composite (C90/105+FRP)
3. FRP

Illustration 7.17: Materials in DIANA model

Vertical supports are applied to the system, at the lines where the deflected elements are supported by the steel plate of the props. The results of the analysis for an element thickness of 20mm can be seen in the following images.

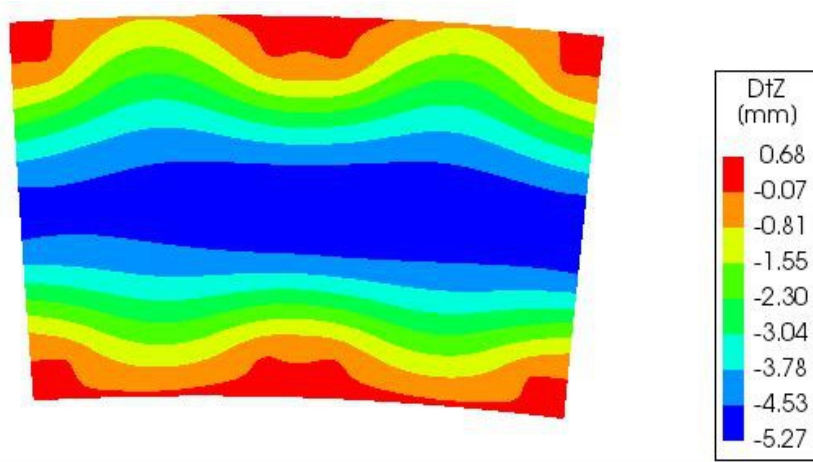


Illustration 7.18: Connection-Deformations z-axis

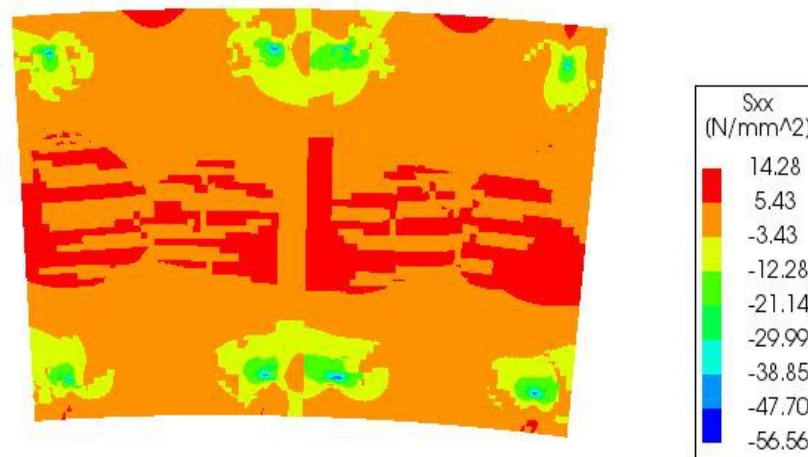


Illustration 7.19: Connection-Stresses x-axis

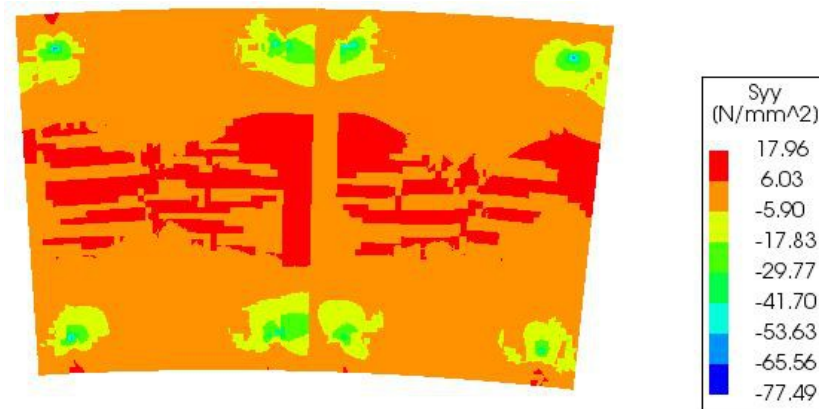


Illustration 7.20: Connection-Stresses y-axis

In order to define how the properties of the connection affect the structural behavior, an analysis is also conducted with an increased thickness of the FRP strip at 6mm. The increased FRP thickness although does not influence the stiffness of the FRP itself, it affects the stiffness of the composite material since the rule of mixture is applied here as well. The difference in the stiffness between the two materials are shown in the following table.

	Thickness 2mm	Thickness 6mm	$\Delta$ [%]
$E_x$ [MPa]	40542	35223	-13,12
$E_y$ [MPa]	64327	95600	48,7
$G_x$ [MPa]	4950	5796	17,1
$G_y$ [MPa]	4950	5796	17,1

Table 7.7: Properties for "composite material" for the 2mm and 6mm FRP strip

The results of the two analyses for an element thickness of 20mm are presented and compared in the following table.

	2mm	6mm	$\Delta$ [%]
$n_{xx,max}$ [N/mm]	115,87	86,17	25,6
$n_{xx,min}$ [N/mm]	-86,13	-66,15	26,7
$n_{yy,max}$ [N/mm]	133,89	124,54	6,9
$n_{yy,min}$ [N/mm]	-113,89	-135,58	19,0
$\sigma_{xx,max}$ [N/mm <sup>2</sup> ]	14,28	11,41	20,1
$\sigma_{xx,min}$ [N/mm <sup>2</sup> ]	-56,56	-37,01	34,6
$\sigma_{yy,max}$ [N/mm <sup>2</sup> ]	17,26	18,24	5,7
$\sigma_{yy,min}$ [N/mm <sup>2</sup> ]	-77,49	-71,29	8,0
$m_{xx,max}$ [kNm/m]	4,36	4,26	2,3
$m_{xx,min}$ [kNm/m]	-1,13	-1,34	18,5

$m_{yy,min}$ [kNm/m]	5,26	8,06	53,2
$m_{yy,min}$ [kNm/m]	-1,36	-1,95	43,4
$u_{z,max}$ [mm]	5,27	3,01	42,3
$\lambda_1$	0,79	0,88	11,4

Table 7.8: Results of analysis of connected elements of 20mm thickness

The analysis of connection with the 2mm thick FRP shows that the maximum compressive stresses can be taken both by the concrete and the FRP material. The following contains the properties of the High Strength CFRP with epoxy resin matrix.

	Standard CF UD
Ult. Tensile Strength 0° [N/mm <sup>2</sup> ]	1500
Ult. Comp. Strength 0° [N/mm <sup>2</sup> ]	1200
Ult. Tensile Strength 90° [N/mm <sup>2</sup> ]	50
Ult. Comp. Strength 90° [N/mm <sup>2</sup> ]	250

Table 7.9: Mechanical properties of epoxy resin matrix HS CFRP

As far as the tensile stresses are concerned, the properties of FRP provide great tensile resistance. For the prefabricated elements themselves, tensile reinforcement is necessary.

For the analysis of the connection with the 6mm thick FRP, although an increase in the stiffness of 48,7% occurs for the composite material, the differences in the resulting quantities are of a smaller magnitude. In this case, the compressive stresses could be resisted by a concrete of lower strength, however tension reinforcement is still necessary to resist the tensile stress. Reinforcement is always required to be provided in the concrete elements in order to prevent brittle failure of the concrete, even if the intrinsic concrete tensile resistance is sufficient to resist the occurring tensile stresses. Another important finding from the analysis is that the number of supports of the elements should be increased due to the low buckling load factor. Another option is the increase of the element thickness.

An increased element thickness of 40mm is also examined for the same connection. The results are shown in the following table.

	2mm	$\Delta$ [%]
$n_{xx,max}$ [N/mm]	40,11	-65,3
$n_{xx,min}$ [N/mm]	-30,63	-64,4
$n_{yy,max}$ [N/mm]	34,08	-74,5
$n_{yy,min}$ [N/mm]	-28,83	-74,6
$\sigma_{xx,max}$ [N/mm <sup>2</sup> ]	4,11	-71,2

$\sigma_{xx,min}$ [N/mm <sup>2</sup> ]	-18,67	-66,8
$\sigma_{yy,max}$ [N/mm <sup>2</sup> ]	4,10	-76,2
$\sigma_{yy,min}$ [N/mm <sup>2</sup> ]	-18,76	-75,7
$m_{xx,max}$ [kNm/m]	4,97	14,0
$m_{xx,min}$ [kNm/m]	0,97	-14,1
$m_{yy,min}$ [kNm/m]	5,07	-3,6
$m_{yy,max}$ [kNm/m]	-1,08	-20,6
$u_{z,max}$ [ mm]	0,98	-81,4
$\lambda_1$	1,09	43,5

Table 7.10: Results of analysis of connected elements for element thickness of 40mm

A significant decrease of the forces is produced with the increase of element thickness to 40mm.. It is interestingly noticed that the compressive and tensile stresses have decreased that much that allow for the use of concrete of a much lower strength, with the necessary reinforcement always provided. A substantial decrease of the bending stresses also occurs, justified by the increased moment of inertia.

## 7.5 Conclusions

The elements work as lost formwork for the wet concrete, without participating in the structural behavior of the complete shell. Their behavior was examined for different stages of the construction process. It was found out that an element thickness of 20mm is not sufficient to withstand the applied construction loads. Thus an increase of the thickness is completely necessary. Another issue concerns the support of the elements by props. At least three supports on each element edge are necessary to minimise deflections. Both of these alterations on the original concept would increase the resistance to buckling from which the elements suffer and subsequently the critical buckling load.

# CHAPTER 8

## 8 Conclusions and Recommendations

### 8.1 Conclusions

The aim of this master thesis was to examine whether the construction of a concrete shell was feasible using flexible mould prefabricated concrete elements. In order to accomplish this, a design case building was chosen, which had to be analysed both as a monolithic structure and as a prefabricated structure. The shell of the 'Bezoekerscentrum Waalbos' has not been constructed yet, thus apart from its constructability it was wise also to check design parameters, such as its dimensions and its geometrical characteristics.

Accompanying the research question, there are set design criteria which have to be satisfied throughout the progress of the thesis. These are the following:

- the structure should satisfy the strength and stiffness requirements for shells.
- the construction and design of the structure should be cost-efficient
- the final design should not diverge greatly from the original design of the architect.

Subsequently, since the structural feasibility of the shell had not been checked, it was examined if this is possible and what modifications in the design were necessary. A limitation to this was the criterion of the least deviation from the original design. The analysis of the structure in a FEA software required first its validation. After a design had been produced, it was necessary to verify the finite element model. The structure was then analysed considering it as a monolithic shell. The structure was then segmented in elements, and a connection model was proposed, in which a cooperation of prefabricated elements and cast in-situ concrete took place.

From the analysis of the approximating structures, it was concluded, that the structural behavior of the central part of the structure could approach the behavior of a flat slab supported on columns or a long barrel shell (shell beam) supported on walls in its transverse direction. Moreover, an effort was made to relate the shell with a catenary arch, however it was proved unsuccessful for two reasons. First the resulting design was differentiating substantially from the original design. Second, the research for the arch geometry did not follow an optimisation process where a critical loading enve-

lopes should be constructed by superimposing the effects of various load cases on the arch. The dead weight was chosen instead, and as a result the rest of the applied loads which had significant magnitude would produce tension across the arch length. Finally, the analysis of the side parts, showed that they behave quite similarly to dome structures. With the analysis of the approximating structure, the validation of the FEA software was also completed.

The architect's designs only included rough dimensions for the building layout, without defining essential features of the shell like its curvature and the design of the facade. A lot of ideas for the shape of the facade were tested with structural and aesthetic criteria. The design was altered, with the main difference located at the front part of the structure, where instead of a continuous opening throughout the whole length of the facade, an arch opening was positioned.

The new model was verified using three checks: sum of reaction forces, deformations at the crown of the arch, stresses. Only small percentages of deviation between theoretical and analytical calculations were present, proving that the structure works as expected. The analysis of the model loaded only by its self-weight produced excessive deformations at the top of the arch opening, which made necessary the introduction of a stiffening arch across the opening. The resulting deformations were decreased by 44%. Before the analysis of the structure with the service loads, a mesh study was performed, where a mesh size of 0,25 m was proved sufficiently small to produce representative results.

The model was then analysed with service loads, and the combinations where the live load is the dominant variable action were the governing ones. LC2 produced the maximum structural quantities but it was not used for the design, as its application is not predicted by Eurocode. LC1 was used instead. The sum of the reaction forces shows that the structure is relatively light. Structural efficiency of the side domes is proved due to much lower deformations at this part. Tensile ( $16,90\text{N/mm}^2$ ) and compressive ( $50,63\text{N/mm}^2$ ) stresses are quite large for LC1, indicating that C25/30, assumed in the beginning, was not suitable for the construction of the building. Global axis stresses showed that the behavior of the central part of the shell resembles the behavior of a doughnut like axisymmetric shell dome, where compressive hoop forces appear at the highest point surrounded by tensile forces. Bending stresses occur where the membrane stresses are insufficient to carry the applied loads, at regions close to the connections with foundation and at the arch support. The first and second buckling load

factors were determined after they have been multiplied with a 'knock-down' factor. There is no load case for which the buckling factor is below 1. The difference between the first and second buckling load factor is big enough to conclude that the shell is not sensitive to imperfections.

Since the thickness of 100 mm for the shell was chosen arbitrarily, a thickness study was also conducted, proving that although the initial thickness is sufficient to withstand the applied loads and provide the necessary stability to the structure, an increase to 120mm, causes a reduction in the tensile and compressive stresses (14,17N/mm<sup>2</sup> 43,47N/mm<sup>2</sup> respectively) and deflections (21,51mm) allowing for use of concrete of lower strength, accompanied by a minor increase in the reaction forces.

After the analysis of the monolithic shell, the segmentation of the shell took place. For this process, certain boundary conditions were taken into account, like the dimensions and the curvature of the elements and the number of reconfigurations of the flexible mould. Finally, the cylindrical part was segmented in 72 (6x12) elements of 1,47m-2,26m x 2,23m-2,36 m. Elements with odd and small shapes were incorporated with the neighboring ones. For the spherical side part, the technique of the ribbed dome was applied producing elements of 0,97m-1,97m x 2,36m-2,63m. For the sides of the domes, a segmentation in quadrilaterals was followed instead of the ribbed dome technique, which would lead in triangular elements.

Following this, a model had to be defined for the connection between the prefabricated elements. First a construction method was applied that makes use of both prefabricated elements and cast in-situ concrete. The properties of the connection between the elements need further investigation in order to ensure that load transfer is realised and for this reason it was decided to consider that the prefabricated elements function solely as a lost formwork, on which the wet concrete will be cast. This method is an enhancement to the traditional shell construction method. The reasons are:

- faster and less arduous production of formwork elements
- it allows for complex shell configuration using the flexible mould
- it skips the process of lowering and removing the formwork, as they are integrated in the final structure

Since the elements function as formwork, it was wise to examine their structural behavior throughout the different stages of the construction process. Initially, a curved element part of the prefabricated shell was checked during its transportation to the building site. Dynamic loading effects were considered with the use of amplification

factors for the static loading. During its lifting by the crane, the element with a thickness of 20mm, using C90/105 is not put at risk since deflections equal to 0,74mm were within the acceptable limits of  $l/250=7,33\text{mm}$  and compressive and tensile forces could be resisted by the concrete. However, reinforcement of the elements is considered advantageous in order to avoid brittle failure of the elements. In a later stage, the elements should be examined when they are placed on top of props, and loaded with the weight of the wet concrete and reinforcement. Considering that the element is point-supported at its four corners, quite large deflections occur for the case of 20mm, equal to 63,27mm. With an increased element thickness at 40mm, the deflections (9,32mm) are greatly decreased, still not satisfying the maximum allowable limits of 7,33mm. An insertion of a third support on each edge of the element decreases the deformations to 32,12mm and 4,76mm for the case of 20mm and 40mm thickness respectively. The reason for the large magnitude of deflections is mainly due to the type of the assumed supports. Punching shear check was performed and finally satisfied on the element for the thickness of 20mm and 40mm assuming a support steel plate of 300mm. For safety reasons, the plate width is increased from 300mm to 400mm.

A connection model was defined at the last part. The main problem of the connection is the transfer of tensile stresses. FRP strips were used for this reason, placed on the bottom side of the elements. The analysis of two connected elements showed that the transfer of tensile forces is facilitated with the use of the FRP strip, however reinforcement is necessary for the prefabricated elements as well. The deformations were within the acceptable limit of 7,33mm for this stage of construction, but buckling occurred for the case of 20mm thick elements. As a conclusion the construction of the shell using flexible mould prefabricated elements as formwork is feasible with a minimum element thickness at 40mm and at least three supports on each element side.

## **8.2 Recommendations**

This project concerned the feasibility of the shell of the 'Bazoekerscentrum Waalbos' as a monolithic and prefabricated shell. Since the structure has not been built yet, optimisation procedures could take place throughout the whole project, from its design to its construction. Unfortunately, these optimisation steps could not all be addressed in this thesis, due to the lack of time. This chapter includes the extra steps that could enhance the quality of the final result.

To begin with, as it was made clear in the thesis report, no finalised dimensions or geometrical characteristics were given, and consequently a certain form was selected and examined based on structural and aesthetic criteria. For this reason, different designs should be examined with various dimension and curvature combinations in order to obtain a more advantageous structural behaviour of the shell. Numerous concepts for the facade opening were tested, without this excluding the possibility of a different design with higher aesthetic quality.

Moreover, specific types of loads were not considered in order to decrease the complexity of the analysis. The use of time-dependent and accidental loads is thus recommended. The wind load was examined in the axis of the development of the building. Applying the wind load in the perpendicular axis is recommended to check whether governing results are produced. Serviceability limit state load combinations were not considered in order to speed up the process. Instead the deformations were determined using the ULS load combinations. A more economic design would have been produced in the opposite case and for this reason, the use of SLS load combinations is recommended.

It is also proposed to combine the optimisation steps of shell thickness and concrete strength and specify regions on the structure where each combination would produce beneficial results.

A linear static analysis simulates reality only when the deflections are infinitesimally small and stresses and strains induced by loads are within the elastic range. The occurring stresses exceed the elastic range and for this reason non-linear analysis is considered wise. A non-linear analysis could be performed to examine the stability problems, taking into account material and geometrical non-linearities, a step that would produce higher buckling factors than the ones obtained from the conservative linear static analysis with the 'knock down' factors.

Proceeding to the segmentation of the shell in prefabricated elements, the main criteria concerned the number of different elements and their dimensions. In addition to this, more parameters could be introduced to Grasshopper such as the curvature and weight of the elements or limits for the occurring stresses, that could enhance even more the quality of the segmented design. Specialised segmentation tools could be also used.

The analysis of the prefabricated shell started with the definition of the construction process, where an in-situ and a prefabricated part would cooperate. In this thesis since

no previous investigation on that model existed, it was conservatively assumed that no cooperation between the cast in-situ and prefabricated part took place. Initially it is recommended to research the constructional feasibility of this model. If this assumption and approach will be followed, an exact thickness for the elements used as lost formwork should be defined, that would satisfy the stability and strength requirements. Moreover, further investigation on the number of props combined with the thickness study can produce more cost-efficient results.

The connection model that uses FRP strips was selected due to its simplicity in design and analysis. However, the model, as it was previously mentioned, has never been studied or applied before and investigation is absolutely necessary. The effects of the connection on the structure should be checked. In this thesis since no structural cooperation between the cast in-situ and prefabricated part was assumed, this was not necessary. Furthermore, different connection types can be applied and the properties of the connection they provide should be determined. Subsequently, the properties of the connection should be applied to the prefabricated shell, in order to proceed to its analysis. The structural response of the prefabricated shell should be compared to the one of the monolithic shell in order to check the feasibility of the method.

This approach is recommended since a different one was followed in the thesis. The assumption of no cooperation between the cast in-sit and the prefabricated shell should be checked.

From the last paragraphs it can be seen that the connection model that employs FRP strips is only a proposal, studied in this thesis with assumptions and simplifications. However, it comprises an interesting research topic that would be complemented by the construction of a physical scale model which would verify its behaviour and its effects on the structural response of the shells.



# BIBLIOGRAPHY

- [1] [www.slideshare.net/IanToisa/shell-structure-basic-concept](http://www.slideshare.net/IanToisa/shell-structure-basic-concept)
- [2] [anhngq.wordpress.com/2009/12/10/r-g-curvature/](http://anhngq.wordpress.com/2009/12/10/r-g-curvature/)
- [3] CIE 5251-09 Reader
- [4] [en.wikipedia.org/wiki/Developable\\_surface](http://en.wikipedia.org/wiki/Developable_surface)
- [5] Joseph Francis Wong, The text of free-form architecture: qualitative study of the discourse of four architects, 2010
- [6] Flugge W., Theory of Plates and Shells, 1960
- [7] Peerdeman B., Analysis of Thin Concrete Shells Revisited: Opportunities due to Innovations in Materials and Analysis Methods, 2008
- [8] Moore R.E., Construction Techniques for Thin Shell Concrete Domes, 1980
- [9] Bösigler H., The Building of Isler Shells, 2011
- [10] [www.globalconstructionreview.com/](http://www.globalconstructionreview.com/)
- [11] Dallinger S., Johann Kollegger, Pneumatic Formwork for Concrete and Ice Shells
- [12] [https://en.wikipedia.org/wiki/Construction\\_3D\\_printing](https://en.wikipedia.org/wiki/Construction_3D_printing)
- [13] Wolfs R.J.M., 3D Printing of Concrete Structures
- [14] Witterholt S., The application of double-curved precast concrete elements for the Project Green Planet, 2016
- [15] [www.ketchum.org](http://www.ketchum.org), Construction of Concrete Shells
- [16] Eisenbach P., Processing of Slender Concrete Shells -Fabrication and Installation, 2017
- [17] Weilandt A., Grohmann M., Bollinger K., Wagner M. ROLEX LEARNING CENTER in Lausanne: From conceptual design to execution, 2009
- [18] Schipper H.R., Double-curved precast concrete elements-Research into technical viability of the flexible mould method, 2015
- [19] [www.richardmeier.com/?projects=jubilee-church-2](http://www.richardmeier.com/?projects=jubilee-church-2)
- [20] [www.archdaily.com/127679/hoto-fudo-takeshi-hosaka-architects](http://www.archdaily.com/127679/hoto-fudo-takeshi-hosaka-architects), Takeshi Hosaka Architects-Hoto Fudo
- [21] [www.arup.com/projects/hoto-fudo](http://www.arup.com/projects/hoto-fudo), A unique restaurant at the foot of Mt Fuji

- [22] <https://www.architectural.com/takeshi-hosaka-architects-hoto-fudo/>, The Monolithic Dome
- [23] [www.monolithic.org/domes](http://www.monolithic.org/domes), The Monolithic Dome
- [24] Cauberg N., Parmentier B., Vanneste M., Mollaert M., Fabric Formwork for Flexible Architectural Concrete, 2009
- [25] [fponsolle.wordpress.com/2016/02/17/carton-a-dessin-feuille70](http://fponsolle.wordpress.com/2016/02/17/carton-a-dessin-feuille70), SUN TRAP – BLOG D'ARCHITECTURE
- [26] [stadiasfile.com/category/articles/features/](http://stadiasfile.com/category/articles/features/), THE GREAT ARENA ROOF: Part III (Nervi's Palazzetto dello Sport)
- [27] <http://mapio.net/s/31923292/>, Spencer Dock,
- [28] Cordek, Spencer Dock Beidge Case Study, 2016
- [29] [nl-nl.facebook.com/Project-Bezoekerscentrum-Waalbos-603174846539508/](https://nl-nl.facebook.com/Project-Bezoekerscentrum-Waalbos-603174846539508/), Project Bezoekerscentrum Waalbos
- [30] Abbey T., Verification VSs. Validation in Relation to FEA, 2015
- [31] [https://www.researchgate.net/post/In\\_finite\\_element\\_analysis\\_verification\\_and\\_validation\\_with\\_field\\_tests\\_universally\\_what\\_is\\_the\\_expected\\_percentage\\_FEA\\_should\\_meet](https://www.researchgate.net/post/In_finite_element_analysis_verification_and_validation_with_field_tests_universally_what_is_the_expected_percentage_FEA_should_meet)
- [32] [elibrary.asabe.org](http://elibrary.asabe.org), Typical properties of soil
- [33] Cement and Concrete Association of Australia, Guide to Long-Span Concrete Floors, 2003
- [34] <https://www.slideshare.net/Tarunkumar689/flat-slab>, Flat slab
- [35] Shueler W., The Design of Building Structures, 1995
- [36] Snavane T., Analysis of Arches, 2006
- [37] [en.wikipedia.org/wiki/Organic\\_architecture](http://en.wikipedia.org/wiki/Organic_architecture), Organic Architecture
- [38] Nielsen K., Organic architecture, 2016
- [39] Clive L. Dym, F.ASCE: and Harry E. Williams, Stress and Displacements for Arches, 2011
- [40] Mekjavić I., BUCKLING ANALYSIS OF CONCRETE SPHERICAL SHELLS, 2011
- [41] Schiper R., Janssen B., Manufacturing Double-Curved Elements in Precast Concrete using a fFlexible Mould-First Experimental Results,2011
- [42] den Hartog E., Prefabrication of concrete shells, 2008
- [43] The International Federation for Structural Concrete-Task Group 6,2, FIB 43 - Structural Connections for Precast Concrete Buildings, 2008
- [44] ter Maten R.N., Ultra High Performance Concrete in Large Span Shell Structures, 2011

- [45] Shandliya Dattakumar Sushanth, Ganeshan Vivek, Converting dynamic impact events to equivalent static loads in vehicle chassis, 2017
- [46] Ruhle H., Raumlische Dachtragwerke Construction und Ausfuhrung, Band 1, 1969
- [47] Ayman S. Mosallam , Khalid M. Mosalam, Strengthening of two-way concrete slabs with FRP composite laminates, 2003
- [48] Pavlovic M., CIE5128, Lecture 12 Retrofitting by FRP, 2016
- [49] [en.wikipedia.org/wiki/Pantheon,\\_Rome](http://en.wikipedia.org/wiki/Pantheon,_Rome)
- [50] Krivoshepko, Hyeng, & Mamieva, Chronology of Erection of the Earliest Reinforced Concrete Shells, 2014
- [51] Luitse Simon Jan Johannes, Deconstruction: A new construction method for prefab shell structures, 2016
- [52] Schipper, H.R., Eigenraam P., Mapping double-curved surfaces for production of precast concrete shell elements, 2016
- [53] [www.e-architect.co.uk/azerbaijan/heydar-aliyev-centre-baku](http://www.e-architect.co.uk/azerbaijan/heydar-aliyev-centre-baku), Heydar Aliyev Centre Baku
- [54] [www.cladglobal.com/CLADnews/architecture-design/Coop-Himmelb\(l\)au-House-of-Bread-Asten-architecture-design-Austria-Backaldrin/322478?source=news](http://www.cladglobal.com/CLADnews/architecture-design/Coop-Himmelb(l)au-House-of-Bread-Asten-architecture-design-Austria-Backaldrin/322478?source=news), Coop Himmelb(l)au design House of Bread museum in Austria



# APPENDIX A

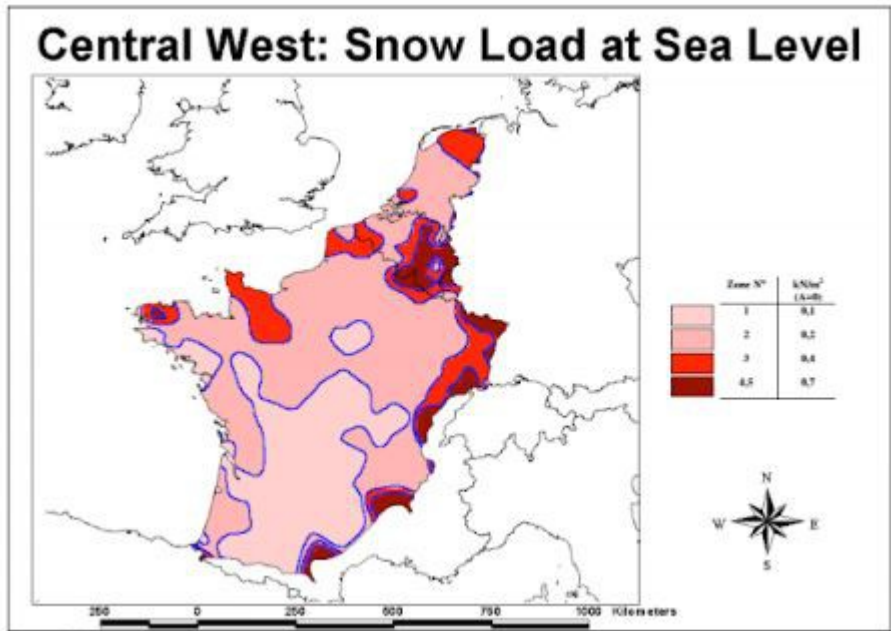


Illustration 1: Snow load map containing the Netherlands according to EN 1991-1-3

5



